

Kristin Bugge Lyche

Snowpack Modeling Forced by Numerical Weather Predictions and Manually Observed Snow Profiles

The Future of Avalanche Forecasting?

Master's thesis in Civil and Environmental Engineering

Supervisor: Oddbjørn Bruland

Co-supervisor: Holt Hancock

June 2023

Kristin Bugge Lyche

Snowpack Modeling Forced by Numerical Weather Predictions and Manually Observed Snow Profiles

The Future of Avalanche Forecasting?

Master's thesis in Civil and Environmental Engineering
Supervisor: Oddbjørn Bruland
Co-supervisor: Holt Hancock
June 2023

Norwegian University of Science and Technology
Faculty of Engineering
Department of Civil and Environmental Engineering



Norwegian University of
Science and Technology

M.Sc. THESIS IN HYDRAULIC ENGINEERING

Candidate: Mrs. Kristin Bugge Lyche

Title: Snowpack Modeling Forced by Numerical Weather Predictions and Field Observations

1 Background

Snow avalanches are major natural hazards in mountainous terrain, and represent a serious risk to both people and infrastructure. Snow avalanche forecasting aims to prevent avalanche accidents, and detailed numerical modeling of snowpack stratigraphy is increasingly relied upon in the forecasts.

The main objective of the study is to investigate how numerical snowpack modeling forced by numerical weather predictions can aid avalanche forecasting.

The study will be carried out in cooperation with the project “Risk governance of climate-related systemic risk in the Arctic” (ARCT-RISK) at the department of Industrial Economics and Technology Management, NTNU.

2 Work description

The thesis shall cover, though not necessarily be limited to the main tasks listed below. The candidate must collect available documents such as reports, relevant studies, and maps. Based on the available documentation the following shall be carried out:

- 1 Literature review on:
 - a. Numerical snowpack modeling, focusing on operational utilized models.
 - b. Define a knowledge gap within the main objective of the thesis.
 - c. Select and set up an appropriate model chain for modelling the snowpack development in a way relevant for avalanche forecasting.
- 2 Define and set up appropriate research methodology.
 - a. Define strategy for data collection from both the numerical weather prediction as well as field observations.
 - b. Set up a numerical model chain consisting of a NWP and a relevant snowpack model, which could be run operationally.
- 3 Collect field data and establish model chain.
 - a. Collect relevant snow and meteorological data.
 - b. Set up and validate model and compare simulation results and observations. Do quantitative and qualitative analysis of the model results.
- 4 Prepare a report with an introduction, relevant theory, method, results, discussion, and conclusions.

3 Supervision

Professor Oddbjørn Bruland will be the main supervisor. PhD Holt Hancock at UNIS will be co-supervisor. The supervisors shall assist the candidate and make relevant information available.

Discussion with and input from other research or engineering staff at NTNU or other institutions are recommended. Significant inputs from others shall be referenced in a convenient manner.

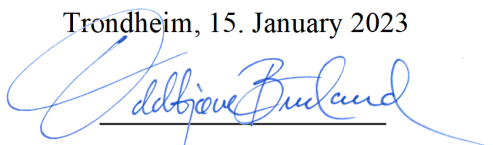
The research and engineering work carried out by the candidate in connection with this thesis shall remain within an educational context. The candidate and the supervisors are free to introduce assumptions and limitations which may be considered unrealistic or inappropriate in contract research or a professional/commercial context.

4 Report format and submission

The report should be written with a text editing software. Figures, tables and photos shall be of high quality. The report format shall be in the style of scientific reports and must contain a summary, a table of content, an article describing the work and a list of references.

The report shall be submitted electronically in B5-format .pdf-file at Inspira. Supplementary working files such as spreadsheets, numerical models, program scripts, figures and pictures shall be uploaded to Inspira. The summary shall not exceed 450 words and the thesis should not exceed 60 pages (or 20.000 words) The Master's thesis should be submitted within 11th of September 2023.

Trondheim, 15. January 2023



Oddbjørn Bruland
Professor

Department of Civil and Environmental Engineering
NTNU

Abstract

Snow avalanches are significant natural hazards in mountainous terrain and represent a severe problem for people and infrastructure. Snow avalanche forecasting aims to prevent avalanche accidents, and detailed numerical modeling of snowpack stratigraphy is increasingly relied upon.

The research presented in this thesis addresses the knowledge gap related to the potential of numerical snowpack modeling forced by numerical weather predictions and observed snow profiles to improve avalanche forecasting. This is achieved by answering the following research questions: 1) To what degree does weather prediction data from AROME-Arctic provide suitable input for numerical snowpack modeling? 2) How accurately does the SNOWPACK model forced by AROME-Arctic and a manually observed snow profile forecast the development of the snowpack? 3) To what extent is the performance of SNOWPACK forced by AROME-Arctic and a manually observed snow profile useful for avalanche forecasting?

This was answered by first evaluating the AROME-Arctic model data output from different grid points. The best-performing option was linked to the SNOWPACK model. Further, the AROME-Arctic and SNOWPACK model chains were run over four model periods, initiated by manually observed snow profiles. The performance of the model chain was qualitatively evaluated using an objective comparison algorithm, comparing the simulated snow profile with a manually observed snow profile.

The results indicate that AROME-Arctic can provide high-quality data for snowpack modeling. The model chain consisting of AROME-Arctic and SNOWPACK, can accurately forecast the development of the snowpack and deliver valuable results for avalanche forecasting. During the fourteen-day field period, the model chain correctly predicted the applicable avalanche problems, demonstrating its operational usefulness.

However, careful consideration should be given to translating the gridded AROME-Arctic output to point data, as the model chain showed sensitivity towards AROME-Arctic grid point selection. Particularly, shortwave radiation was found to significantly influence the snowpack's temperature and, thereby, the metamorphism of the snowpack. The model's inability to incorporate wind deposition and resulting wind slabs poses practical implications for avalanche forecasting. Nevertheless, the promising results from this validation study encourage further exploration of the model chain, both for site-specific avalanche forecasting and for including the developed model in regional forecasting.

The research suggests that numerical snowpack modeling, forced by numerical weather predictions and manually observed snow profiles, can effectively aid avalanche forecasting.

Sammendrag

Snøskred er en utbredt naturfare i bratt terreng og utgjør en alvorlig trussel for både mennesker og infrastruktur. Formålet med snøskredvarsling er å forhindre ulykker i forbindelse med snøskred, og blir i økende grad basert på detaljert numerisk modellering av snøens lagdeling.

Denne studien har undersøkt om numerisk snødekkmodellering basert på data fra numeriske værprognoser og observerte snøprofiler kan bistå i snøskredvarsling. For å besvare dette, undersøkes følgende tre forskningsspørsmål: 1) I hvilken grad gir meteorologiske data fra værmodellen AROME-Artic brukbare data for numerisk snødekkmodellering? 2) Hvor nøyaktig kan snødekkmodellen SNOWPACK med værprognoser fra AROME-Artic og manuelt observert snøprofil forutsi utviklingen av snødekke? 3) I hvilket omfang vil resultater fra SNOWPACK-modellen basert på input fra AROME-Artic og manuelt observert snøprofil være nyttig for snøskredvarsling?

De tre spørsmålene ble besvart ved først å evaluere data fra AROME-Artic i forskjellige rutenettpunkter ved Longyearbyen, Svalbard. Det rutenettpunktet med minst avvik i forhold til observerte værddata ble valgt til SNOWPACK-modellen. En modellkjede bestående av AROME-Artic og SNOWPACK ble deretter kjørt over fire modellperioder og sammenlignet mot manuelt observert snøprofiler. Kvaliteten på resultatene fra modellkjeden ble evaluert ved hjelp av en sammenligningsalgoritme. Algoritmen målte den simulerte snøprofilen mot en manuelt observert valideringsprofil.

Resultatene fra testperioden viser at AROME-Artic kan levere data av høy kvalitet for snødekkmodellering. Modellkjeden bestående av AROME-Artic og SNOWPACK kan nøyaktig forutsi utviklingen av snødekket, og gi verdifulle data for snøskredvarsling. I løpet av feltperioden på 14 dager beregnet modellkjeden de aktuelle skredproblemene, noe som igjen viser den operative nytten av modellkjeden.

Modellkjeden har svakheter som bør tas hensyn til. Konverteringen av rutenettdata fra AROME-Artic til punktdata bør utføres med stor nøyaktighet, da modellkjeden viste følsomhet overfor valg av rutenettpunktet i AROME-Artic. Videre, har kortbølgestråling signifikant innvirkning på simuleringen av snødekkets temperatur, og dermed den modellerte metamorfosen. Modellen har en manglende evne til å fange opp vinddrift og dermed flakdannelse i snøen, noe som igjen medfører praktiske implikasjoner for snøskredvarsling. Til tross for de påpekte svakhetene, er resultatene fra denne studien lovende og gir grunnlag for videre utforskning av modellkjeden til bruk i stedsspesifikk- og regional snøskredvarsling.

Den gjennomførte studien viser at numerisk snødekkmodellering basert på numeriske værprognoser og manuelt observerte snøprofiler effektivt kan bistå snøskredvarsling.

Preface

This master's thesis is conducted as a completion of the study program Civil and Environmental Engineering at the Norwegian University of Science and Technology (NTNU). The work is carried out at the Department of Hydraulic and Environmental Engineering, Faculty of Engineering.

During this master's program, the author's academic interest in snow science and avalanche dynamics inspired the author to spend a semester at the University Centre on Svalbard (UNIS) and a year at Montana State University (MSU), pursuing knowledge in this field. At NTNU, the interdisciplinary research project Risk governance of climate-related systemic risk in the Arctic (ARCT-RISK) at the Department of Industrial Economics and Technology Management made a master thesis within snow- and avalanche science possible. A collaboration with ARCT-RISK motivated the choice of snowpack modeling and avalanche forecasting as the topic for this master's thesis.

Acknowledgments

I want to thank my supervisor, Prof. Oddbjørn Bruland, for enthusiastically supporting my choice of topic and believing in my abilities and work capacity. I am also grateful to Arnt Grøver at SINTEF for helping a novice programmer with the demanding task of setting up this project's model chain.

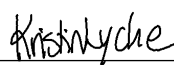
Additionally, I would like to thank The Norwegian Water Resources and Energy Directorate (NVE) and Norsk skredfaglig forening for the opportunity to complete NVE's Observatør kurs 4a as part of preparations for this research's field studies.

Furthermore, I want to express my deepest gratitude to my co-supervisor Holt Hancock, Ph.D., and Siiri Wickström, Ph.D., in the ARCT-RISK project. Thank you both for inspiring me to pursue snow science when I first came to UNIS in 2021 and for your continuous support during the work with this thesis. I especially want to thank you for the rewarding discussions and the extraordinary hospitality and guidance during my fieldwork in Longyearbyen. Without your advice, this thesis would not be possible.

I would like to thank my Hydraulic and Environmental Engineering classmates for enjoyable and formative years together. Simultaneously, I want to thank Prof. Leif Lia for providing additional support for us, the students of Hydraulic Engineering.

A final thank you goes to my family and my partner for their never-ending help and support.

Trondheim
June 28, 2023



Kristin Lyche

Contents

Abstract	i
Sammendrag	iii
Preface	v
Acknowledgments	vii
Contents	ix
List of Figures	xiii
List of Tables	xv
List of Abbreviations	xvii
1 Introduction	1
1.1 Background	1
1.2 Research scope and questions	3
1.3 Structure and outline of the thesis	4
2 Theory	5
2.1 Concepts and terminology from snow science	6
2.2 Snow avalanche characteristics	8
2.3 Avalanche forecasting	9
2.4 Snow cover modeling	11
2.5 The SNOWPACK model	12
2.5.1 Computational key features of SNOWPACK	12
2.5.2 Boundary conditions	13
2.5.3 Input parameters, initial state, and model output	14
2.6 Numerical weather predictions	15
2.7 AROME-Arctic	16
2.7.1 AROME-Arctic model performance	16
2.8 Knowledge gap	17
3 Study area	19
3.1 Physiographic setting	20
3.2 Climate and meteorology	20
3.3 Snow climate	21
3.4 Seasonal conditions winter 2023	22
3.5 Avalanche warning in Longyearbyen	24

4	Methods	25
4.1	Research design	26
4.2	AROME-Arctic	28
4.2.1	AROME-Arctic grid point	29
4.3	Manually observed snow profiles	30
4.4	SNOWPACK model setup	34
4.5	Model chain validation	34
4.5.1	Layer mapping	35
4.5.2	Stratigraphy	35
4.5.3	Temperature gradient	36
4.5.4	Grain size	37
4.5.5	Grain shape	38
4.5.6	Overall agreement score	38
4.5.7	Sensitivity analysis	38
5	Results	39
5.1	AROME-Arctic weather predictions	40
5.1.1	AROME-Arctic model performance	40
5.1.2	Best performing AROME-Arctic grid point	40
5.2	Manually observations of the snowcover	44
5.2.1	The snowpack development	44
5.3	SNOWPACK simulations	47
5.3.1	Grain shape	47
5.3.2	Temperature	48
5.3.3	Liquid water content	49
5.3.4	Snow Profile	49
5.4	SNOWPACK model validation	51
5.4.1	Layer mapping	51
5.4.2	Qualitative agreement score	53
5.4.3	Grid point sensitivity	53
6	Discussion	57
6.1	AROME-Arctic as data source for SNOWPACK	58
6.1.1	From grid to point value	59
6.2	Predicting the development of the snowpack	59
6.2.1	Performance beyond the case study	60
6.2.2	Sensitivity	61
6.3	Implications for avalanche forecasting	63
6.3.1	Implications beyond the case study	64
6.4	Limitations	65
6.5	Future research	66
7	Conclusion	67
7.1	Concluding remarks	68
	References	69

Appendices	77
A Snow Science	79
A.1 Stratigraphy	80
A.2 Metamorphism	80
A.2.1 Dry metamorphism	81
A.2.2 Wet metamorphism	81
A.3 Spatial variability	82
B SNOWPACK simulations	85
B.1 Model period 1	86
B.2 Model period 2	88
B.3 Model period 3	90
B.4 Model period 4	91
C Sensitivity analysis	93
C.1 Point B	94
C.2 Point C	96

List of Figures

2.1.1	The energy balance	7
2.3.1	The conceptual framework and data types in avalanche forecasting .	10
2.8.1	The knowledge gap	17
3.1.1	The physiographic setting of Svalbard	20
3.3.1	An idealized snow profile in a typical high-Arctic maritime snowpack	22
3.4.1	The seasonal conditions in the study area	23
3.4.2	Seasonal wind patterns in the study area	23
4.1.1	The study area	26
4.1.2	The workflow of the AROME-Arctic and SNOWPACK model chain	27
4.2.1	AROME-Arctic grid point	29
4.3.1	Density measurements and a snow profile example	33
4.5.1	Snow profile alignment and layer mapping	35
4.5.2	Comparison method of temperature gradients snow profiles	36
5.1.1	AROME-Arctic model output from the four selected grid points . .	41
5.1.2	AROME-Arctic grid point performance	42
5.1.3	AROME-Arctic model data from best-performing grid point	43
5.2.1	Initial state of the snowpack	45
5.2.2	An overview of the snowpack development over the field period. . .	46
5.2.3	Snow surface characteristics from 21. April & 24. April	46
5.3.1	Simulated grain shape development over four model periods	47
5.3.2	Simulated temperature development over four model periods	48
5.3.3	Simulated liquid water content over four model periods	49
5.3.4	Simulated snow profiles over four model periods	50
5.4.1	Layer mapping between observed and simulated snow profiles	52
5.4.2	Simulated grain shape development, AROME-Arctic grid point A .	54
5.4.3	Simulated temperature development, AROME-Arctic grid point A .	54
5.4.4	Simulated liquid water content, AROME-Arctic grid point A	55
5.4.5	Simulated snow profile development, AROME-Arctic grid point A .	55
6.2.1	Weather, snow process, and agreement score	61
A.1.1	Snow stratigraphy	80
A.2.1	Overview of the processes in snow metamorphism	82
A.3.1	Spatial variability over different scales	83
A.3.2	The scale triplet in spatial variability research	83
B.1.1	Detailed grain shape development for Model Period 1	86
B.1.2	Detailed thermal development for Model Period 1	86

B.1.3	Detailed liquid water content for Model Period 1	87
B.2.1	Detailed grain shape development for Model Period 2	88
B.2.2	Detailed thermal development for Model Period 3	88
B.2.3	Detailed liquid water for content Model Period 4	89
B.3.1	Detailed grain shape development for Model Period 3	90
B.3.2	Detailed thermal development for Model Period 3	90
B.4.1	Detailed grain shape development for Model Period 4	91
B.4.2	Detailed thermal development for Model Period 4	91
C.1.1	Simulated grain shape development, point B simulations	94
C.1.2	Simulated temperature development, point B simulations	94
C.1.3	Simulated liquid water, point B simulations	95
C.1.4	Simulated snow profile development, point B simulations	95
C.2.1	Simulated grain shape development, point C simulations	96
C.2.2	Simulated temperature development, point C simulations	96
C.2.3	Simulated liquid water, point C simulations	97
C.2.4	Simulated snow profile development, point C simulations	97

List of Tables

2.5.1	SNOWPACK input parameters	14
2.5.2	Required Snow Profile parameters to initiate a SNOWPACK simulation	15
4.2.1	AROME-Arctic model runs	28
4.2.2	AROME-Arctic variables used as SNOWPACK input parameters . .	28
4.3.1	Hand Hardness Scale	31
4.3.2	Classification of grain shape	32
4.3.3	Determining liquid water by the snowball test	32
4.3.4	Documentation of the ECT test results	33
4.4.1	SNOWPACK model setup	34
4.5.1	The matrix for comparing snow grain shape	38
5.2.1	ECT results	44
5.4.1	The Qualitative agreement score for all four model periods.	53

List of Abbreviations

Abbreviation	Explanation
ARCT-RISK	Risk governance of climate-related systemic risk in the Arctic
ECT	Extended Column Test
MEPS	MetCoOp Ensemble Prediction System
MET	The Norwegian Meteorological Institute
NVE	The Norwegian Water Resources and Energy Directorate
NWP	Numerical Weather Prediction
RMSE	Root Mean Square Error
SLF	The Swiss Federal Institute for Snow and Avalanche Research
UNIS	The University Centre in Svalbard

Chapter 1

Introduction

Snow avalanches are significant natural hazards in mountainous terrain and represent a severe problem for people and infrastructure (McClung & Schaerer, 2006; Rudolf-Miklau et al., 2015). Yearly, snow avalanches account for approximately 250 fatalities worldwide (Schweizer et al., 2015), and infrastructure damages occasionally exceeding 500 million Euros for single avalanche cycles alone (Fuchs & McAlpin, 2005).

Human injuries and damages to infrastructures from avalanches can be mitigated by either regulating the presence of people and structures or by controlling the avalanche itself (McClung & Schaerer, 2006). Due to extensive avalanche mitigation throughout the twentieth century, avalanche casualties on roads or in permanent settlements have become less frequent in areas like the European Alps and North America. Consequently, most snow avalanche fatalities in these regions today occur while people are recreating in the mountains (Techel et al., 2016). However, accidents affecting permanent settlements are still a relevant problem (Jóhannesson et al., 2019).

1.1 Background

Despite a decreasing number of accidents affecting permanent settlements (Techel et al., 2016), catastrophic events over the last decades have kept the attention of the public on snow avalanche danger and the associated risk (Jóhannesson et al., 2019). For instance, a severe winter storm resulted in the release of a dry snow avalanche in the arctic settlement of Longyearbyen, Svalbard, in 2015. The avalanche tragically killed two people, destroyed 11 houses, and led to the evacuation of 200 people (The Norwegian Directorate for Civil Protection, 2016). The destructive powers of snow avalanches were again made highly relevant, as another community experienced a fatal accident in northern Norway during this master thesis research period. In this event, unusual weather, with heavy precipitation and winds from an uncommon wind direction resulted in the release of a dry snow avalanche in Reinøya, Tromsø, in March 2023. Two people, along with their livestock, were tragically killed as the rare, or even first-time avalanche, hit and swept the farm out on the sea (Lindin, 2023).

With ongoing climate change, the regional snowfall and snow cover may change significantly (Le Roux et al., 2021), affecting the frequency, type, and scale of snow avalanches (Hao et al., 2023; Strapazzon et al., 2021). Research suggests that the

frequency of wet snow avalanches might increase due to the continued effects of global warming (Hanssen-Bauer et al., 2019; Hanssen-Bauer et al., 2017; Strapazzon et al., 2021). Simultaneously, the risk of snow avalanches at mid-high altitudes is escalating (Hao et al., 2023). However, whether climate change contributes to an overall lower or higher probability of snow avalanches is widely disputed, and all associated studies and results are associated with a very high level of uncertainty (Dyrrdal et al., 2020). Within this context, it's becoming evident that infrastructure systems are often too inflexible to swiftly adjust to a shifting climate and the unpredictable future. This lack of adaptability could jeopardize the delivery of infrastructure services and public well-being (Gilrein et al., 2019).

Simultaneously, modern societies generally require a higher safety and risk awareness than earlier (Techel et al., 2016), and the risk threshold is usually lower for settlements and transportation corridors compared to voluntary recreational activities in the mountains (Faber, 2007). In this way, an adequate level of avalanche safety is a prerequisite to maintaining and further developing mountain regions as habitable areas, destinations for tourism, and transportation options (Jóhannesson et al., 2019). As a necessary consequence, developing avalanche protection measures to meet the requirements of a changing climate has become increasingly important (e.g., Eckert & Giacona, 2023).

Avalanche forecasting can serve as such a flexible strategy to mitigate avalanche risks, as avalanche forecasting aims to predict the current and future snow instability and resulting avalanche conditions (LaChapelle, 1980; McClung & Schaerer, 2006). Currently, avalanche forecasting at a micro-scale, or site-specific avalanche forecasting, is recognized as a temporal mitigation strategy. In contrast, permanent technical solutions in the form of structures or protective forests are regarded as permanent (Building Acts and Regulations, 2017; McClung & Schaerer, 2006; Wilhelm et al., 2000). In Norway, site-specific avalanche forecasting combined with action planes and temporary evacuation is currently employed to mitigate several exposed settlements (Lindin, 2023).

To predict snow avalanche hazards, snow profiles are a key element in avalanche forecasting. Traditionally, this information has been provided through manually observed snow profiles. However, physically-based models are becoming increasingly utilized to provide information about the snowpack (Morin et al., 2020). These models rely on meteorological input data (Lehning et al., 2002b; Morin et al., 2020).

As the extent and quality of numerical weather prediction (NWP) are improving (Aguado & Burt, 2015), research has been investigating the performance and utilization of snowpack modeling forced by NWP instead of observed weather data (e.g., Bellaire et al., 2011). However, the research fields on how numerical snowpack modeling forced by NWP can aid avalanche forecasting are incomplete. The existing knowledge gaps in the convergence of the three research areas of numerical modeling in avalanche forecasting, the SNOWPACK¹ model driven by NWP, and numerical snowpack modeling in Arctic conditions, with a main focus on site-specific avalanche forecasting, motivated this master thesis.

¹SNOWPACK refers to the numerical snowpack model, while snowpack refers to the accumulated snow on the ground.

1.2 Research scope and questions

The research conducted in this master thesis explicitly builds upon existing knowledge within the field of numerical snowpack modeling forced by NWP. The scope of the research is to investigate further how numerical snowpack modeling forced by NWP, and manual snow observations can aid avalanche forecasting. A main focus will be on site-specific avalanche forecasting. To help address existing knowledge gaps within that field, a case study on the performance and usefulness of the physical snowpack model SNOWPACK forced by the AROME-Arctic NWP and a manual snow profile in an Arctic environment were conducted. The primary research questions for this work therefore included:

1. To what degree does weather prediction data from AROME-Arctic provide suitable input for numerical snowpack modeling?
2. How accurately does the SNOWPACK model forced by AROME-Arctic and a manually observed snow profile forecast the development of the snowpack?
3. To what extent is the performance of SNOWPACK forced by AROME-Arctic and a manually observed snow profile useful for avalanche forecasting?

1.3 Structure and outline of the thesis

The thesis is organized into seven Chapters to address the stated research questions, including this introductory Chapter.

Chapter 2 presents concepts and knowledge needed to discuss the research questions. The first part of the chapter presents the necessary theory before the knowledge gap that motivates and influences the rest of the report is described. A brief review of highly related studies is included.

Chapter 3 introduces the study area of Svalbard and Longyearbyen, describing the physiographic setting, typical meteorological patterns, and snow climate. A review of weather and snow conditions leading up to the conducted field period is included, alongside a description of the history and current status of avalanche forecasting in Longyearbyen.

Chapter 4 presents the project methodology for approaching the research questions stated in Section 1.2. This includes a description of the research design and an explanation of how AROME-Arctic was utilized and evaluated. Further, the method for gathering manual snow profiles is given before the operated setup of the SNOWPACK model is described. The methodology for model validation through a qualitative, objective snow profile comparison algorithm is explained. The chapter concludes with a description of the conducted sensitivity analysis.

Chapter 5 provides an overview of the most significant results, while Chapter 6 discusses the three research questions. This Chapter also includes the most pronounced limitations of the conducted study.

Chapter 7 closes the report by answering the three research questions based on the preceding discussion.

Chapter 2

Theory

This chapter provides concepts and knowledge needed in order to discuss the research questions stated in Section 1.2 through eight sections.

Section 2.1 provides an introduction to snow as a material, before a brief description of important terminology from snow science utilized in this thesis is given. Even though these concepts are assumed to be familiar to the reader, a more detailed description of each process is provided in Appendix A as they are used throughout the presented study.

Section 2.2 provides a brief description of the definition of a snow avalanche, the typical stratigraphy leading to a slab avalanche, as well as a description of avalanche terrain.

Section 2.3 further introduces the framework of avalanche forecasting, including a description of site-specific and regional forecasting, along with the associated data requirements.

The following Section 2.4 introduces snow cover modeling and focuses on the snow models most relevant for avalanche forecasting. Section 2.5 provides detailed information regarding the snow model utilized for this research. This section includes a discussion on the differences between SNOWPACK and the other most common physical modeling tool. Further, the computational key features of SNOWPACK are described, as well as the utilized boundary condition. A description of input, initial state, and output data conclude this section.

Section 2.6 offers a description of numerical weather prediction, with a focus on the numerical weather predictions in Norway. Section 2.7 provides relevant background information regarding the NWP utilized for this research, the AROME-Arctic model. The performance of the AROME-Arctic model is described.

While the first sections of this Chapter present well-known concepts and descriptions, Section 2.8 provides an overview of the knowledge gap that motivated this thesis. The rest of the study will focus on this area of research, as the three research questions all aim to contribute to further knowledge in this aspect. A review of the related research is provided in this concluding section.

2.1 Concepts and terminology from snow science

Alpine snow, from which avalanches originate, possesses unique characteristics distinguishing it from other Earth surface materials. Snow is made out of a continuous ice structure, with a typical porosity ranging from 97 to 35% (McClung & Schaerer, 2006). As the temperature of snow typically is close to its melting point, transformations within the snowpack are constantly occurring. At the melting point, liquid water may exist in the snowpack. In this way, all three phases of water can coexist in the snow cover (Fierz et al., 2009).

The following concepts within snow science are essential in this thesis. A more detailed description of stratigraphy, metamorphism, and spatial variability is provided in Appendix A.

Stratigraphy refers to the various layers within the snowpack (Dingman, 2015). Each stratigraphic layer differs in at least one respect from the layer above or below (Fierz et al., 2009). The stability of the snowpack is largely connected to the stratigraphic arrangement of the snowpack and the properties of each layer (McClung & Schaerer, 2006).

Metamorphism is the transformations the snow crystals undergo due to the thermodynamic relationships among the water phases (Jordan et al., 2008). The metamorphism process begins as soon as snow accumulates on the surface and continues until melting is completed (Dingman, 2015). Even though the initial state of a stratigraphic layer depends on the initial state of the snow crystal, the vast variability in snow microstructure is a result of snow metamorphism (Jordan et al., 2008; McClung & Schaerer, 2006). There are distinct differences between wet and dry metamorphism, depending on the presence or absence of liquid water. Depending on the temperature gradient in the snowpack, dry metamorphism is divided into equilibrium and kinetic growth form, leading to the construction and deconstruction of snow crystals (Jordan et al., 2008).

Spatial variability is a pronounced feature of the seasonal snow cover and most manifested in the heterogeneity of snow depth. The stratigraphy of the snowpack is affected, however, most studies demonstrate that critical weak layers in the stratigraphic sequence are continuous at slope scale. The phenomenon is caused by both external and internal processes, which interact with topography during and post-deposition (Schweizer et al., 2008).

The energy balance consists of the net flux of energy from the atmosphere and ground, as well as the change of internal energy. These fluxes include shortwave radiation, longwave radiation, latent heat exchange, sensible heat exchange, sensible heat from rain as well as sensible heat via conduction with the ground. In this way, it represents the rate at which energy becomes available for the snowpack (Dingman, 2015). The interaction between the energy fluxes and snow surface is displayed in Figure 2.1.1. Further, the components of the energy fluxes are described in Equation 2.2. The fluxes are considered positive when going into the snow surface and negative when radiating from the snow to the atmosphere.

$$F_E = Q_{melt} + \frac{\delta U}{\delta t} \quad (2.1)$$

where: F_E = Net flux of energy [W/s]

Q_{melt} = Rate of external energy input [$\frac{J}{m^2s}$]

δU = Change of internal energy [-]

δt = Time period [s]

$$F_E = SW + LW + \lambda E + H + R + G \quad (2.2)$$

where: F_E = Net flux of energy [W/s]

SW = Net shortwave radiation [W/s]

LW = Net longwave radiation [W/s]

λE = Net flux of latent heat [W/s]

H = Net flux of sensible heat [W/s]

R = Flux of sensible heat from rain [W/s]

G = Net flux for sensible heat via conduction with the ground [W/s]

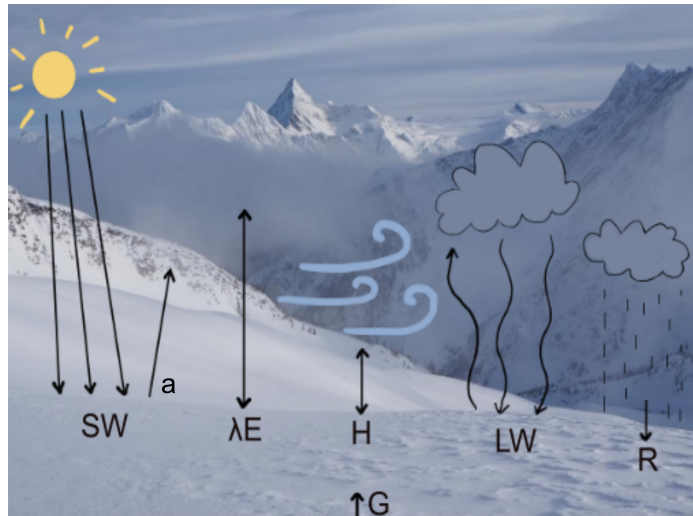


Figure 2.1.1: A simplification and visualization of the fluxes in the energy balance. The fluxes of shortwave radiation(SW), latent heat (λE), sensible heat(H), longwave radiation(LW) and sensible heat from rain(R), ground heat(G), as well as reflection caused by albedo(a) are visible in the Figure.

The magnitude of the energy fluxes varies continuously, both on hourly, daily, and monthly averages. However, Dingman (2015) points out general patterns found after reviewing studies of melt period energy balances. Whereas the net radiation and turbulent exchange are significant, the heat from rain and ground are both typically trivial parameters in the energy balance.

Looking closer at the components of net radiation, the net shortwave radiation is highly dependent on the snowpack's reflectivity, the albedo. The albedo of snow exhibits a significant range from approximately 0.2 to 0.9, signifying that between 20% and 90% of incoming shortwave radiation is reflected. Consequently, when quantifying the net shortwave radiation, albedo plays a crucial role. It is essential to note that albedo is not a static parameter but a variable characteristic, depending on numerous factors. These include the physical properties of the snow, such as grain shape and size, liquid water content, and color, among others.

The net input of longwave radiation is the difference between incoming longwave fluxes emitted by the atmosphere, clouds, and surrounding objects and the outgoing radiation from the snowpack. The outgoing radiation is governed by the snow surface temperature, which in turn is dependent on all the fluxes in the energy balance (Dingman, 2015). This adds to the complexity of the energy balance.

Due to the storage of heat and geothermal heating from the ground, the temperature is usually stable at the ground/snow interface. Further, the snow temperature usually decreases toward the surface, which is exposed to the energy fluxes from the atmosphere (Dingman, 2015; McClung & Schaerer, 2006). The general pattern of energy balance illustrates that as the snowpack accumulates, the net inputs tend to be negative. This typically results in a decrease in snow cover temperature and an increase in snow-water equivalent. The melting period commences when the seasonal snowpack's input fluxes generally become positive, eventually leading to melting and a progressing decreasing snow-water equivalent (Dingman, 2015).

2.2 Snow avalanche characteristics

A snow avalanche is a rapid downward movement of snow, typically exceeding 100 m^3 (European Avalanche Warning Service, n.d.) The two primary types of snow avalanches are loose-snow- and slab avalanches. A loose-snow avalanche initiates from a single point and expands as it progresses down the slope. In contrast, a slab avalanche involves a cohesive block of either dry or wet snow, simultaneously detaching from the snow cover (Lied & Kristensen, 2003; McClung & Schaerer, 2006). Additional forms of snow avalanches include cornice fall, ice fall, glide, and slush avalanches (Landrø et al., 2020). However, the focal point of this study lies with slab avalanches, as they are responsible for most of the damages and fatalities related to avalanches (McClung & Schaerer, 2006).

The trigger of a slab avalanche is marked by a swift fracture propagation along all boundaries of the slab. Investigations into previous avalanche events have revealed

a typical stratigraphy conducive to the formation of a slab avalanche: A relatively thick, cohesive slab lies above a weak and thinner layer of snow crystals, which in turn overlays another cohesive layer (McClung & Schaerer, 2006). This tri-layered structure: A slab, a weak layer, and a gliding plate encapsulate the structural essence leading to slab avalanches (McClung & Schaerer, 2006; Tremper, 2018).

The collapse or fracture of the weak layer is initiated when the applied load surpasses the strength of the crystalline bonds of the weak layer. A slab avalanche, thus, is a culmination of both the initiation and subsequent propagation of fractures within that same layer (Gaume et al., 2019). The snow stability is, in this way, the ratio of strength to stress in a weak layer or interface (Schweizer & Wiesinger, 2001).

If the slope gradient is sufficient, the detached slab descends rapidly down the slope. Most dry snow avalanches transpire on slopes between 35 and 40 degrees. After releasing, the avalanche progresses through an avalanche path consisting of a starting zone, an avalanche track, and ending in a deposition or run-out zone. Together they are all referred to as avalanche terrain. The starting zone is the location where the unstable snow fails and begins to move (McClung & Schaerer, 2006).

2.3 Avalanche forecasting

Avalanche forecasting is a structured approach to estimate the current and future snow instability and resulting avalanche conditions. This evaluation is based on a mixture of meteorology, snow physics, human influence, and empirical evidence across different spatial and temporal scales (LaChapelle, 1980; McClung, 2002).

By evaluating various types of information, avalanche forecasters tempt to identify instability within the snowpack. The three types of relevant information can be divided into direct snow stability observations (Class I), snowpack factors (Class II), and meteorological data (Class III) (LaChapelle, 1980; McClung, 2002). This is visualized in Figure 2.3.1. A lower class number represents stronger evidence of snow instability.

Snow profiles, which are a core part of this thesis, are Class II data. They reveal important information about the stratigraphy of the snowpack and are part of some of the best data for stability evaluations (Schweizer & Wiesinger, 2001). However, an accurate prediction of avalanche conditions requires consideration of data from all three distinct classes across various spatial scales. Avalanche forecasting is commonly divided into regional and site-specific avalanche forecasting. Regional forecasting spans over mountain ranges or a significant fraction thereof (McClung & Schaerer, 2006). The regional forecasts in Norway are largely aimed towards recreational activities and emergency responses (Varsom, 2023). Further, the regional avalanche forecasts in Norway are provided by NVE and published at [Varsom.no](https://varsom.no)¹.

¹<https://varsom.no/snoskred/varsling/>

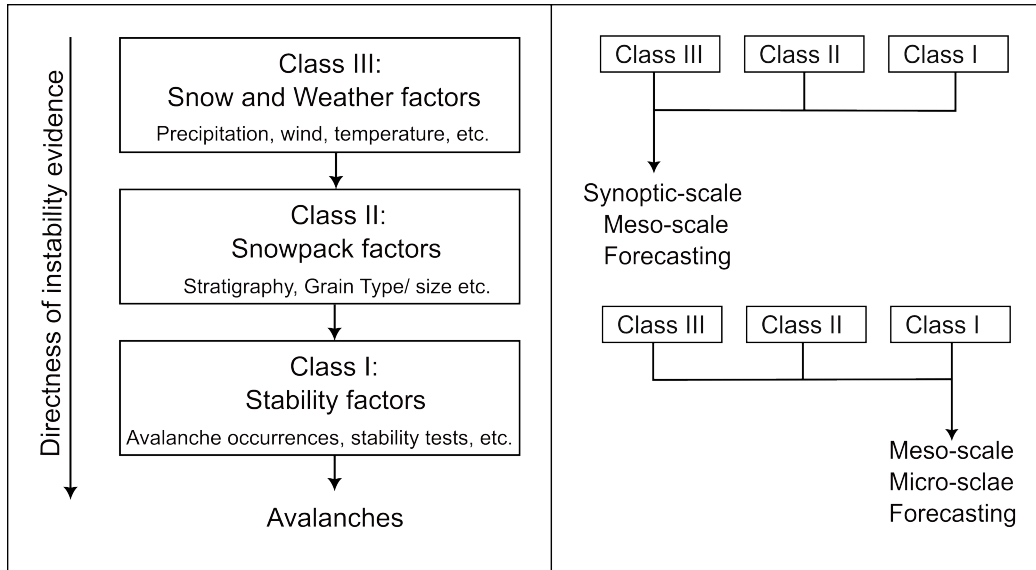


Figure 2.3.1: The conceptual framework and relative influence of the three data types at different spatial scales in avalanche forecasting. The left Figure shows the three classes into which avalanche information is commonly divided. The right Figure shows how the three classes of information are included and valued in forecasts at different spatial sales. The Figure is adapted from McClung and Schaerer (2006).

Site-specific forecasting on the other hand, is an assessment of the probability of an avalanche to release in one or several specific avalanche paths and whether its runout might endanger people or infrastructure (European Avalanche Warning Services, 2022), and is often accessible only to the directly involved partners (Jaedicke et al., 2018). Avalanche phenomena and the associated forecasting mechanisms evolve across a temporal spectrum. This ranges from the crucial moments leading up to an avalanche’s inception to periods spanning weeks or even months during which snowpack conditions conducive to snow instabilities and potential avalanche occurrences are shaped (LaChapelle, 1980; McClung & Schaerer, 2006; Statham et al., 2018).

Both the spatial as well as temporal scale significantly influences the relative contribution of the three data classes relevant to avalanche forecasting (Figure 2.3.1). In order to develop a forecast for the given spatial scale, the physical processes leading to the release of the avalanche have to be understood based on available, scale-appropriate data. Available, synoptic scale weather data are of greater relative importance for a regional avalanche forecast than to site-specific forecasts, where snowpack factors, and thereby snow profiles, and stability factors must be incorporated to achieve adequate forecasting precision (McClung, 2000).

2.4 Snow cover modeling

A large number of snow models have been designed over the past few decades (Brun et al., 2008), and there are currently a large number of physically based snow models for a range of different applications (Krinner et al., 2018). Simultaneously, there has been a growing use of numerical snowpack modeling in avalanche forecasting (Morin et al., 2020). As of 2020, SNOWPACK (Lehning & Bartelt, 2002; Lehning et al., 2002a; Lehning et al., 2002b), Crocus (Brun et al., 1992; Brun et al., 1989), seNorge (Endrizzi & Skaugen, 2009; Saloranta, 2012) and SNOWGRID (Olefs et al., 2013) are the operationally used snowpack models (Morin et al., 2020). While seNorge and SNOWGRID focus on the spatial extent and variability of the snow cover over larger areas, SNOWPACK and Crocus are one-dimensional, detailed, physically-based models, focusing on reproducing the stratigraphy of the snowpack (Morin et al., 2020).

SNOWPACK and Crocus are currently the most advanced snow cover models, and both utilize meteorological parameters as input data. Based on this information, both models calculate and visualize the results of the complex processes of handling new snow amounts, settling rates, possible surface hoar formation, temperature, density profiles, as well as the metamorphic development of the snow crystals in the individual layers (Bellaire et al., 2011; Lehning & Bartelt, 2002).

Regardless of the complexity of a one-dimensional model, these model types fail to capture some key processes shaping the mountain snow cover. This includes impacts from local topography, redistribution processes driven by wind erosion, and re-distribution and impact from surrounding vegetation. Several snow models focus on the consequence and interaction of these parameters, including The Prairie Blowing Snow Model (Pomeroy et al., 1993), SYTRON3 (Durand et al., 2005), SnowTran-3D (Liston et al., 2007) as well as models developed by Krinner et al. (2018), Lehning et al. (2008), Liston et al. (2007), and Vionnet et al. (2014). However, as of 2020, none of these were known to be utilized by operational avalanche forecasting centers. Currently, Crocus and SNOWPACK are the most utilized snow cover models for avalanche purposes (Morin et al., 2020).

Although SNOWPACK and Crocus operate on very similar underlying physical principles, they show marked differences in their application for operational tasks. This is most notable in the way process and present the results to the end user (Bellaire et al., 2011; Morin et al., 2020). The Crocus model chain is often used to simulate the snow cover for larger areas (Bellaire et al., 2011), and SNOWPACK, on the other hand, simulates the local snowpack at a specific point, similarly to a traditional snow profile (Lehning & Bartelt, 2002). This study will utilize the SNOWPACK model, and the model choice is further elaborated in Section 4.1.

2.5 The SNOWPACK model

SNOWPACK was designed at The Swiss Federal Institute for Snow and Avalanche Research (SLF) (Lehning et al., 1999). The model builds on existing knowledge from the French Crocus model, as well as previous model experience at SLF through the snow model Daisy (Lehning & Bartelt, 2002). The model was developed for, and still mainly used for avalanche forecasting, and critical avalanche forecasting problems and needs were core concerns during development. These concerns include the handling of new snowfall events, snow settling rate, the ability to produce a description of the current situation of the snowpack, and providing grain size, shape, and grain bounding, as well as the density and water content of each snow layer. Further, the model needed to handle surface melt, transportation of melt-water, refreezing of water in the snowpack, and removal of snow through wind erosion and melt as well. The following Sections summarize the computational key features with regard to its operational implementations, aiming to solve the previously mentioned needs.

2.5.1 Computational key features of SNOWPACK

SNOWPACK approaches snowpack modeling by solving the instationary heat transfer equations through the use of a Lagrangian finite element method. Lagrangian finite element method allows for the incorporation of numerous numerical layers and the historically dependent behavior of snow (Lehning et al., 2002b; Morin et al., 2020).

The snow itself is represented as a porous material consisting of three phases: ice, water, and air. In this way, SNOWPACK facilitates mass and energy-conserving phase changes between all three components. Further, the development of grain type is governed by the general laws of snow metamorphism (Lehning & Bartelt, 2002). Snow metamorphism is defined in Section 2.1 and described in Appendix A.

SNOWPACK handles new snow density as a function of air temperature, relative humidity, and wind speed, and is added to the model by introducing new finite elements to the existing mesh. The process of surface hoar formation is also represented, contributing an additional layer if certain threshold criteria are met before a snowfall. The bond radius between snow crystals is explicitly represented, influencing the thermal conductivity and viscosity of the snowpack (Lehning & Bartelt, 2002).

Shortwave radiation is handled as a volumetric heat source, with the intensity of absorbed radiation decreasing exponentially with depth. In terms of water dynamics, water percolation and refreezing within the snowpack are accounted for. The melt-water output results in the removal of mesh elements, symbolizing the loss of snow mass due to melting (Lehning et al., 2002b).

The comprehensive methodology of SNOWPACK, along with its limitations as a one-dimensional model, necessitates certain assumptions. All slope-parallel velocities, including creep and water flow, are presumed to be zero. The computations additionally assume zero lateral gradients of temperature and vapor pressure. Finally, SNOWPACK sets a uniform temperature for ice, water, and moist air within the snowpack at any given time (Lehning et al., 2002b; Morin et al., 2020).

2.5.2 Boundary conditions

The most critical boundary condition is the one that manages the energy transfer at the surface of the snowpack. Two possibilities are incorporated in SNOWPACK, and a time-dependent setting, adjusted based on meteorological measurements, is recommended. In general, the energy balance at the snow surface is solved using Dirichlet boundary conditions, presented in Equation 2.3 (Lehning & Bartelt, 2002).

$$\text{Upper boundary} \rightarrow T_s = T_{ss} \quad (2.3a)$$

$$\text{Lower boundary} \rightarrow T_s = T_G \quad (2.3b)$$

where: T_s = Snow temperature (K°)
 T_{ss} = Snow surface temperature (K°)
 T_G = Ground temperature (K°)

However, during ablation periods, the surface temperature is constantly equal to 0°C . Therefore, the Dirichlet boundary conditions cannot be used, as this would underestimate the melt. Hence, as the surface temperature draws close to the melting point, the model transitions to the Neumann boundary condition. The recommended boundary threshold is -1°C . When switching to Neumann conditions, the model will simulate the heat flux required for the phase transition from solid to liquid. However, it is possible to turn off the switch mechanism, and utilize either Dirichlet or Neumann condition for all temperature ranges (Lehning & Bartelt, 2002).

$$\text{Upper boundary} \rightarrow k_s \cdot \frac{\partial T_s}{\partial z} = q_{lw} + q_{sh} + q_{lh} + q_{rr} \quad (2.4a)$$

$$\text{Lower boundary} \rightarrow k_s \cdot \frac{\partial T_s}{\partial z} = T_G \quad (2.4b)$$

where: k_s = Thermal conductivity of snow (W/m^2)
 $\frac{\partial T_s}{\partial z}$ = Vertical temperature gradient (K°/m)
 T_G = Ground temperature (K°)
 q_{lw} = Net longwave radiation (W/m^2)
 q_{sh} = Sensible heat exchange (W/m^2)
 q_{lh} = Latent heat exchange (W/m^2)
 q_{rr} = Heat flux from rain (W/m^2)

2.5.3 Input parameters, initial state, and model output

SNOWPACK requires atmospheric input parameters. The input parameters should be provided in an ASCII format, named a .smet file. The smet file contains a header of metadata, including location expressed with latitude, longitude, and elevation, before the meteorological data is provided. However, the included input parameters can vary, and SNOWPACK can be driven on a range of input parameters (Table 2.5.1). As described in Table 2.5.1, some variables can be substituted by statistical estimations or assumptions. Other parameters are determined by the utilized boundary condition (Lehning et al., 2002a).

Table 2.5.1: SNOWPACK input parameters. Air Temperature, Relative Humidity, and Wind Speed are required, whereas the reminding parameter is determined based on the utilized boundary condition or could be substituted with either other input parameters or statistically obtained values.

Meteorological Input Parameter	Comment
Air Temperature	Required
Relative Humidity	Required
Wind Speed	Required
Shortwave Radiation	Provided as Incoming, Outgoing, or Net shortwave radiation. If Net Shortwave radiation is not provided, a statistical albedo value can be utilized
Longwave Radiation	Required for Neumann boundary condition
Surface Temperature	Required for Dirichlet boundary condition
Precipitation	Can be substituted with measured Snow Height
Ground Temperature	Optional, assumed to be 0°C if not provided

The initial state of the snowpack needs to be provided as an input file. When running SNOWPACK over an entire season, it is usually initiated on bare ground. However, in the case of a simulation initiated with snow on the ground, a CAAML² file (Gerber et al., 2013) has to provide the information regarding the state of the snowpack. The snow profile needs to provide the required parameters described in Table 2.5.2.

SNOWPACK generates two primary types of output data: time series and snow profile outputs. Time series output data provide a dynamic view of snowpack characteristics as they change over time. This data type captures fluctuations in variables such as grain shape, snow temperature, and liquid water content at consistent intervals. The snow profile output offers a cross-sectional view of the snowpack at a specific moment in time. This output delineates the vertical stratification of the snowpack, providing detailed information about each layer’s characteristics, including its thickness, density, temperature, and grain properties.

²Canadian Avalanche Association Markup Language

Table 2.5.2: Required Snow Profile parameters to initiate a SNOWPACK simulation.

Snow profile parameter	Comment
Meta data	Location Weather consideration
Snow depth	Stratigraphy not considered
Temperature profile	Stratigraphy not considered
Density profile	Stratigraphy not considered
Finger hardness	By layer
Grain size	By layer
Grain shape	By layer
Liquid water content	By layer

2.6 Numerical weather predictions

NWPs are the primary method for weather forecasting. These types of models employ computational models to simulate atmospheric behavior and calculate the evolution of various atmospheric parameters, e.g., wind, pressure, and temperature over designated timescales (Aguado & Burt, 2015). Numerical weather forecasting is further an initial value problem, where the forecast’s accuracy hinges on the model’s precision as well as the initial state’s quality. Therefore, environmental observations frequently update initial states via data assimilation (Randriamampianina et al., 2019).

Many NWP models employ grid-based representations for computational efficiency, where the atmospheric equations are solved at grid points. Grid resolution selection is a compromise between computational expense and model accuracy. Hence, NWP model capabilities correlate with computer technology advancements, allowing for higher grid resolutions and enhanced prediction accuracy as computational capacity increases (Aguado & Burt, 2015). Even though NWPs are the backbone of modern weather forecasting, they still have a relatively short history and have a potential for improvements. Cloud development, and hence also radiation, is for instance known to be difficult to accurately predict (Gregow et al., 2020).

The Norwegian Meteorological Institute (MET) operates two forecasting systems reliant on separate NWP models: MetCoOp Ensemble Prediction System (MEPS) and AROME-Arctic (Norwegian Meteorological Institute, 2019). Both models were created within the AROME model scheme (Stoll et al., 2020).

2.7 AROME-Arctic

The AROME-Arctic model is a high-resolution, regional, short-range forecast system with 2.5 km grid spacing and 65 vertical levels (M. Müller et al., 2017b). As of June 2017, the operational AROME-Arctic employs the cycle version 40h1.1, generating forecasts four times a day with a 66-hour lead time. The AROME-Arctic output is a wide array of variables, including but not limited to temperature, precipitation, wind speed and direction, cloud cover, and snow albedo, among others. This system serves as the core basis for operational weather services within Svalbard and neighboring regions, exemplified by the spot forecasts available on yr.no (Norwegian Meteorological Institute, 2019).

However, AROME-Arctic closely aligns with the MEPS setup operated in mainland Norway, with some critical distinctions. Where MEPS runs ensemble simulations, AROME-Arctic is a deterministic model, running singularly for each model period as of now. An ongoing project is working on running AROME-Arctic with ensemble simulation. This configuration is not run operationally as of today (Singleton, 2022).

Further, Arctic-specific challenges, such as snow on ice and shifting sea ice, significantly influence regional humidity and surface temperatures. Additionally, the scarcity of conventional observational data in the Arctic region amplifies the reliance on remote sensing data (Grote et al., 2022; M. Müller et al., 2017a).

2.7.1 AROME-Arctic model performance

The AROME-Arctic model has known strengths and shortcomings considering model performance (e.g., Køltzow et al., 2019; M. Müller et al., 2017a; Stoll et al., 2020). When compared with other NWP models, AROME-Arctic consistently exhibits lower biases and reduced Root Mean Square Error (RMSE) (Køltzow et al., 2019; M. Müller et al., 2017a). This could be attributed to AROME-Arctic’s effective surface and upper-air assimilation combined with its high-resolution grid (Køltzow et al., 2019).

However, AROME-Arctic has known shortcomings. The model underestimates precipitation along coasts and fjords and displays a more rapid growth of errors compared to lower-resolution models. This suggests that the enhanced performance of this refined model is dependent on the forecast lead time (Køltzow et al., 2019). Moreover, the model’s performance is inconsistent across its operational domain, with noticeably better results over mainland Norway. AROME-Arctic’s performance further displays a seasonal trend. During the winter months, a larger RMSE is usually observed. This is addressed to the high variability of temperature and winds during winter (M. Müller et al., 2017a). Even though the quality of Arctic weather predictions has been on an upward trajectory, it still falls short of forecasts in the mid-latitudes (Randriamampianina et al., 2021).

2.8 Knowledge gap

The research questions stated in Section 1.2 are motivated by the knowledge gaps existing in the convergence of three research areas: SNOWPACK forced by NWP, Snowpack modeling in avalanche forecasting and snowpack modeling in Arctic conditions (Figure 2.8.1). Before investigating this nexus, state-of-the-art research on these highly related themes is summarized.

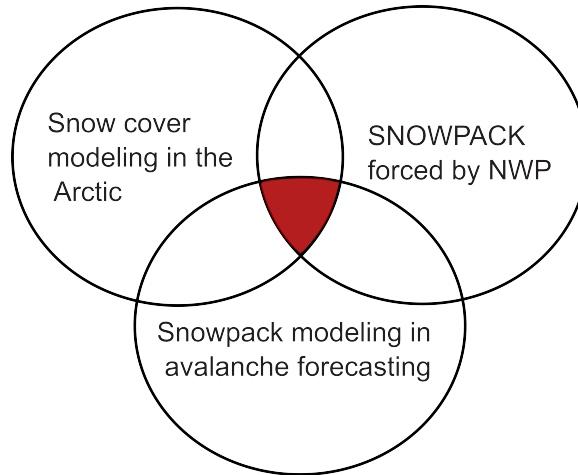


Figure 2.8.1: The knowledge gap existing in the convergence of the three research areas of numerical modeling avalanche forecasting, SNOWPACK models driven by NWP, and numerical snowpack modeling in Arctic conditions.

SNOWPACK forced by numerical weather predictions. Extensive research regarding both snow cover modeling coupled with NWP and utilization for operational avalanche forecasting has been and is currently being, conducted in the Canadian snow avalanche research community. Bellaire et al. (2011) found that the performance of SNOWPACK when powered by NWP models was promising in avalanche forecasting in western Canada, despite challenges related to forecasting precipitation. Through further studies, Bellaire and Jamieson (2013) strengthened the positive impression by highlighting the success of this model chain in simulating the formation of the critical layers of surface hoar and melt refreeze crust in the same area. Continuing the research Bellaire et al. (2017) found promising results when utilizing a similar SNOWPACK and NWP model chain for predicting wet avalanches, despite a high ratio of false alarms.

Snowpack modeling in avalanche forecasting. The review paper of Morin et al. (2020) stated that as numerical modeling has become increasingly used for avalanche forecasting, the information post-processing and visualization component in the model chain was the weakest link for operational avalanche forecasting. Horton et al. (2020) has since developed a visualization design framework aiming to improve the operational value of snowpack models, utilizing SNOWPACK forced by NWP. This has been tested for Canadian avalanche forecasters. An updated version of Lehning et al. (2001) objective algorithm for comparing modeled and observed snow profiles were developed by Herla et al. (2021a) in order to evaluate the performance of their extensive modeling efforts. Further, Herla et al. (2022) presented an averaging algorithm for snow profiles that converts numerous profiles into one representation of the current conditions. Horton

and Haegeli (2022) further investigated if the reliability of the simulated snowpack for regional-scale assessment could be linked with the ability to forecast snow depth, an easier validation parameter than stratigraphy. The study concluded that the model replicated the snow depth in a moderate or good way. Furthermore, if a strong agreement was found between observed and simulated snow depth, the simulated stratigraphy was found to be more reliable. Further validation studies, focusing on the model chain's ability to forecast avalanche hazard scenarios, performed by Herla et al. (2023) showed that the model chain consisting of the NWP and SNOWPACK were able to represent weak layers of concern in avalanche forecasting.

Simultaneously, Mayer et al. (2023) has developed an instability model that assesses the probability that a simulated SNOWPACK profile indicates instability. The research found that considering snow stratigraphy is crucial when persistent weak layers are present in the snowpack, as less new snow is needed to potentially cause a natural slab avalanche. Furthermore, the authors suggest that if applied to one-dimensional SNOWPACK simulations driven by either data from an automated weather station or a NWP, this data can benefit operational avalanche forecasting.

In mainland Norway, a snowpack model chain was also implemented in avalanche forecasting. Vikhamar-Schuler et al. (2011) implemented the Crocus model chain forced by AROME-MetCoOp³ in 2011. The author recommended further evaluations of both Crocus and SNOWPACK for possible establishments in operational avalanche forecasting. However, the Crocus model chain itself was discontinued as of the 2017/2018 season due to unreliable results and lack of model chain maintenance (Morin et al., 2020).

Snow cover modeling in the Arctic. For Arctic conditions, the most recent studies on snow cover modeling is the work of Myhre (2018), Praz (2018), and Zweigel et al. (2021). After investigating the performance of Crocus in conjunction with AROME-Arctic for reproducing the snowpack conditions leading up to the avalanche accidents in 2015 and 2017, Myhre (2018) concluded that the model chain yielded promising, however incomplete, results. The author highlighted the potential for a hybrid approach integrating modeling with manual observations. He further acknowledged AROME-Arctic as a credible provider for snow modeling input data, mostly due to the data consistency. Zweigel et al. (2021) further utilized the Crocus forced by AROME-Arctic as one module in a model chain in order to simulate ground-surface temperatures and end-of-season snow distribution. The authors found a high performance from the snowpack modeling. Regarding the usage of the SNOWPACK model, Praz (2018) validated the model performance in an arctic environment and ran on observed weather data. The author found the results to be satisfactory and encouraging. As such, further studies to explore the potential for operational usage of SNOWPACK in avalanche forecasting within an Arctic setting were recommended.

³A NWP system that was disabled in 2014, and replaced by MEPS

Chapter 3

Study area

This chapter introduces Longyearbyen and Svalbard as the study area used to investigate the three research questions stated in Section 1.2 through five Sections.

Section 3.1 provides an overview of the physiographic setting of Svalbard and the research site.

Section 3.2 describes the climatic and meteorologic patterns typical for the area, including a section describing the changing conditions.

Section 3.3 describes the typical snowpack features found in the distinct climate of Svalbard, and a description of the conceptual model for the high-Arctic maritime snow climate is included.

Section 3.4 provides a description of weather and snow conditions leading up to the conducted field period.

Lastly, Section 3.5 provides a description of the history as well as current avalanche forecasting in Longyearbyen.

3.1 Physiographic setting

The archipelago of Svalbard is situated in the Arctic Ocean, between 74° and 81° north and 10° to 35° east. The administrative center and main settlement, Longyearbyen, is located on the west coast of the largest island, Spitsbergen. Svalbard features a mountainous and glaciated landscape, with continuous permafrost (Humlum et al., 2003) and approximately 57% of the land area currently covered by glaciers (Nuth et al., 2013). Due to the harsh climate, no high vegetation or trees grow on the archipelago (Hancock, 2021).

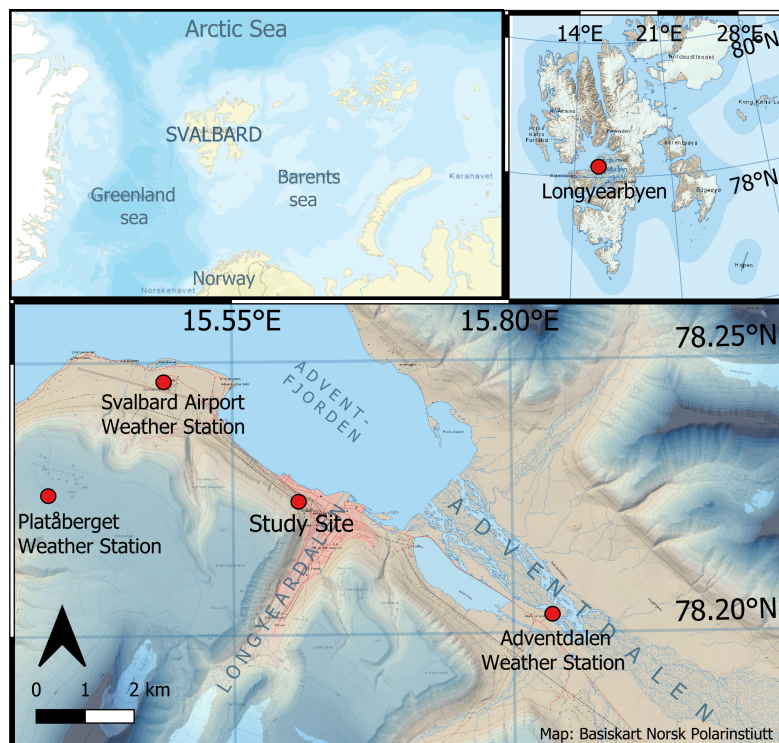


Figure 3.1.1: The upper left map shows Svalbard’s location in between the Arctic-, Greenland- and Barents Sea. The upper right map shows the location of the administrative center and main settlement, Longyearbyen, on the island of Spitsbergen. The bottom map displays the area surrounding Longyearbyen, where a light-red background marks the city of Longyearbyen. The Svalbard Airport weather station, the Adventdalen weather station, the Platåberget weather station as well as the study site are marked as red dots on the map.

3.2 Climate and meteorology

Svalbard is significantly milder, wetter, and cloudier than other locations at similar latitudes (Hanssen-Bauer et al., 2019). The typical winter weather pattern is dominated by high-pressure systems with stable, cold, clear periods punctuated by warm, wet low-pressure systems bringing heat and moisture from the south (Isaksen et al., 2016). This is mainly caused by the semi-permanent low-pressure system, the Icelandic Low, and the warm West Spitsbergen Current transporting heat and moisture to the region. The West Spitsbergen Current flows along the west coast of Spitsbergen and plays a significant role in defining the island’s climate. Particularly in winter,

as the release of heat impact the sea-ice concentration and contributes to the highly noticeable variability in winter temperatures (Hanssen-Bauer et al., 2019).

Svalbard Airport weather station, located close to Longyearbyen, can be used to represent conditions in Longyearbyen and surrounding areas. For the 1971-2000 climate normal period, annual air temperature at this point averaged 5.9°C , with an average of -9.6°C during spring months. Further, measured annual precipitation averages approximately 190 mm, with roughly half of this precipitation occurring during winter (Vikhamar-Schuler et al., 2019). This wintertime precipitation is of primary interest for the current study. However, these measurements are subject to uncertainties due to the inherent difficulties associated with accurately measuring snow precipitation (Christiansen et al., 2013).

The archipelago is encountering some of the most substantial climate changes globally. It is positioning in a warming hotspot, and the alterations are pronounced, even when viewed in the context of arctic amplification¹ (Hanssen-Bauer et al., 2019; Rantanen et al., 2022). Further, the frequency of rain-on-snow events appears to be increasing (Wickström et al., 2020) and the occurrence of extreme precipitation events is expected to increase in the future (Hanssen-Bauer et al., 2019). Simultaneously, the extent and concentration of sea ice are decreasing (Onarheim et al., 2014). These trends are expected to persist, and it is anticipated that Svalbard will become progressively warmer and wetter (Hanssen-Bauer et al., 2019).

3.3 Snow climate

The distinct climate of Svalbard gives rise to snowpack features, classified as the high-Arctic maritime snow climate (Eckerstorfer & Christiansen, 2011a). This is caused by low air temperatures and relatively dry conditions, culminating in a thin and cold snowpack. Depth hoar usually appears during the early season and represents a structural weakness throughout the season (Hancock, 2021). The continuous permafrost results in a basal snowpack temperature well below zero (Humlum et al., 2003).

Due to strong winds and limited vegetation, wind slabs are a leading stratigraphic aspect in the snowpack at Svalbard (Hancock, 2021; Jaedicke & Sandvik, 2002). Additionally, warm winter storms, often accompanied by rain, also result in widespread ice layering. This combination of distinctive characteristics sets the high-Arctic maritime conditions apart from other snow climates. As such, a typical high-Arctic maritime snowpack consists of basal depth hoar, dense wind slabs, and ice layers, separated by faceted crystals (Eckerstorfer & Christiansen, 2011a). This is visualized in Figure 3.3.1.

The definition of the high-Arctic maritime snow climate primarily draws from research conducted approximately a decade ago. However, given the ongoing climatic changes in Svalbard, it is essential to recognize that the snow climate has likely experienced considerable alterations (Hancock, 2021). A multitude of factors, such as increasing air temperatures (Hanssen-Bauer et al., 2019), more frequent rain-on-snow events, and changing winter storm characteristics (Wickström et al., 2020), are all influencing the

¹A phenomenon where Arctic regions are warming more rapidly than lower latitudes (e.g., Hanssen-Bauer et al., 2019; Isaksen et al., 2022)-

snow climate. Recent studies have further identified new changes in the physical properties of the snowpack, including the formation of thicker basal-ice layers, a shift attributed to the ongoing climatic transformation (Peeters et al., 2019)

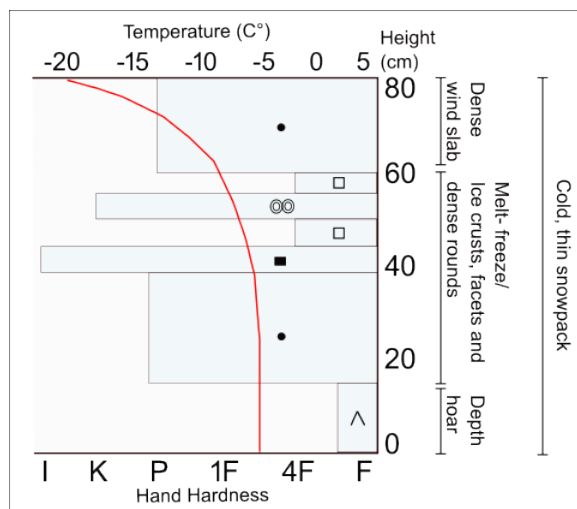


Figure 3.3.1: An idealized snow profile visualizing a typical high-Arctic maritime snowpack. The Figure is adapted from Hancock (2021) and utilizes the definition of Eckerstorfer and Christiansen (2011a) and the symbology described in Fierz et al. (2009).

3.4 Seasonal conditions winter 2023

Based on observations from the Svalbard Airport weather station and the ultrasonic snow depth sensor close to this study’s research site, a substantial seasonal snowpack began developing at the beginning of January (Figure 3.4.1). The snow depth steadily increased throughout the winter until reaching a total snow depth of 162 cm before the middle of April. Figure 3.4.1 further indicates a rapid increase in snow depth in March, which could be explained by an intense event of snow drift or a possible sensor error. April began with precipitation and a heavy increase in snow height. Additionally, an event of increasing snow depth was detected right before the beginning of the field period. There was 10 - 15 cm of measured snowfall in Longyearbyen on the 09. April, combined with strong winds from the southwest.

59 mm of precipitation were measured at the Svalbard Airport weather station between the 1. December 2022 until 12. April 2023. Throughout the winter, there have been several events with positive temperatures, making both melt and events of rain likely. The month of March where notably colder than both January, February, and April.

Due to the topographic channeling effects, wind speed and wind direction differ between the weather station of Platåberget and Svalbard Airport (Christiansen et al., 2013; Eckerstorfer & Christiansen, 2011b) (Figure 3.4.2). Due to the study’s location on a slope facing Adventfjorden, it is expected to experience some of the same channeling effects as Svalbard Airport. Therefore, the weather station at Svalbard Airport is chosen as the most representative option for this study. In this location, the season has been dominated by southeasterly winds, mostly between 5 and 10 m/s.

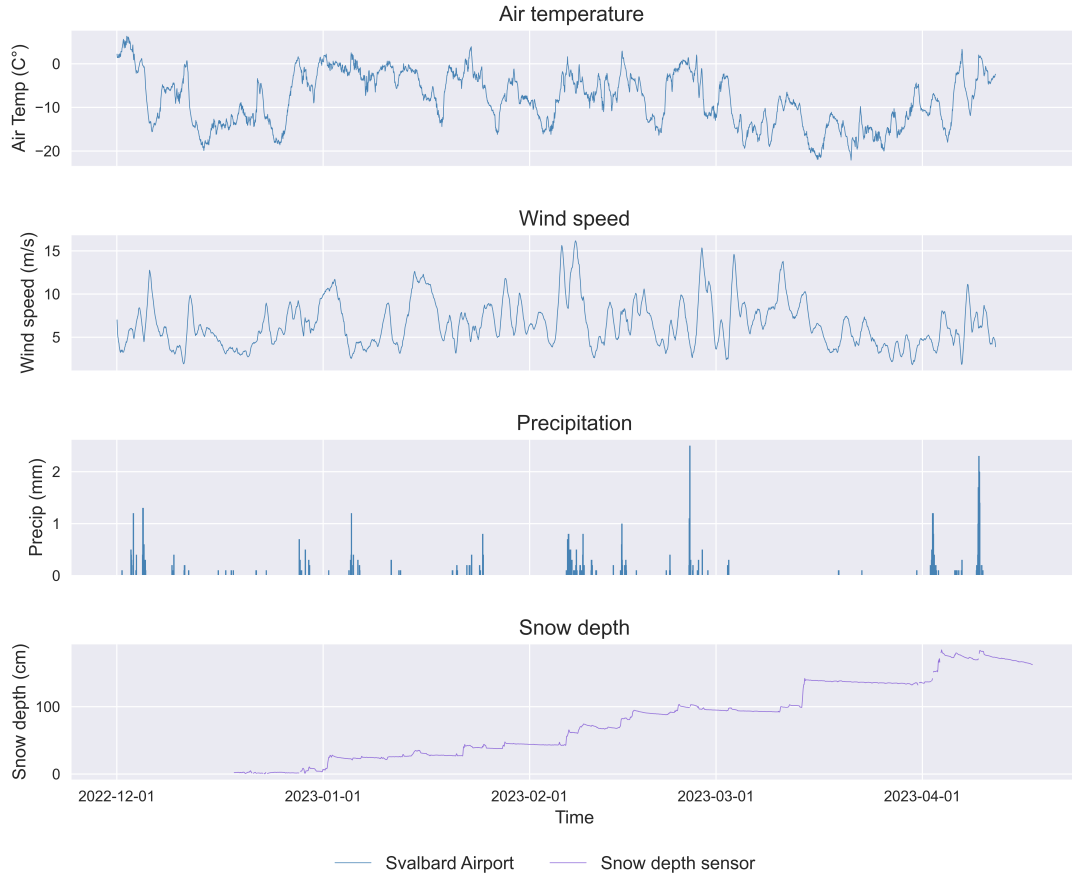


Figure 3.4.1: An overview of the seasonal conditions in the study area leading up to the conducted fieldwork. Air temperature, wind speed, and precipitation data were collected from the Svalbard Airport weather station, while the ultrasonic snow depth sensor is located approximately 50 meters from the study site. The winter consisted of positive air temperatures, as well as longer periods with air temperature around -20°C . Precipitation events, occasionally accompanied by winds, contributed to the development of a consistent snowpack from January onwards, leading to a steady increase in snow depth throughout the season.

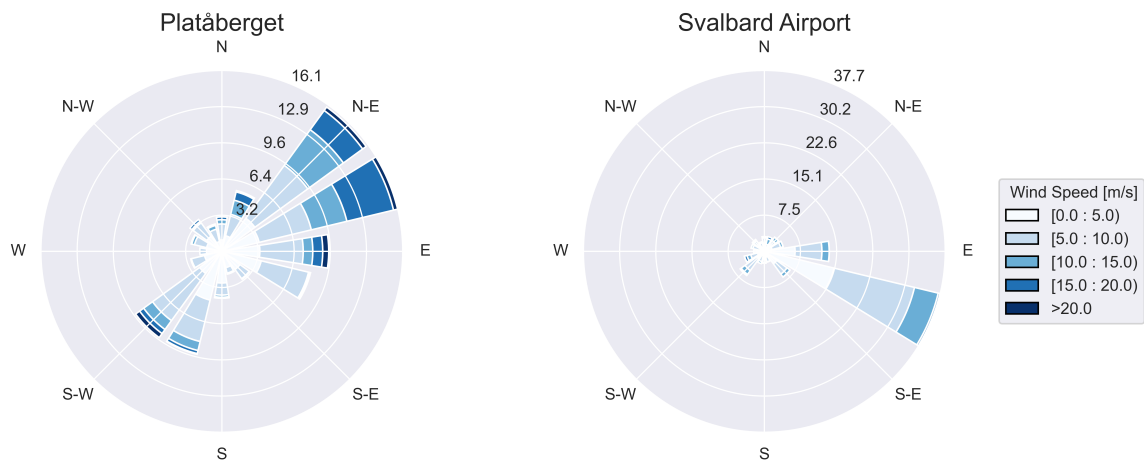


Figure 3.4.2: The wind roses from Platåberget and Svalbard Airport shows a notable difference in wind patterns caused by the channeling effects of Adventdalen. Due to the location of the study site, it is expected to experience a similar pattern as Svalbard Airport.

3.5 Avalanche warning in Longyearbyen

Svalbard has an extensive snow avalanche problem, posing a threat to infrastructure and houses in Longyearbyen (Engeset et al., 2020). In response to the severe snow avalanche accident in December 2015, claiming two lives while in their home in Longyearbyen, NVE launched a site-specific avalanche warning in Longyearbyen. The intention was to mitigate the avalanche risk in Longyearbyen until permanent solutions were implemented (Engeset et al., 2020).

Furthermore, NVE and The University Centre in Svalbard (UNIS) launched a regional public avalanche warning service for the Nordenskiöld Land region at Svalbard, incorporated in the Varsom system² (Engeset et al., 2020). Currently, NVE issues the daily regional forecasts, while the site-specific forecasts for Longyearbyen are provided by the Norwegian Geotechnical Institute (Sysselimesteren på Svalbard, 2023).

However, several factors make avalanche forecasting on Svalbard challenging. This includes the short history of observations and, thereby, a lack of historical data and recordings. Further, the Arctic polar night stretching from December to February makes visual observation difficult and increases the risk for the observers in the field (Engeset et al., 2020). On top of these facts, the ongoing climate shift and its consequences for the snow cover influence the snow avalanche regime. In the forthcoming decades, climate change is expected to influence and change the occurrence of all kinds of snow avalanches in Svalbard. This is particularly connected to the predicted rise in extreme events involving intense snowfall or heavy rain on snow, consequently leading to a possible escalation in wet snow avalanches as well as slush flows (Engeset et al., 2020; Hanssen-Bauer et al., 2019).

²Accessible at <https://varsom.no/snoskred/varsling/>

Chapter 4

Methods

This Chapter presents the project methodology for investigating the three research questions stated in Section 1.2. The Chapter is divided into five sections.

The Chapter begins with Section 4.1, which provides an overview of this study's research design. The model choices and the selection of the field site are discussed. This Section further provides an overview of the workflow of the model chain.

Section 4.2 elaborates on how AROME-Arctic was used in this study, including the retrieved parameters and the utilized model grid points. The method used to evaluate AROME-Arctic's performance is described. The results of this analysis will be utilized to answer the first research question in Section 1.2.

Section 4.3 describes the method used to collect a manual snow profile before Section 4.4 presents the setup of the SNOWPACK model, including the model period and an overview of the data input for each model period.

Section 4.5 offers an algorithm to compare a manually observed snow profile with a model simulation. This Section is significant for qualitatively evaluating the model chain's performance. The Chapter concludes with a description of the conducted sensitivity analysis.

4.1 Research design

The knowledge gap motivating this study was explored by evaluating the performance of SNOWPACK forced by AROME-Arctic weather data with a manual snow profile as the initial condition over a fourteen-day field campaign. The connection to the ARCT-RISK project made Longyearbyen, Svalbard, the field area for this study. However, the specific study site was chosen due to a range of safety precautions, including avoiding avalanche hazard exposure and considering polar bear safety. To meet these requirements, the study site was selected based on recommendations from the UNIS safety center as a spot close to the city center of Longyearbyen with limited associated risks and a snowpack thickness of approximately 100 cm.

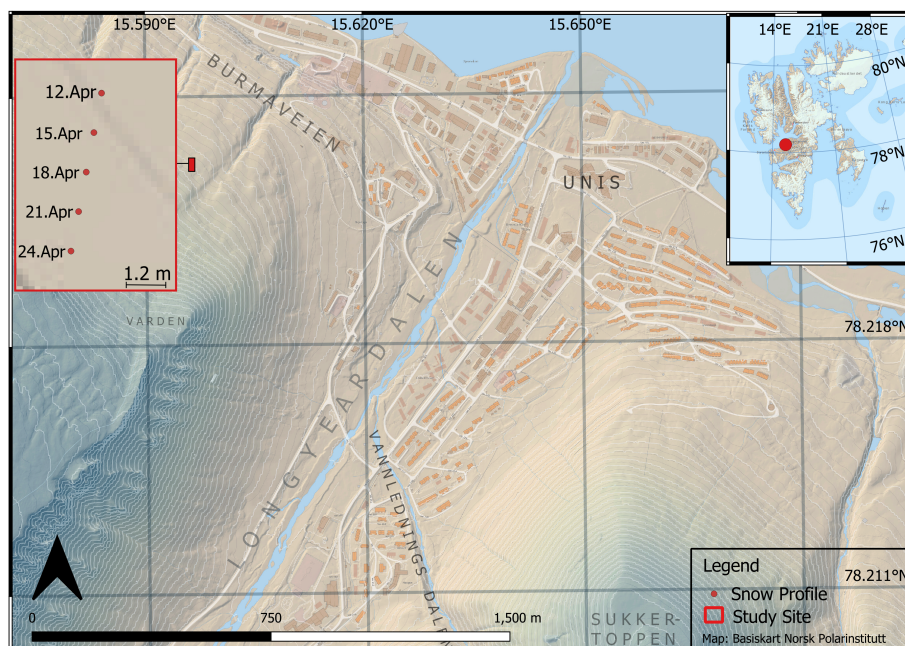


Figure 4.1.1: An overview of the study area. The study site is delineated by a red rectangle, with a magnified view of the area provided. The sites where snow profiles were taken are indicated by red dots and labeled according to their survey time.

The snow cover model, SNOWPACK, was chosen due to the explicit wishes of an ARCT-RISK collaboration partner, Skred AS, who expressed an interest in a SNOWPACK performance analysis. This choice is supported by the suitability of SNOWPACK's output for site-specific avalanche warnings, as it provides point predictions (Section 2.4). This aligns with the primary focus of site-specific avalanche forecasting in the ARCT-RISK research scope. Additionally, the relevance of the SNOWPACK model is currently high, as new adaptations and utilization methods are being developed and validated in Canada and Switzerland (Section 2.8). All these factors made the SNOWPACK model most relevant for the conducted study. The AROME-Arctic model was chosen due to its position as a recognized and most utilized NWP in the area (Section 2.7).

A workflow was established to connect two models and evaluate the performance. Firstly, data from the AROME-Arctic model and a manual initiation profile were collected (Figure 4.1.2). These were then formatted and utilized in SNOWPACK. This resulted in a forecasted snowpack, which in turn was qualitatively compared with a validation snow profile using an objective snow profile comparison method as validation criteria. This resulted in an objective agreement score. Lastly, sensitivity analyses were conducted.

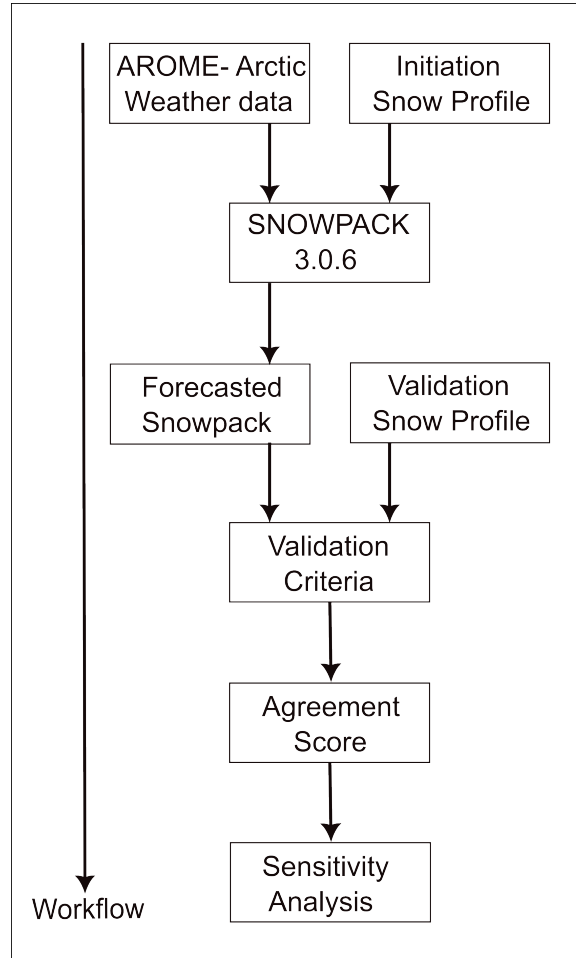


Figure 4.1.2: The workflow of the AROME-Arctic and SNOWPACK model chain. AROME-Arctic weather data and an initial snow profile were used to force the SNOWPACK (3.0.6) model. Further, the model output and a validation profile were utilized to perform a validation of the model results. This algorithm resulted in an agreement score. Lastly, a sensitivity analysis was conducted.

4.2 AROME-Arctic

Forecasted weather data from the AROME-Arctic model were accessed from the MET THREDDS server, a service for shared model and research data. For this research, the MET AROME-Arctic archive data¹ were downloaded in a NetCDF format. The extraction of data was done by modifying the AROME-Arctic extraction program developed by Frank (2023). The script was modified to download and format the specific weather parameters necessary for the project, as well as extract the relevant AROME-Arctic grid points. Bugs regarding AROME-Arctic grid point selection were fixed. Furthermore, the formatting of precipitation data into hourly values was included, and the required data formatting to automatically produce a SMET file was implemented

Four model runs were downloaded. Which model runs that were used were based on the time of the observed initiation snow profile, with the goal of as similar starting time as possible. The data from each model run were separately stored as SMET files. The downloaded AROME-Arctic model runs, as well as the corresponding time of the initiation snow profile, are shown in table 4.2.1. All 66 hr of model data were included, despite the risk of spin-up errors in the early hours of the data set.

Table 4.2.1: This overview details the employed AROME-Arctic model runs, the resulting SMET file, and the used lead time. The initiation time for the snow profile is included as downloaded model runs were anchored to the time of the manual observation

SMET file	Time of Initiation Snow Profile	AROME-Arctic Model run	Lead time Downloaded
1	2023-04-12 16:00	arome_arctic_det_2_5km_20230412T15Z.nc	66 hr
2	2023-04-15 12:00	arome_arctic_det_2_5km_20230415T12Z.nc	66 hr
3	2023-04-18 12:00	arome_arctic_det_2_5km_20230418T12Z.nc	66 hr
4	2023-04-21 10:00	arome_arctic_det_2_5km_20230421T09Z.nc	66 hr

For this study, only the AROME-Arctic output variables corresponding to SNOWPACK's required input parameters were downloaded. The relationship between AROME-Arctic variables and SNOWPACK input data is shown in 4.2.2.

Table 4.2.2: The AROME-Arctic variables used as SNOWPACK input parameters. The unit for each parameter is included.

SNOWPACK parameter	Corresponding AROME-Arctic variable	Unit
Air temperature	air_temperature_2m	K°
Relative humidity	relative_humidity_2m	-
Wind speed	wind_speed	m/s
Net shortwave radiation	surface_downwelling_shortwave_flux_in_air	W/m^2
Incoming longwave radiation	surface_downwelling_longwave_flux_in_air	W/m^2
Surface temperature	air_temperature_0m	K°
Precipitation	precipitation_amount_acc	mm

¹<https://thredds.met.no/thredds/catalog/aromearcticarchive/catalog.html>

4.2.1 AROME-Arctic grid point

As described in Section 2.7, AROME-Arctic has a 2.5 grid resolution. As the closest point is not necessarily the most representative point (Zweigel et al., 2021), four AROME-Arctic grid points were selected for performance evaluation.

The data from point A², point B³, point C⁴, and point D⁵ were downloaded and evaluated. Points B and A were chosen as they were the closest points at representative heights above sea level. Additionally, Points C and D were examined as they were both land-based, had a matching aspect and had a comparable topographic characteristic to the study site. Points E⁶, F⁷, and G⁸ were excluded due to being in water or at a substantially higher elevation. The AROME-Arctic grid point distributed around the research site is displayed in Figure 4.2.1.

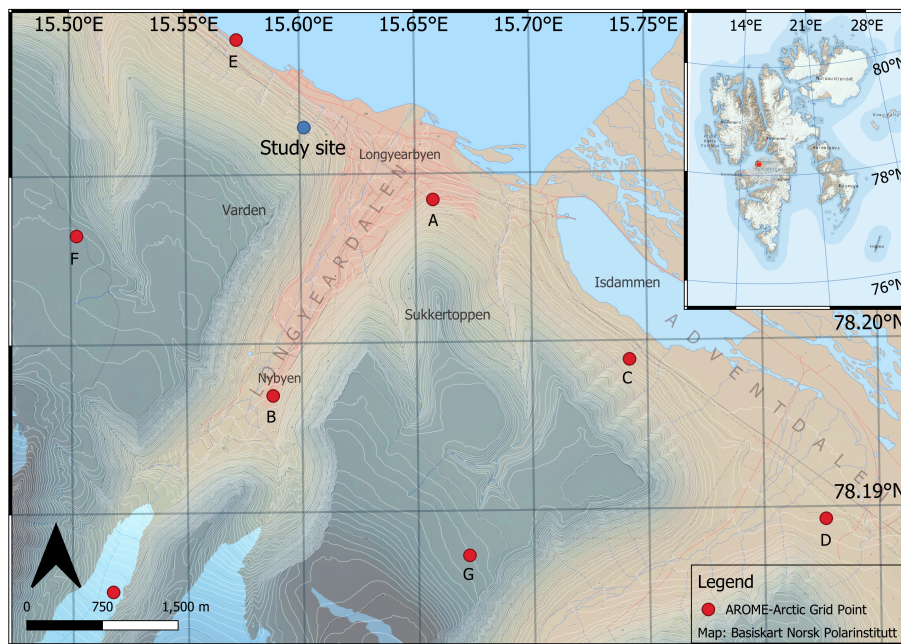


Figure 4.2.1: AROME-Arctic grid point relevant to the study site.

To assess the quality of the AROME-Arctic performance, observed weather parameters were collected from Svalbard Airport. This station was chosen due to its proximity to the research site and its known representativeness of the area (Section 3.2). Parameters that were not available from this weather station were supplemented with values from the Adventdalen weather station (Figure 3.1.1). Snow surface temperature was not observed at either of these weather stations or at any other weather stations in the area. Therefore, the modeled data for this parameter are not included in the quality evaluation.

²AROME-Arctic point [515, 230]

³AROME-Arctic point [514, 230]

⁴AROME-Arctic point [515, 231]

⁵AROME-Arctic point [515, 232]

⁶AROME-Arctic point [515, 229]

⁷AROME-Arctic point [514, 229]

⁸AROME-Arctic point [515, 229]

Weather parameters from all four model grid points were compared with observed weather measurements for the model run periods. This comparison was conducted by first calculating a RMSE value between modeled and observed variables, as described in Equation 4.1a. Subsequently, a scaled RMSE for each variable was calculated in accordance with Equation 4.1b. The scaled RMSE for each parameter was then summarized within each grid point to assess overall performance. RMSE was chosen as the performance criterion, as it is recognized as a widely used initial candidate for model performance (Bennett et al., 2013). Moreover, it aligns with model performance evaluations conducted in M. Müller et al. (2017a). The grid point that yielded the overall lowest RMSE value was chosen as the data provider for the model chain employed and evaluated in this study.

$$RMSE = \sqrt{\frac{1}{n} \sum_{i=1}^n (y_i - \hat{y})^2} \quad (4.1a)$$

$$RMSE_{scaled} = \frac{RMSE - RMSE_{min}}{RMSE_{max} - RMSE_{min}} \quad (4.1b)$$

where: $RMSE$ = Root Mean Squared Error
 y_i = Observed value
 \hat{y} = AROME-Arctic model prediction of y_i
 n = number of samples
 $RMSE_{scaled}$ = Scaled Root Mean Squared Error
 $RMSE_{max}$ = Maximum RMSE for the specific parameter
 $RMSE_{min}$ = Minimum RMSE for the specific parameter

4.3 Manually observed snow profiles

Manually observed snow profiles were used for both model initiation as well as validation of the results. The procedures for collecting the data were largely based on the recommendations by the NVE for snow profiles related to avalanche forecasting presented in Haslestad and Larsen (2022), the work of K. Müller et al. (2015) as well as Greene et al. (2010). Additionally, for a stability assessment, the Extended Column Test (ECT) was performed following the methodology described by Simenhois and Birkeland (2006).

Firstly, metadata were recorded, which included the coordinates of the snow pit, along with the date, time, and information about the slope incline, aspect, height above sea level, total snow depth, cloudiness, precipitation, wind speed, wind direction, and snow surface conditions.

Next, the snow pit was excavated with sidewalls parallel to the slope's fall line. The face of the snow pit had approximate dimensions of 1.5m x 1.0m to accommodate necessary tests. The sidewall shaded from sunlight was used for snow observations, while the stability tests were conducted on the main face of the profile. The faces

of the snow pit were cut smooth and vertically using a snow saw. All five snow profiles were dug as close to each other as possible, however, at least 1.2 meters were left between the profiles to ensure the snow had not been affected by previous snow profiles and disturbances.

A ruler was positioned in one corner of the snow profile and served as a reference depth, facilitating the identification of stratigraphic layers and snow properties. Subsequently, the temperature profile was measured first to prevent the snow temperature from being affected by the atmosphere. The surface temperature was recorded by placing the thermometer just at the snow cover surface, shaded from sunlight.

Further temperature measurements were taken at every full 10 cm interval, with additional measurements every 10 cm until reaching the ground. The air temperature was also recorded at a height of 1.5 m above the snow surface, shaded from direct sun exposure.

To analyze the snow stratigraphy, layer boundaries within the snow cover were identified by both visual inspection and searching for hardness differences with a finger and the crystal card. The different layers were marked and mapped to the reference depth.

Each layer was systematically examined for hardness, grain shape, grain size, moisture, and density. Hardness was expressed according to the hand hardness scale presented in Fierz et al. (2009) and given in Table 4.3.1. It is determined by gently pushing a standardized set of objects into the snow layers with a force of approximately 10-15 Newton. The largest of the items that can penetrate the snow layer sets the hand hardness value.

Table 4.3.1: The Table provides the objectives as well as code for the hand hardness investigations of a snow profile. The hand hardness scale is adapted from Fierz et al. (2009).

Object	Code
Fist	F
Four Fingers	4F
One Finger	1F
Pencil	P
Knife Blade	K
Ice	I

Grain shape and size were identified by examining the snow in each layer using a crystal screen and magnifying glass. Further, it was categorized according to the classification system described in Fierz et al. (2009) and given in Table 4.3.2. The study was limited to the main classes, as well as the subclass of melt refreeze crust. The grain size was considered to be the average length along the longest axis.

Liquid water content was determined through the snowball test, where the liquid water content of the snow is linked to the snow's ability to bind. The liquid water content was classified as described in Table 4.3.3.

Table 4.3.2: Conventions, including class, code, symbol, and color for main morphological grain shape classes, as well as the subclass of melt refreeze crusts. Table is adapted from Fierz et al. (2009)











Class	Code	Symbol	Color
Precipitation Particle	PP	+	
Decomposing and Fragmented precipitation particles	DF	/	
Rounded Grains	RG	•	
Faceted Crystals	FC	□	
Depth Hoar	DH	∧	
Surface Hoar	SH	∨	
Melt Forms	MF	○	
Melt Fefreeze crust	MFcr	∞	
Ice Formations	IF	■	
Machine Made snow	MM	⊙	

Table 4.3.3: Describes the snowball method, the standardized way of determining the liquid water content of snow based. The Table is adapted from Norwegian Water Resources and Energy Directorate (2022).

Liquid Water Content	Code	Description
Dry	0	Individual snow grains that do not adhere when an attempt is made to form a snowball.
Moist	1	Snow that binds together well when an attempt is made to form a snowball.
Wet	2	Snow that not only binds together well but also feels damp, though water cannot be squeezed out from the formed snowball.
Very Wet	3	Snow from which water can be squeezed out upon the formation of a snowball.
Soaked	4	Water runs out from the snow, and the snow no longer maintains its structure.

A bulk snow density was measured using the Wasatch density cutter (Figure 4.3.1). The sampling cylinder was inserted vertically, and great care was given to ensure a full, but not compacted content of the cylinder before weighing. Three density samples were taken for each measurement, where the average value is presented. If the difference between the measurements were more than 10%, a fourth sample was collected, and the outlier data point was discarded. This is done to avoid measuring errors.

For stability testing, the ECT was used. This involved isolating a 90 cm wide by 30 cm high column along the slope. Dynamic force was applied through a series of 30 steps, including 10 taps using the weight of the hand, 10 taps using the weight of the underarm, and 10 taps using the weight of the hole arm. The number of taps required to initiate a fracture and the behavior of fracture propagation was observed and documented according to the standard procedure, described in Table 4.3.4

Table 4.3.4: The code alongside the description of the documentation of the ECT test results. The Table is adapted from Norwegian Water Resources and Energy Directorate (2022)

Code	Description
ECTPV	Fracture propagates during isolation.
ECTP#	Fracture with propagation along the entire column after # dynamic loads
ECTN#	Fracture without propagation after # dynamic loads
ECTX	No fracture during test

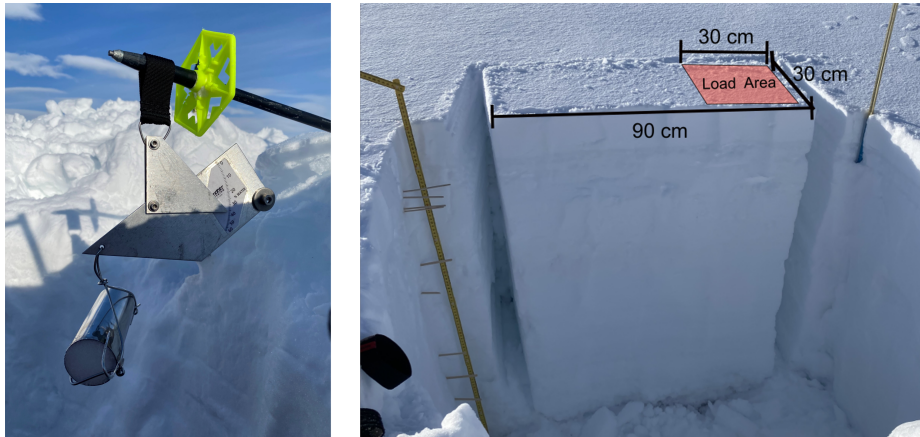


Figure 4.3.1: The Wasatch density cutter is visualized in the Figure to the left, and a snow profile is pictured to the right. The snow profile displays the setting for the ECT procedure, as well as how the snow inspections are conducted at the sidewall of the snow profile. The procedure with reference height as well as layer markers is seen left in the snow profile

All manual observed snow profiles were converted to a CAAML files by registering the observed results in the open source NiViz software ⁹, developed by the SLF.

⁹<https://niviz.org/>

4.4 SNOWPACK model setup

SNOWPACK version 3.6.0 was used to simulate the snowpack. The initial state was given as a manually observed snow profile in a CAAML format. Input data were provided as the AROME-Arctic output formatted as a SMET file. Four 66 hr model runs were conducted between 12.04.2023 and 24.04.2023. The model periods, input snow profile and utilized AROME-Arctic model run are described in Table 4.4.1. The SMET files are numbered as described in Table 4.2.1.

Table 4.4.1: The SNOWPACK model periods, with the utilized start time, end time, initiation snow profile, and utilized SMET file

Model Period	Start Time	End Time	Initiation Snow Profile	SMET file
1	2023.04.12 - 16:00	2023.04.15 - 08:00	Profile nr.1	1
2	2023.04.15 - 12:00	2023.04.18 - 05:00	Profile nr.2	2
3	2023.04.18 - 12:00	2023.04.21 - 05:00	Profile nr.3	3
4	2023.04.21 - 10:00	2023.04.24 - 02:00	Profile nr.4	4

The SNOWPACK output time step was set to 60 min to match the hourly resolution of the AROME-Arctic input data. The atmospheric conditions were assumed to be neutral for all four model periods, similarly to e.g., Bellaire et al. (2011). The energy exchange at the surface was governed by a shifting boundary condition, as explained in Section 2.5.2. The water transport model was set to Bucket, and the SNOWPACK stability evaluation was not utilized. Other parameters were assigned to the program’s default parameters.

4.5 Model chain validation

The performance of the model output was qualitatively assessed with an objective snow profile comparison algorithm. Several elements in the presented algorithm are based on the method proposed in Herla et al. (2021a), an advancement of the objective compartment scheme presented in Lehning et al. (2001). The original algorithm was developed as a tool to improve the SNOWPACK model, whereas Herla et al. (2021a) modified the algorithm to be more oriented towards validation model outputs in light of avalanche hazard evaluations (Herla et al., 2021a). Due to the research scope of this study, including both model validation as well as the usefulness for avalanche forecasting, the suggesting of Herla et al. (2021a) has been followed, and additional elements of the Lehning et al. (2001) have been included.

The presented algorithm consists of a layer mapping before the agreement of several snow material parameters is calculated based on suitable goodness of fit criteria for each parameter. This is expressed as an agreement score ranging from zero to one. One represents a perfect replication, whereas zero indicates no resemblance.

4.5.1 Layer mapping

Due to the spatially variable nature of snow, it is necessary to perform a mapping between the layers of the two snow profiles when making a quantitative comparison (Hagenmuller et al., 2018; Herla et al., 2021a; Lehning et al., 2001). This involves explicitly identifying and correlating layers with similar properties that occur at the same position within the stratigraphic sequence (Hagenmuller et al., 2018). In their work, Hagenmuller et al. (2018) uses Dynamic Time Warping¹⁰ in order to perform a mapping between the layers. This method has become state-of-the-art and is also conducted in the studies of Herla et al. (2021a). However, numerical solutions for automatic layer mapping are beyond the scope of this study. Therefore, the mapping of layers between the observed and modeled snow profiles was performed manually by visually optimizing the pairing of layers with similar properties. This has been conducted according to the recommended process presented by Hagenmuller et al. (2018) and Herla et al. (2021b) (Figure 4.5.1).

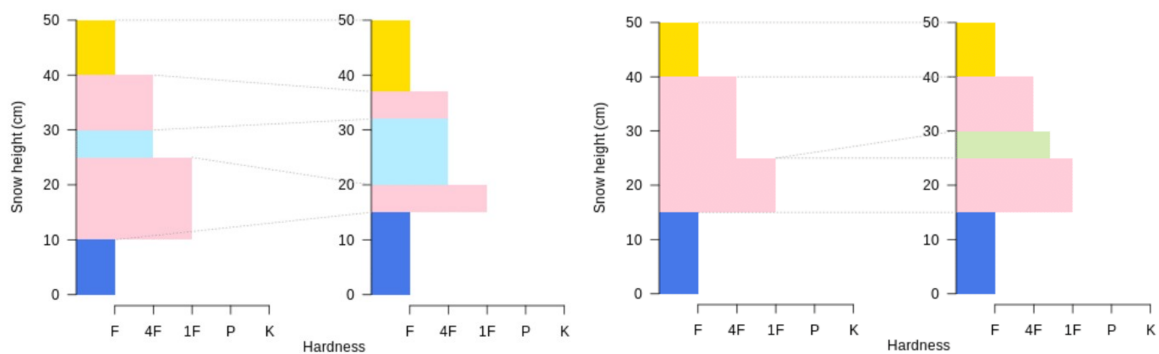


Figure 4.5.1: The Figure illustrates two examples of snow profile alignment and layer mapping presented by Herla et al. (2021b). Layers possessing similar features are superimposed on each other, denoted by dotted lines. Layers that do not align are left unmapped. For additional examples, see Herla et al. (2021b).

4.5.2 Stratigraphy

To evaluate the model’s ability to replicate the stratigraphy of the observed snow profile, the concept of the F-criterion from Casas-Mulet et al. (2015) was employed. The F-criterion is a comprehensive measure of the model’s ability to replicate observed events. It factors in the matching area as well as the extent of overestimation and underestimation. As this evaluation is conceptually equal to what is desired in comparing the stratigraphy between observed and modeled snow profiles, a slight adaptation of the F criterion is employed to establish an agreement score for the snow stratigraphy, as shown in Equation 4.2.

¹⁰An established method to match sequences in data science (Herla et al., 2021a).

$$\kappa_s = \frac{L_{Matching}}{L_{Obs} + L_{Sim} - L_{Matching}} \quad (4.2)$$

where: κ_s = Stratigraphy agreement score
 $L_{Matching}$ = Nr. of matching layers
 L_{Obs} = Nr. of observed layers
 L_{Sim} = Nr. of simulated layers

4.5.3 Temperature gradient

The temperature measurements of the observed and modeled snow profiles might contain different amounts of data points and should not be directly compared (Lehning et al., 2001). Further, the snow temperatures mainly fluctuate close to the surface and are more stable near the ground interface (Section 2.1). Therefore, the snow surface was used as a datum, and the observed and modeled temperatures at equal distances from the surface were compared. When differences in snow depth resulted in an unequal amount of temperature measurements, the arrays were forced to be equal by not considering the last measurements of the longest data series. The comparison method is visualized in Figure 4.5.2

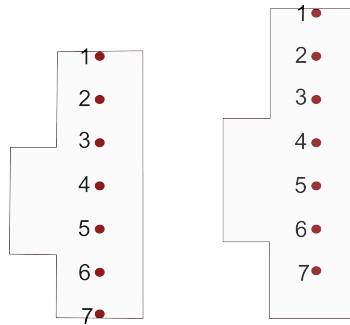


Figure 4.5.2: The two idealized snow profiles features identical stratigraphic patterns, but varying snow depth. The comparison method is visualized through evenly spaced temperature measurements in both profiles, where measurements with equal numbers are compared. The distance to the snow surface is used as the reference point. Due to different amounts of measurements, the deepest portion of the larger profile has been excluded from this comparison.

As the correlation between the two temperature gradients and the possible offset are of interest, the Kling-Gaupa criteria (Equation 4.3a) has been utilized. The Kling-Gaupa criteria balance three components: Correlation, bias ratio, and variability ratio to measure model performance, making it an elegant approach (Bennett et al., 2013).

$$\kappa_{temp} = \sqrt{(r - a)^2 + (\beta - 1)^2 + (\gamma - 1)^2} \quad (4.3a)$$

$$\beta = \frac{\mu_{sim}}{\mu_{obs}} \quad (4.3b)$$

$$\gamma = \frac{\sigma_{sim}/\mu_{sim}}{\sigma_{obs}/\mu_{obs}} \quad (4.3c)$$

where: κ_{temp} = Agreement score of temperature gradient
 r = Correlation between simulated and observed temperature
 β = bias
 μ = Mean
 σ = Standard deviation

4.5.4 Grain size

To compare grain size, the method presented in Lehning et al. (2001) is utilized. It is done by first normalizing grain size for each layer in both the observed and simulated profile by dividing them by the size of the largest grains in their respective profiles (Equation 4.4a). After that, the agreement score of each mapped layer is calculated (Equation 4.4b). Finally, the whole profile agreement score is obtained by an average over the number of mapped layers (Equation 4.4c). A layer thickness weighting is not performed, as thin layers are important to judge the stability of a snowpack (Lehning et al., 2001).

$$rg_n = \frac{rg}{rg_{Max}} \quad (4.4a)$$

$$\kappa_{i,size} = 1 - |rg_{n,Obs} - rg_{n,Sim}| \quad (4.4b)$$

$$\kappa_{size} = \frac{1}{L} \sum_{i=1}^L \kappa_{i,size} \quad (4.4c)$$

where: rg_n = Normalized grain size (-)
 rg = Grain size (mm)
 $\kappa_{i,size}$ = Layerwise agreement score of grain size
 κ_{size} = Profile agreement score of grain size
 L = Number of layers in mapped snow profile

4.5.5 Grain shape

The comparison of grain type is done accordingly to the normalized similarity of all combinations of main grain types published in Herla et al. (2021a), presented in Table 4.5.1. The matrix is based on the international morphological classification in Fierz et al. (2009). For this study, only the main forms were utilized. Based on the agreement score of each layer, a total profile agreement score for grain shape was determined using the same principle as Equation 4.4c

Table 4.5.1: The matrix of normalized distances for all combinations of main classes of grain shape. Table adapted from Herla et al. (2021a), which is a modification of the original matrix presented in Lehning et al. (2001).

Symbol	+	/	•	□	∧	○	∨
+	1	0.8	0.5	0.2	0	0	0
/	0.8	1	0.8	0.4	0	0	0
•	0.5	0.8	1	0.4	0.1	0	0
□	0.2	0.4	0.4	1	0.5	0	0.3
∧	0	0	0.1	0.5	1	0	0
○	0	0	0	0	0	1	0
∨	0	0	0	0.3	0	0	1

4.5.6 Overall agreement score

The individual scores were combined in a weighted sum to provide a single overall score between the two profiles (Herla et al., 2021a). For this study, all parameters were weighted equally, turning the weighted sum into an average, calculated as shown in Equation 4.5

$$\kappa_{profile} = \sum_{i=parameter} \kappa_i \quad (4.5)$$

where: $\kappa_{profile}$ = Total agreement score
 κ_i = Agreement score of parameter i
 i = temperature, grain size, grain type

4.5.7 Sensitivity analysis

In order to check the model sensitivity regarding the chosen AROME-Arctic grid point, SNOWPACK was forced with the output of all the four selected AROME-Arctic grid points described in Section 4.2.1. All other parameters, such as model period, input snow profiles, and settings in SNOWPACK were kept constant. The results of the sensitivity analyses were qualitatively evaluated.

Chapter 5

Results

This Chapter presents the research findings following the methodology given in Chapter 4. These results consist of four Sections and will form the fundamental when discussing the research questions stated in Section 1.2 in Chapter 6.

Section 5.1 shows the AROME-Arctic weather predictions for all selected grid points before the assessment of the performance is given. Lastly, the Section presents the data from the optimal AROME-Arctic grid point.

Subsequently, Section 5.2 presents the results of the manual observations of the snowpack, including a description of the initial state. This is followed by an overview of the observed snowpack development through snow profiles, accompanied by the results from the conducted stability tests.

Section 5.3 presents the simulations run by the AROME-Arctic and SNOWPACK model chain. An overview of the simulated development of grain shape, temperature, and liquid water content is visualized. The simulation of the snow profile from the last time step in the model run is further presented. The detailed time series of the model chain output can be found in Appendix B.

Finally, Section 5.4 provides the results of the validation of the simulations. This section begins with the results of the conducted layer mapping, followed by a presentation of agreement scores for layer and total characteristics. The Section ends with an overview of the most pronounced results of the investigation on the model chain's sensitivity towards AROME-Arctic grid point selection.

5.1 AROME-Arctic weather predictions

Divergent data outputs were yielded from the four grid points selected from the AROME-Arctic atmospheric model (Figure 5.1.1). The data gathered from all four model periods are presented in conjunction with the observed data from Svalbard Airport weather station and the Adventdalen weather station. Upon visual examination, the air temperature and longwave radiation parameters consistently align across the grid points throughout all model periods. The surface temperature remains consistent over the first two model periods before diverging in the last two periods. A broader discrepancy is noted in the predictive outcomes for precipitation, net shortwave radiation, and relative humidity. Notably, the net shortwave radiation parameter displays the most substantial variance, where differences among each grid point are significantly pronounced. Overall, no signs of model spin-up errors are detected. It should be noted that all AROME-Arctic data sets predict surface temperatures above 0°C . This is not physical, as snow temperatures do not exceed 0°C (Dingman, 2015).

5.1.1 AROME-Arctic model performance

The numerical assessment of the model's goodness of fit (Figure 5.1.2) revealed a similar performance across all four grid points for the parameters of air temperature and longwave radiation. Greater discrepancies were observed for wind speed, relative humidity, and precipitation. The greatest divergence was evident in the net shortwave radiation parameter. Point D displayed the lowest RMSE value for six out of five parameters, with relative humidity being the exception.

Upon evaluating the overall performance of each grid point, point D, which is the farthest from the study site, exhibited the lowest RMSE value. This suggests that it best replicated the observed weather conditions based on the selected goodness-of-fit criteria. In contrast, point A, which is nearest to the study site, demonstrated the highest normalized RMSE value. Considering the selection criteria delineated in Section 4.2.1, point D emerges as the preferred choice for input parameters to the SNOWPACK model. Point D is therefore utilized when model performance is evaluated, whereas the other three grid point is only included in the sensitivity analysis.

5.1.2 Best performing AROME-Arctic grid point

A visual review of the weather forecast from selected point D (Figure 5.1.3), illustrates the model's alignment with observed weather patterns. No significant bias is observed for air temperature or wind speed. However, the AROME-Arctic output for relative humidity has a negative bias. The longwave radiation is also slightly underestimated, with larger discrepancies occurring during the first model period. Net shortwave radiation is consistently overestimated throughout the entire field period, with this overestimation being most pronounced during the first model period. The main patterns in the precipitation are captured during the model period, however, both the timing as well as the amount is not precise.

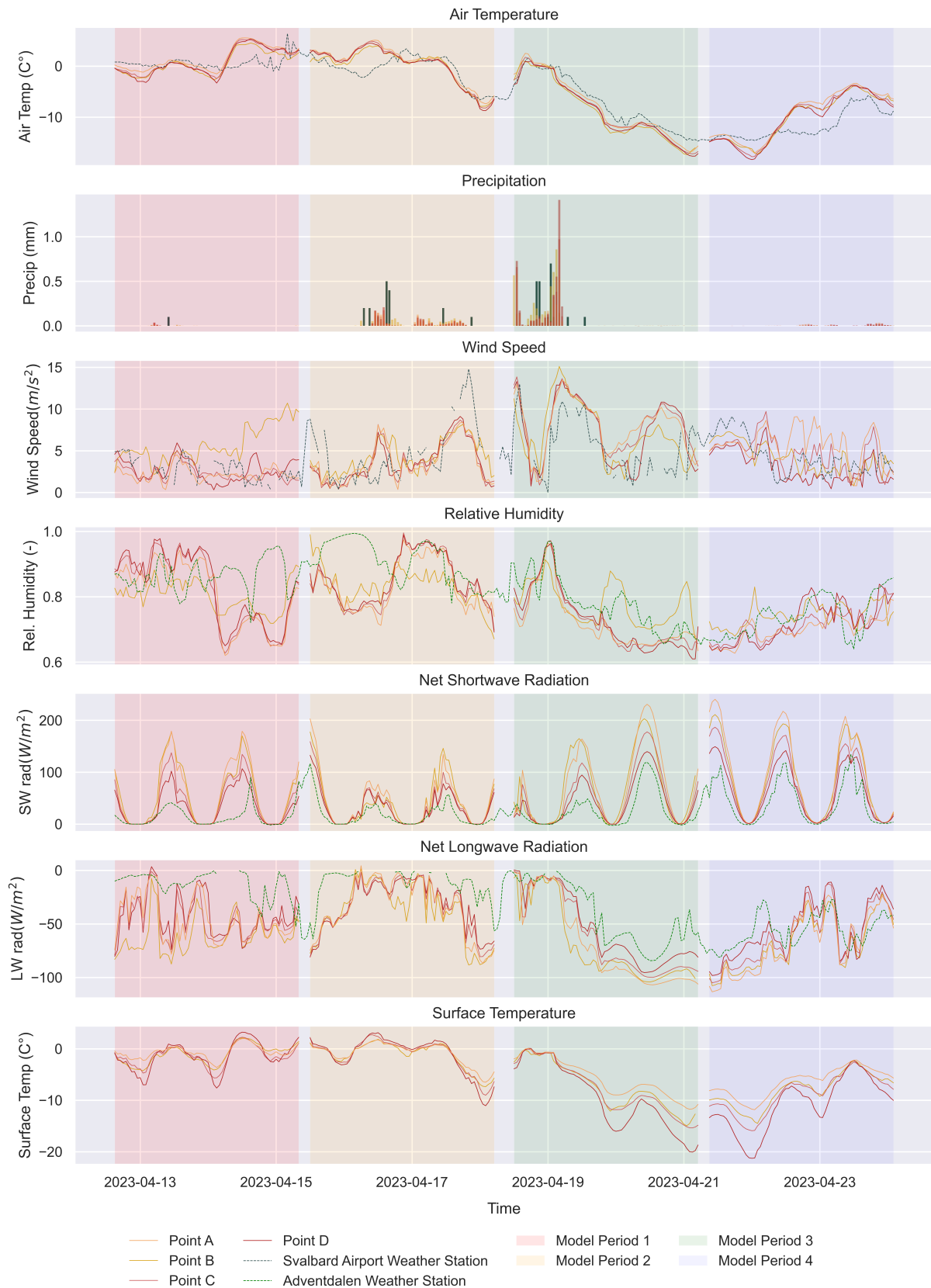


Figure 5.1.1: The collected AROME-Arctic weather predictions from the four relevant grid points. The data across all four model periods are presented alongside the observed data from Svalbard Airport weather station for air temp., precip. and wind speed. The parameters of rel. humidity, net shortwave rad., and net longwave rad. are presented alongside data from the Adventdalen weather station.

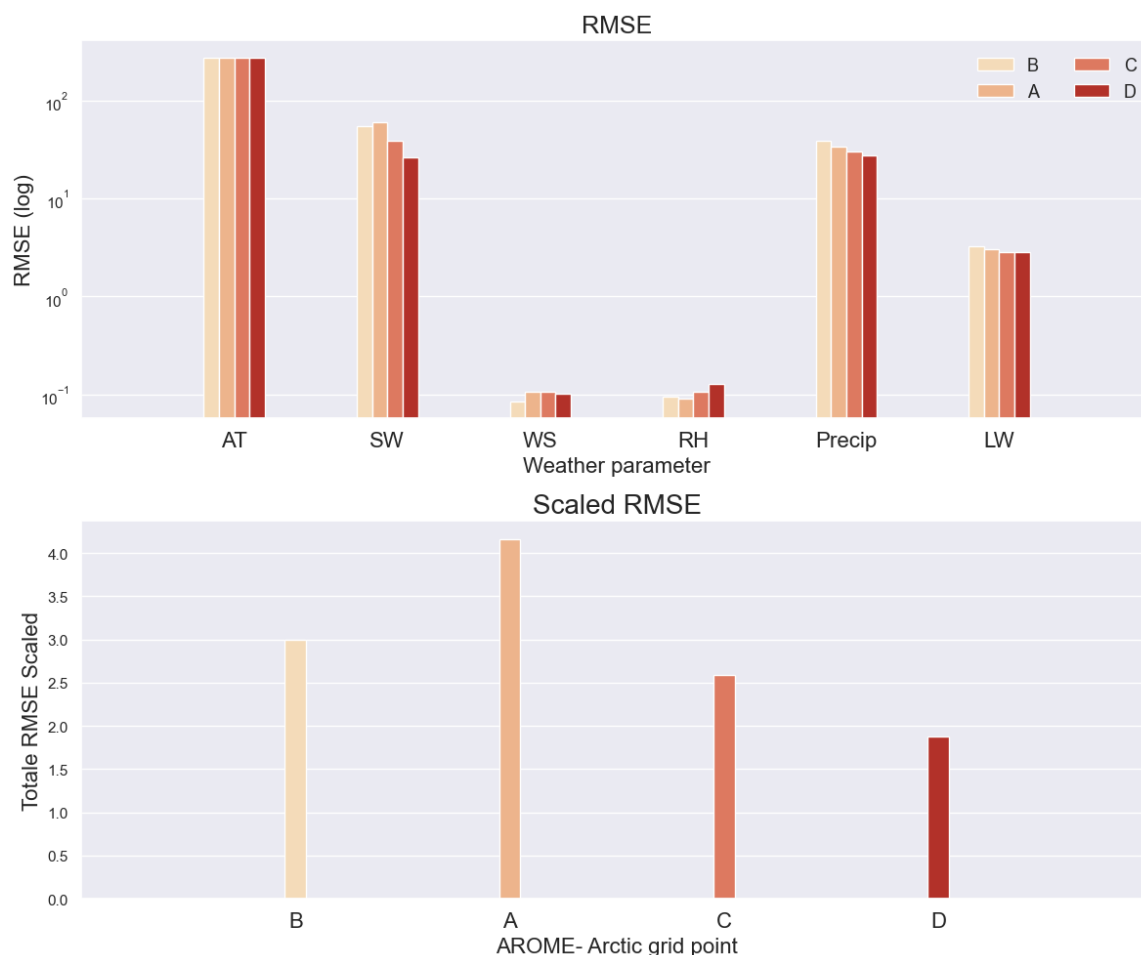


Figure 5.1.2: This Figure displays the RMSE for each AROME-Arctic parameter across all four grid points, as computed in accordance with Section 4.2.1. The upper graph illustrates the performance of each grid point per parameter, with the y-axis in a logarithmic scale. The lower graphic summarizes the overall grid point performance by accumulating the scaled RMSE for each grid point. A lower score, evident in both graphs, denotes a more accurate replication of observed events.

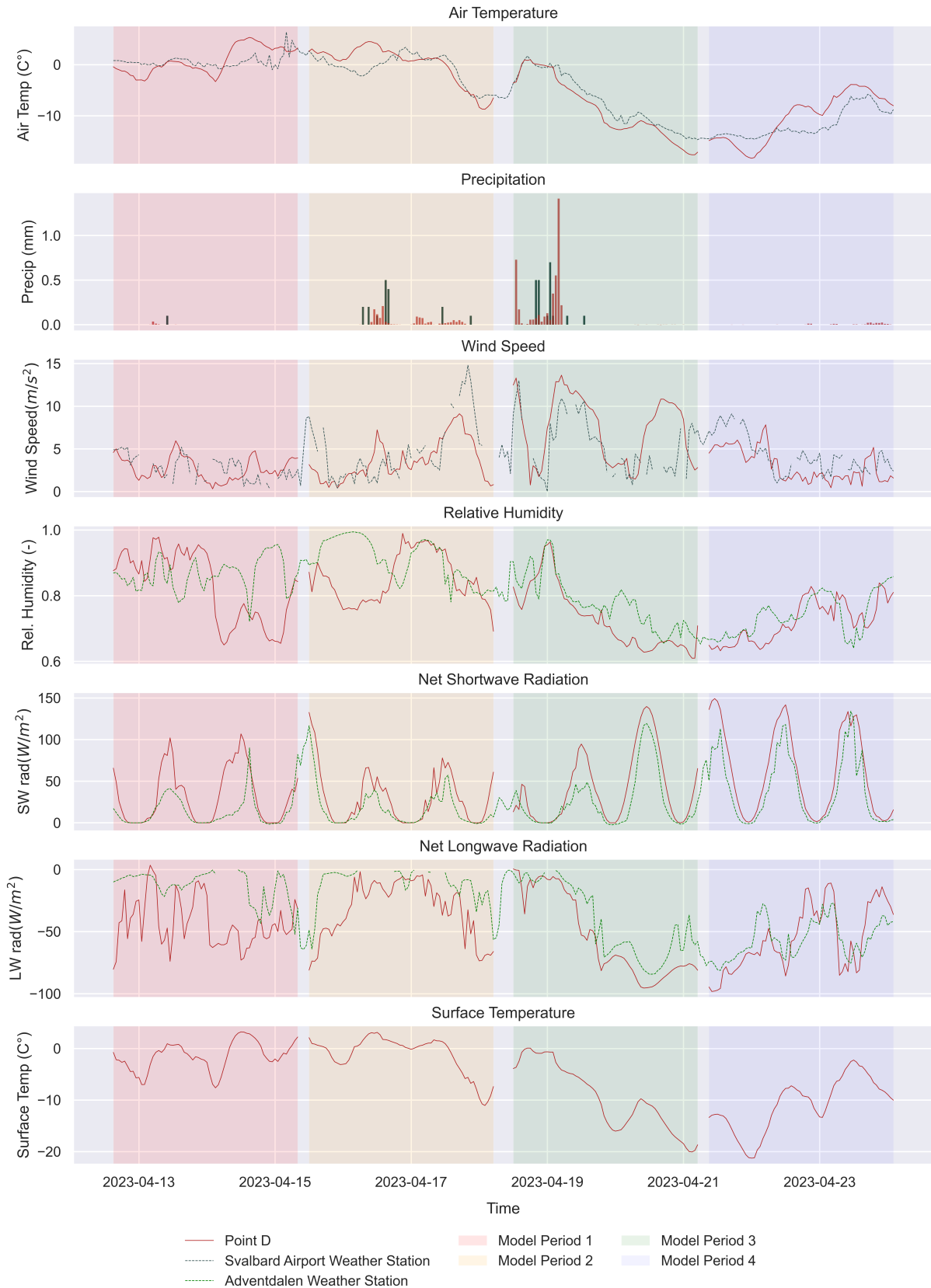


Figure 5.1.3: The collected AROME-Arctic data from the best-performing point. The data across all four model periods are presented alongside the observed data from Svalbard Airport weather station for air temp., precip. and wind speed. The parameters of rel. humidity, net shortwave rad., and net longwave rad. are presented alongside data from the Adventdalen weather station.

5.2 Manually observations of the snowcover

The initial state of the snowpack had a snow depth was 100 cm, and the snow profile showed 12 distinct stratigraphic layers (Figure 5.2.1). At the surface, a thin 2 mm layer of precipitation particles was identified, covering a 2 cm-thick melt refreeze crust. Beneath this crust, a loosely cohesive layer of decomposing and fragmented precipitation particles was identified was found, preceding another melt refreeze crust layer. Underneath, 5 cm of 1 mm faceted crystals was observed, which was succeeded by 60 cm of rounded grains, exhibiting variable hardness. Approaching the ground, softer faceted crystals were detected. An ice layer was discerned just above a stratum of large depth hoar crystals located at the ground interface. There is a temperature gradient of approximately $0.55 \text{ C } ^\circ\text{pr. cm}$ for the top 20 cm of the snowpack. Beneath, the temperature is stable. The ECT resulted in a non-propagating fracture when the load nr.13 was applied.

5.2.1 The snowpack development

Throughout the study period, the gathered snow profiles reveal that the snow cover underwent several types of metamorphosis (Figure 5.2.2). The melt refreeze crust at the top of the first snow profile (Figure 5.2.1) experienced both melting and refreezing during the first half of the field period. Furthermore, the layer of decomposing and fragmented precipitation particles transformed into faceted crystals. A new layer of wind-affected snow was observed at the surface. These layers exhibited uneven spatial distribution, observed during fieldwork (Figure 5.2.3).

An ice layer was observed in the first and fifth snow profiles. Further, the bottom half of the detected show profiles all show similar features. However, layer thickness, hardness, as well as the number of stratigraphic layers differ. All five snow profiles have a weak temperature gradient at the bottom half of the snowpack. Further, the temperature in this section of the snowpack stayed stable over the field period. The stability test indicated a propagating collapse occurred at isolation and dynamic load nr. 12 in the same layer of faceted crystals at the 18. April, as well as the 21. April. The other three stability tests resulted in a non-propagating fracture (Table 5.2.1).

Table 5.2.1: The ECT results from the five conducted stability tests, all performed on the manually observed snow profiles. The results indicated collapse for all five ECT, with propagating on the 18. April, 21. April

Snow Profile	Date	ECT Result
1	12. April	ECTN13
2	15. April	ECTN9
3	18. April	ECTPV
4	21. April	ECTP12
5	24. April	ECTN15

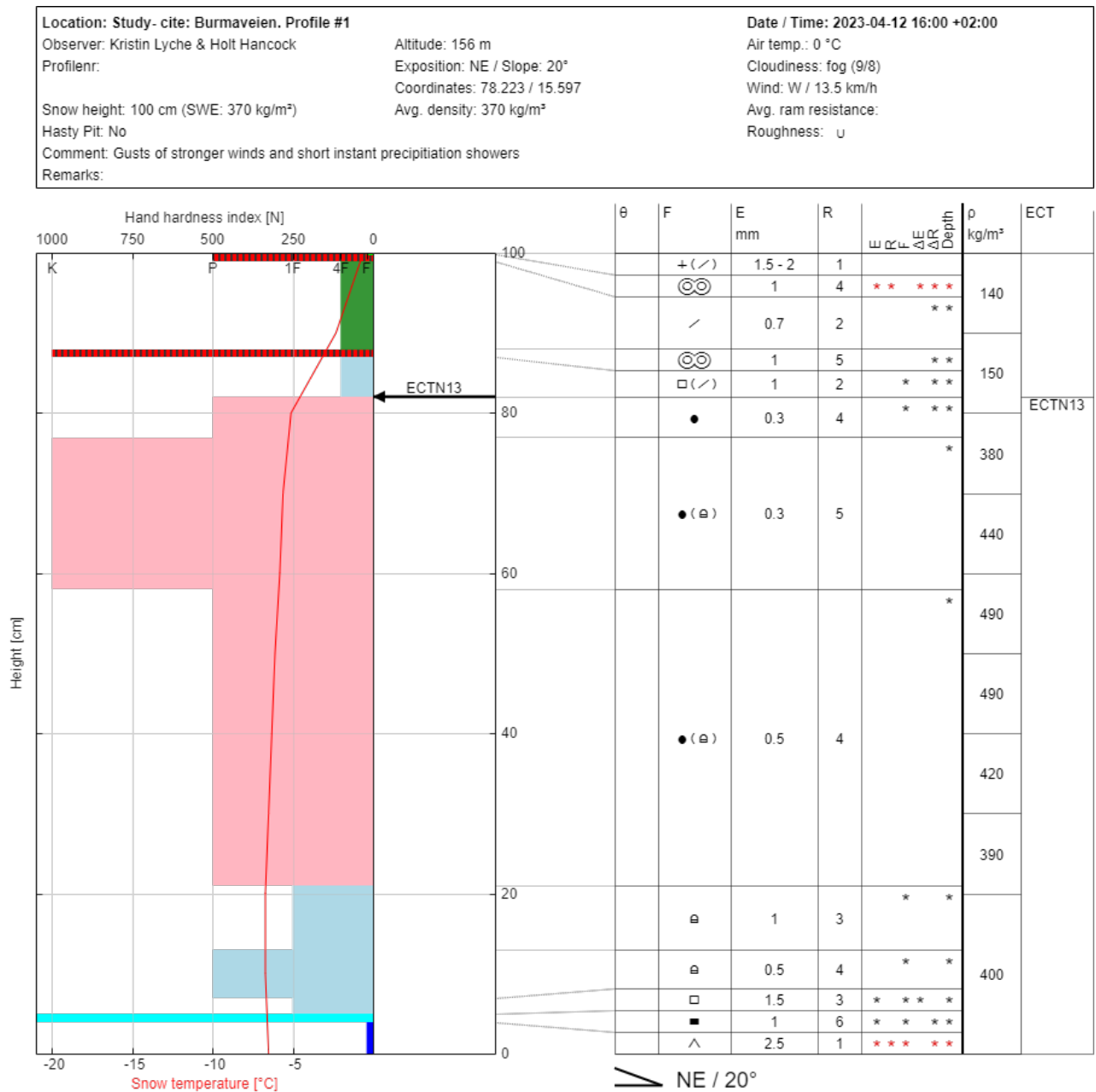


Figure 5.2.1: The initial state of the snowpack presented through the snowpack profile conducted on the first day of fieldwork. The figure is an original output from the NiViz software. The hand hardness of each layer is expressed through the width of the layers, readable from the graph’s top line. Grain shape is denoted through both color-coding and symbols as described in Table 4.3.2. The measured temperature is indicated by a red line, using the bottom x-axis as a reference. Snow height is expressed in cm with the box’s right end as the reference point. Metadata from the observation time is provided at the top of the Figure. The right panel offers information about grain shape (F), density (ρ), grain size(E), and moisture content (θ). The black arrow visualizes the point where the ECT led to a collapse, with the ECT test result annotated at the arrow.

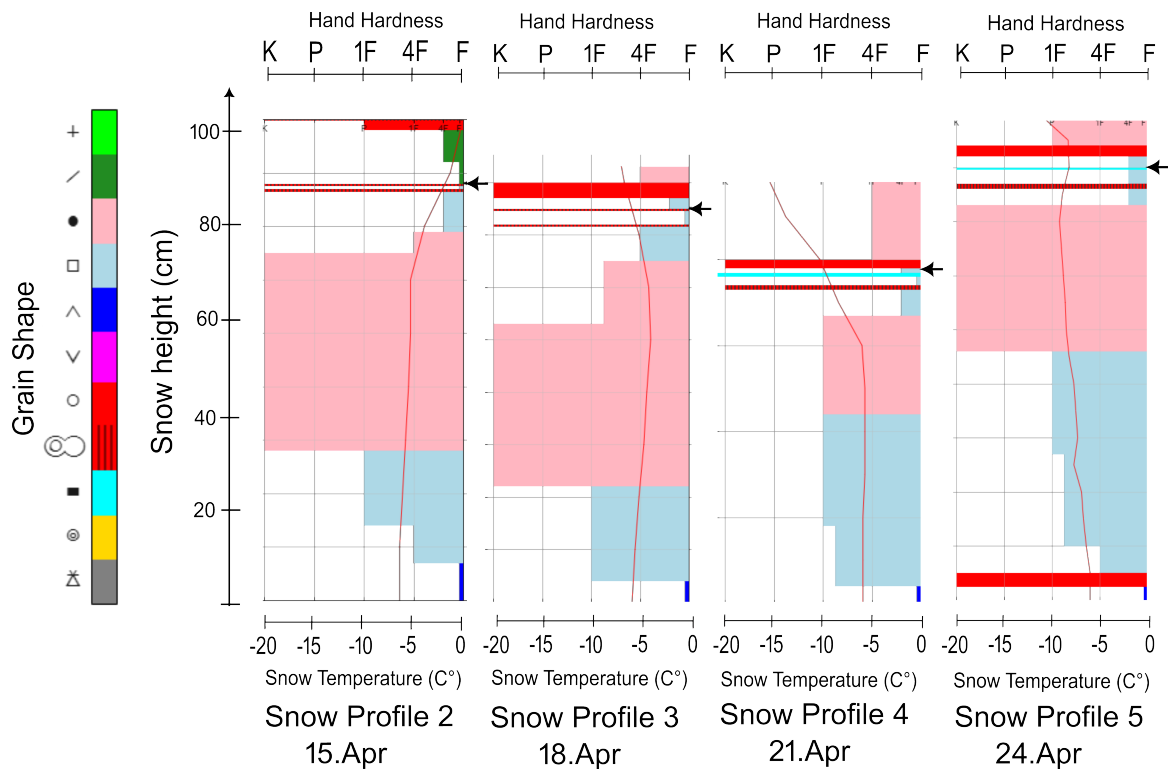


Figure 5.2.2: The development of the snowpack is visualized by four snow profiles. Each snow profile shows the hand hardness of each layer expressed through the width of the layers, readable from the graph's top line. Grain shape is denoted through both color coding and symbols described in Table 4.3.2. The measured temperature is indicated by a red line, using the bottom x-axis as a reference. Snow height is expressed in cm with the box's right end as the reference point. The black arrows indicate the place where the fracture during the ECT occurred. The results of the ECT are displayed in Table 5.2.1.



Figure 5.2.3: The two pictures shows unequally distributed snow surface characteristics. The picture to the left shows the uneven snow surface east of the study site at 21. April. The picture to the right shows the snow surface looking south from the study site taken at 24. April. The mitten is included as a scale.

5.3 SNOWPACK simulations

The following section presents the SNOWPACK predicted development based on the AROME-Arctic model, grid point D, and manually observed snow profiles.

5.3.1 Grain shape

Figure 5.3.1 illustrates the SNOWPACK model’s temporal tracking of grain shape across all four model periods. In the first model period, two melt/refreeze cycles are forecasted, with melting being modeled within the surface layer during two intervals. These transformations are difficult to discern in Figure 5.3.1; however, they can be viewed in detail in Appendix B, Figure B.1.1.

The second model period encompasses two primary transformations. Initially, the surface layer changes into melt forms around the middle of the model period. Subsequently, a transformation from decomposing and fragmented precipitation particles to faceted crystals commences approximately at the onset of the second day.

In the third model period, the snowpack forecast anticipates new precipitation, which rapidly transforms into faceted crystals. Towards the end of the model period, the surface rounded grains at the uppermost part of the snowpack convert into faceted crystals. For all three model periods, the lower part of the snowpack is kept stable over the 66-hour model period. The final model period exhibits a stable snowpack with no observable changes in grain shape.

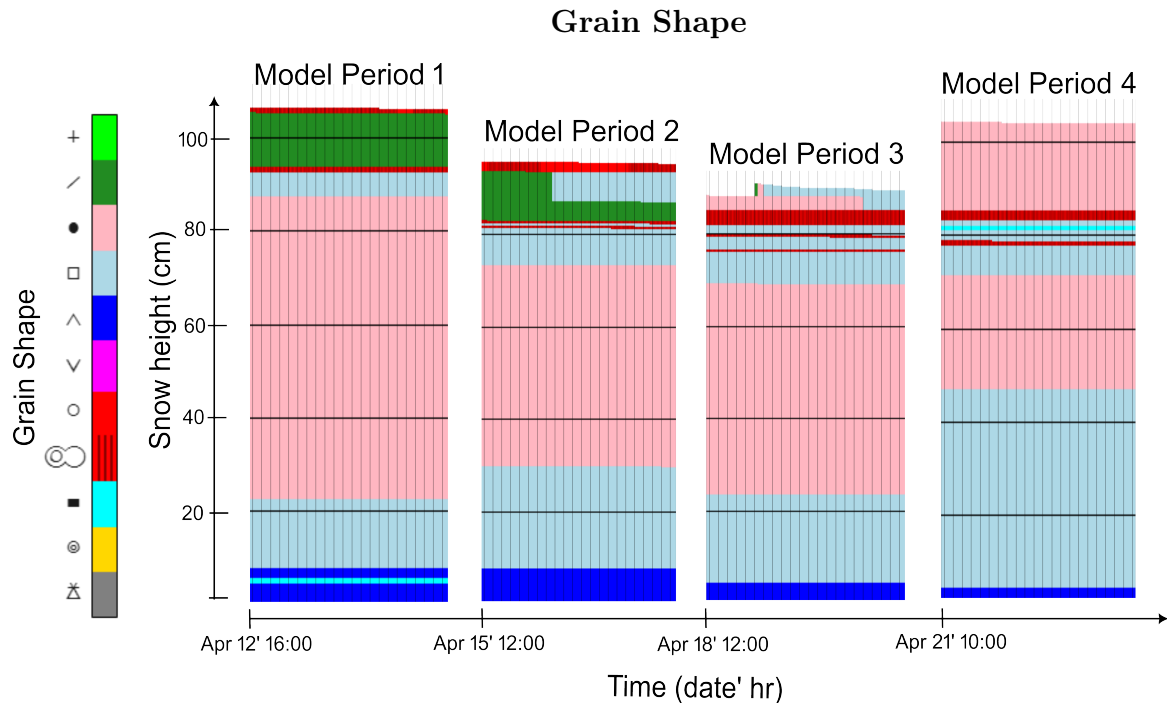


Figure 5.3.1: The simulated grain shape evolution over four model periods as generated by the model chain is displayed. The horizontal black lines indicate snow depth, with vertical lines positioned at every three-hour intervals within the model periods. The start time of each simulation is denoted by the date and time at the beginning of the model period.

5.3.2 Temperature

The thermal evolution of the snowpack, visualized in Figure 5.3.2, reveals a consistent trend of cooling throughout the fourteen-day observation period.

The first model period is characterized by temperatures nearing 0°C in the upper section of the snowpack. These warmer temperatures are seen to propagate downwards over the course of the model period.

Both the second and third model periods are divided into warmer and colder sections. In the first half of these periods, the snowpack retains warmer temperatures and exhibits a stronger temperature gradient. Conversely, a cooling trend is observable in the snow cover towards the latter part of both model periods. This cooling trend is more pronounced in the third model period, with surface temperatures nearing -15°C .

The fourth model period commences with cold surface temperatures before rapid warming to approximately -6°C is simulated around the first day. Toward the end of this model period, the temperature approaches uniformity across the entire depth of the snowpack.

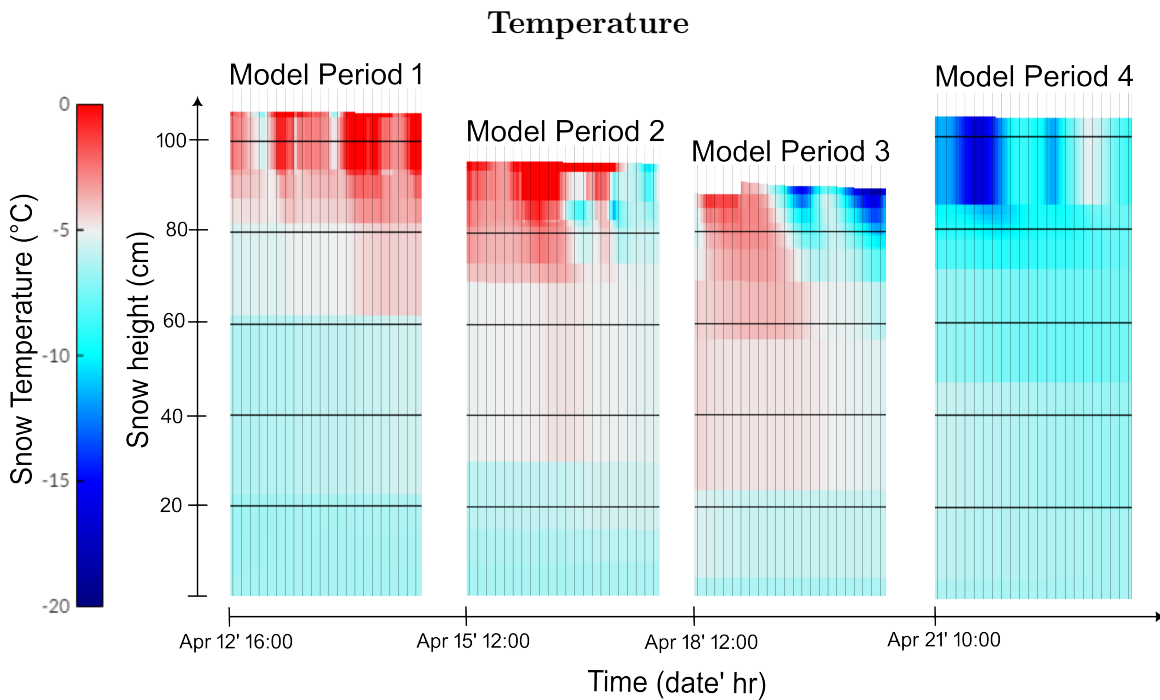


Figure 5.3.2: The simulated temperature evolution over four model periods as generated by the model chain is displayed. The framework of the Figure is equal to Figure 5.3.1, and should be read similarly.

5.3.3 Liquid water content

The simulation results suggest that liquid water is present only during the first and second model periods (Figure 5.3.3). In the first model period, a slight presence of liquid water is observed, manifesting as a moist layer at the top of the snowpack. In contrast, the second model period models a significantly wetter condition, with a layer with relatively high (3%) liquid water content apparent at the surface.

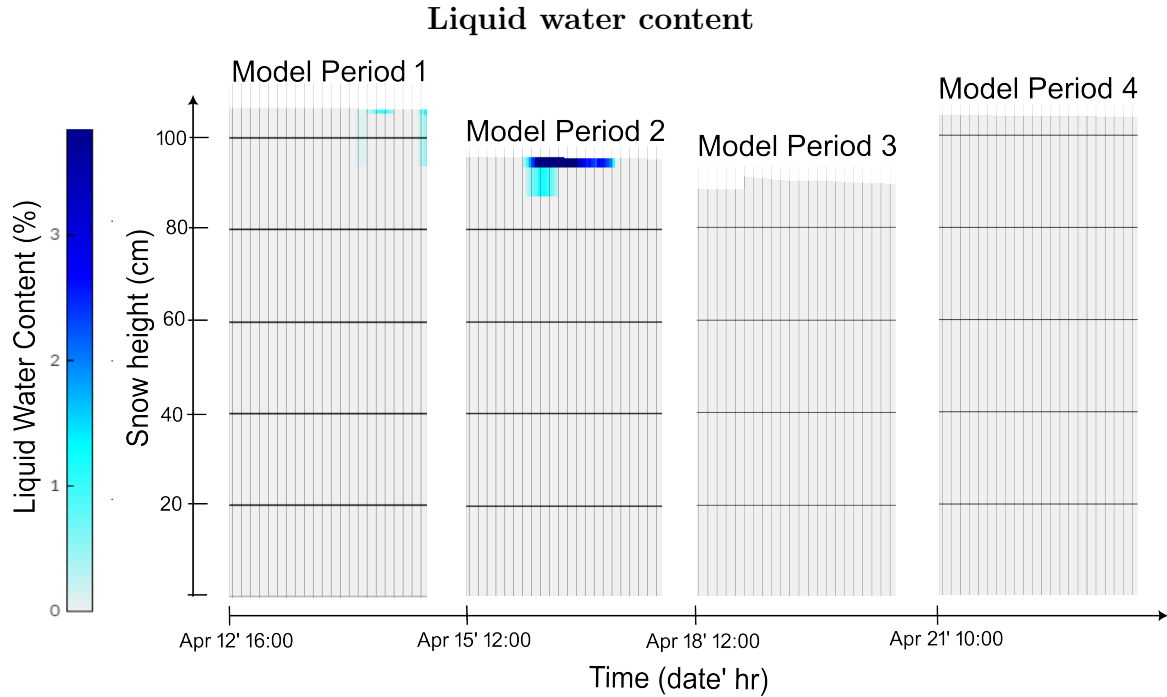


Figure 5.3.3: The simulated liquid water content over four model periods as generated by the model chain is displayed. The framework of the Figure is equal to Figure 5.3.1, and should be read similarly.

5.3.4 Snow Profile

The snow profiles from the final time step of each model period are visualized in Figure 5.3.4. For the first model period, the snow profile reveals two knife-hard layers of melt forms and melt refreeze crust in the upper section. These are separated by a fist-soft layer of decomposing and fragmented precipitation particles. Underneath the second ice layer, there is a fist-soft layer of faceted crystals, preceding a gradually hardening section composed of rounded grains. The bottom section is dominated by faceted crystals and depth hoar, with an ice layer proximal to the ground.

Similar features are found in the snow profile representing the final time step of the second model period. However, beneath the melt refreeze crust, a layer of soft faceted crystals is simulated before a layer of decomposing and fragmented precipitation particles is observed. Two thin ice layers are detected, followed by a layer of faceted crystals. The main features of the lower half of the snowpack are similar to those found in the profile generated from the first model period, however, the ice layer near the ground is absent. The snowpack in the second profile is generally softer than that of the first model period.

This trend of softening continues in the profile representing the third model period. This profile showcases the overall softest snowpack. Furthermore, three ice layers are simulated for the upper section of the snowpack, interspersed solely by faceted crystals. A fist-soft layer of faceted crystals is simulated at the top of the snowpack. No ice layer at the bottom of the snow cover is detected.

The fourth model period displays a surface layer of 4F-hard rounded grains atop three hard ice layers. These ice layers are separated by faceted crystals. The bottom part of the snowpack is characterized by an equal distribution of faceted crystals and rounded grains, with depth hoar detected at the ground interface.

All the snow profiles exhibit temperature gradients that remain consistent for the bottom half of the profiles, while larger fluctuations are observed in the upper sections. For model periods 1 and 2, these fluctuations are towards 0°C , while for model periods 3 and 4, colder surface temperatures are simulated. The temperature of model period 4 is approaching an isotherm state. The temperature's temporal development is more detailed expressed in Figure 5.3.2

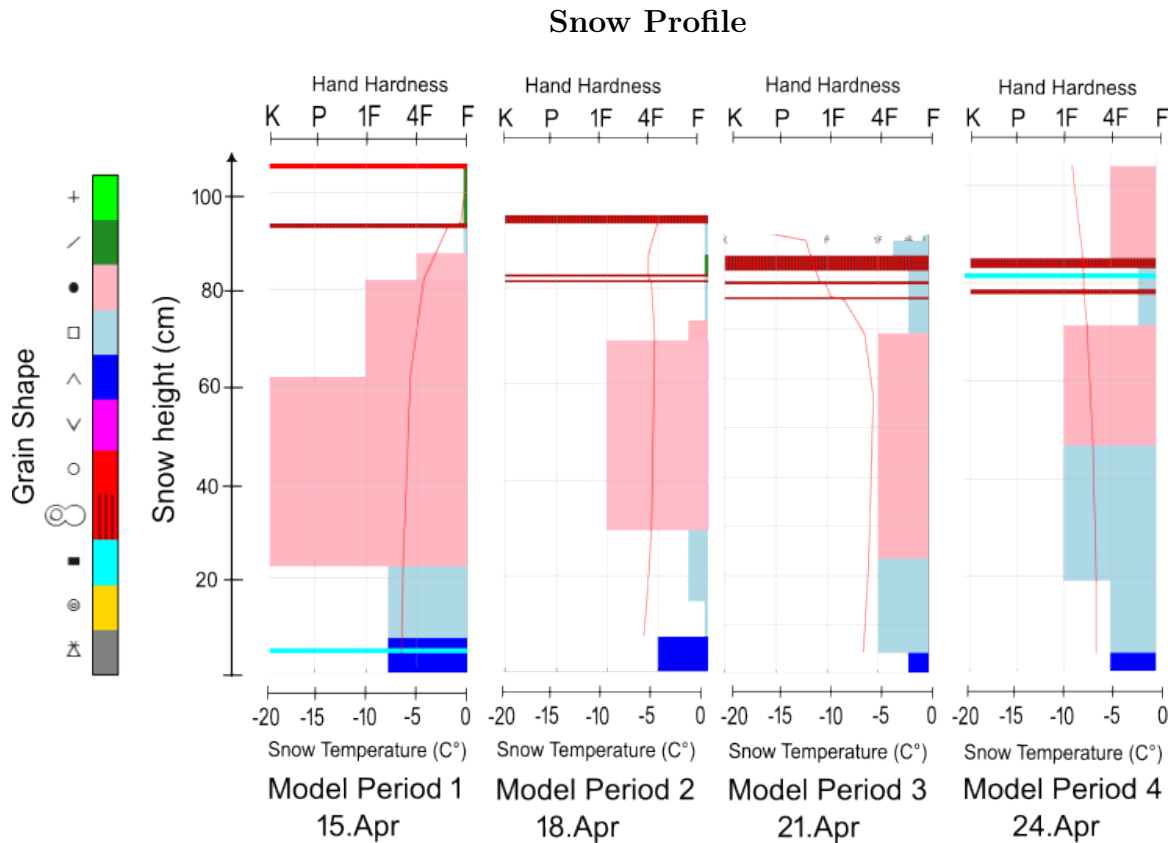


Figure 5.3.4: The Figure displays the simulation of the snowpack as a snow profile for the last time step of the model period. Each snow profile shows the hand hardness of each layer expressed through the width of the layers, readable from the graph's top line. Grain shape is denoted through both color coding and symbols as per Table 4.3.2. The measured temperature is indicated by a red line, using the bottom x-axis as a reference. Snow height is expressed in cm with the box's right end as the reference point.

5.4 SNOWPACK model validation

This section presents the results of the visualized layer mapping between the observed validation snow profile and the simulated snow profile. This is followed by the outcomes from the objective compartment algorithm.

5.4.1 Layer mapping

The layer mapping between the validation snow profile and the simulated snow profile for the final time step of all four model periods is visualized in Figure 5.4.1. The mapping, conducted manually as outlined in Section 4.5.1, reveals different degrees of correlation across the model periods.

For the first model period, the simulation identifies nine corresponding layers in the snow profile. However, it misses four layers and simulates three layers that are not observed. The simulation fails to capture a 2 mm thin surface layer of precipitation, which is barely graphically visible, and a sequence of two thin ice layers separated by faceted crystals. Here, only one ice layer is simulated. Additionally, an ice layer near the ground is observed but not simulated.

During the second model period, the model chain simulates 11 layers, with 10 of these corresponding to the observed stratigraphy. The model fails to detect a layer of decomposing and fragmented precipitation particles in the upper section of the snowpack and a layer of soft faceted crystals above the final stratigraphic layer of depth hoar.

In the third model period, all observed layers are simulated, yielding 11 matching layers. The simulation further predicts an extra surface layer not observed, resulting in one superfluous layer in the simulation.

Lastly, the simulation for the fourth model period yields 11 simulated stratigraphic layers, compared to 13 observed layers. 11 layers align with the mapping algorithm. During observation, an ice layer near the ground is detected but not simulated. Furthermore, a layer of faceted crystals at the bottom of the snowpack is overlooked.

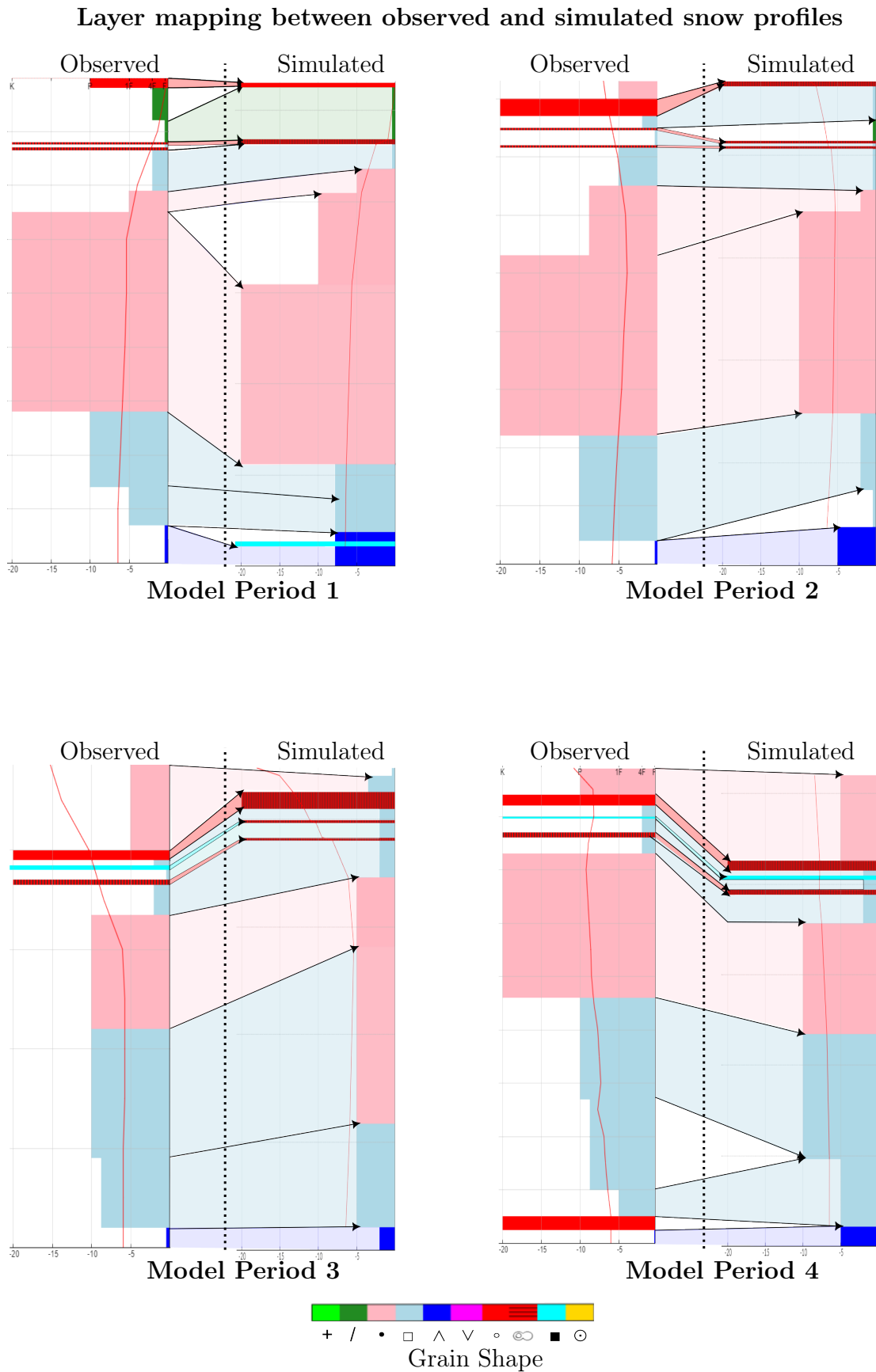


Figure 5.4.1: The results of the layer mapping conducted between manually observed snow profiles and the corresponding simulation. The vertical dotted line elevates the border between the observed and simulated snow profiles.

5.4.2 Qualitative agreement score

The calculations for the quantitative comparison method, as outlined in Section 4.5, were conducted based on the layer mapping visualized in Figure 5.4.1. The results are given in Table 5.4.1.

These results indicate that total agreement scores across the four model periods exhibit a range between 0.85 to 0.91. Notably, the third model period achieves the highest score. The total agreement score averages a value of 0.88.

An examination of the model's performance across different aspects reveals disparities. The agreement score for stratigraphy is 0.79, whereas the model's representation of grain shape yields an agreement score of 0.97.

Furthermore, it's important to note that the alignment of stratigraphy for the first model period is significantly lower than the values for the subsequent periods.

Table 5.4.1: The results of the model validation conducted according to Section 4.5 is presented. The agreement score for each property and the total score for each model run are provided. The mean value derived from all four model runs and the mean value of the overall agreement is included for each property.

Model Period	κ_{strat}	κ_{temp}	κ_{size}	κ_{shape}	κ_{tot}
1	0.56	0.96	0.90	1	0.85
2	0.83	0.68	0.91	1	0.86
3	0.92	0.88	0.96	0.89	0.91
4	0.85	0.74	0.98	1	0.89
Mean value	0.79	0.82	0.94	0.97	0.88

5.4.3 Grid point sensitivity

A sensitivity analysis was performed by driving the SNOWPACK model with data from four selected AROME-Arctic grid points. All other parameters were kept constant. An overview of the results from grid point A is presented in the following section due to the most significant differences detected, while the results from grid points B and C are detailed in Appendix C.

Grid point A

For grid point A, the model chain simulated significant grain shape metamorphism (Figure 5.4.2). Model periods 1 and 2 featured the faceting of decomposing and fragmented precipitation particles and extensive melt processes in the upper layers.

The simulation further showed significant warming during the first and second model periods (Figure 5.4.3). This was coupled with the simulation of liquid water content, producing saturated conditions in the upper layers of the snowpack during these periods (Figure 5.4.4). This pronounced melting is also evident in the upper sections of the snow profiles for the corresponding model periods (Figure 5.4.5).

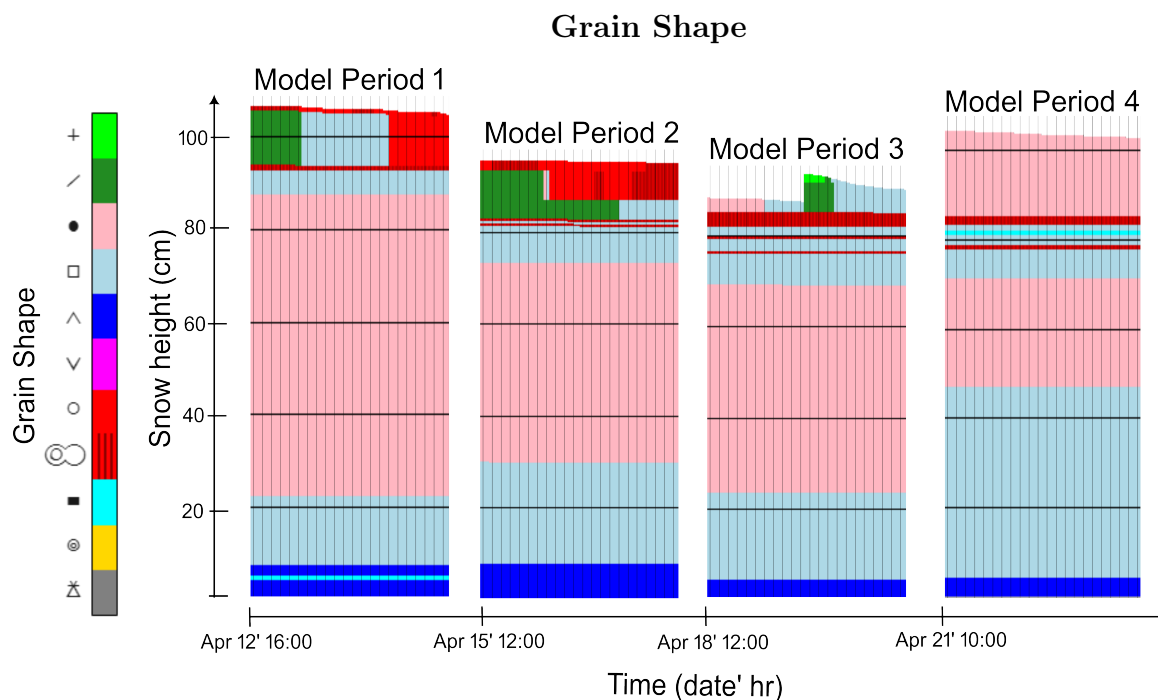


Figure 5.4.2: Simulated grain shape development over the four model periods when SNOWPACK was forced by AROME-Arctic output from point A. The horizontal black lines indicate snow depth, with vertical lines positioned at every three-hour intervals within the model periods. The start time of each simulation is denoted by the date and time at the beginning of the model period

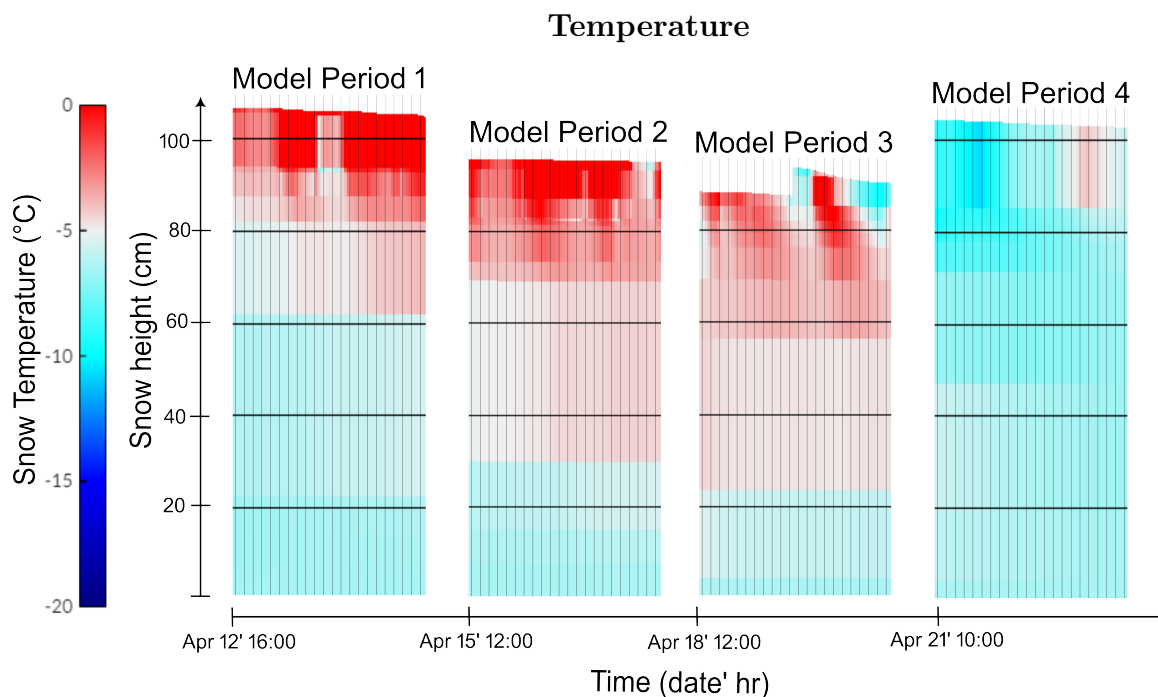


Figure 5.4.3: Simulated grain shape development over the four model periods when SNOWPACK was forced by AROME-Arctic output from point A. The Figure should be read the same way as Figure 5.4.2

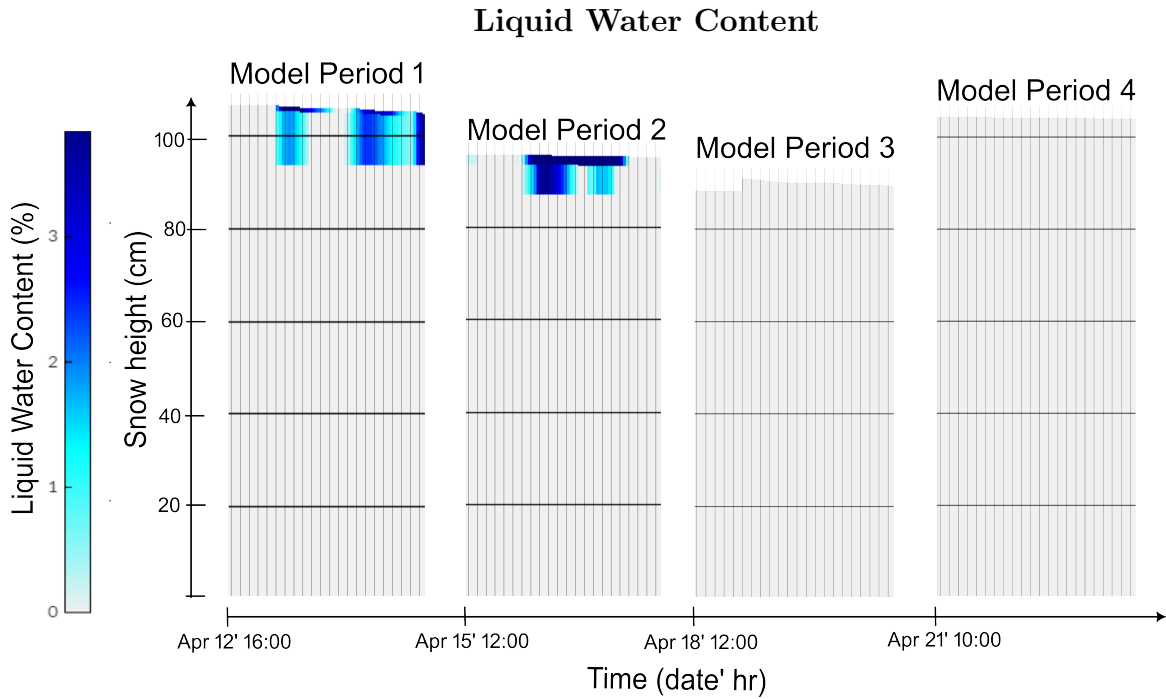


Figure 5.4.4: Simulated development of liquid water content over the four model periods when SNOWPACK was forced by AROME-Arctic output from point A. The Figure should be read the same way as Figure 5.4.2

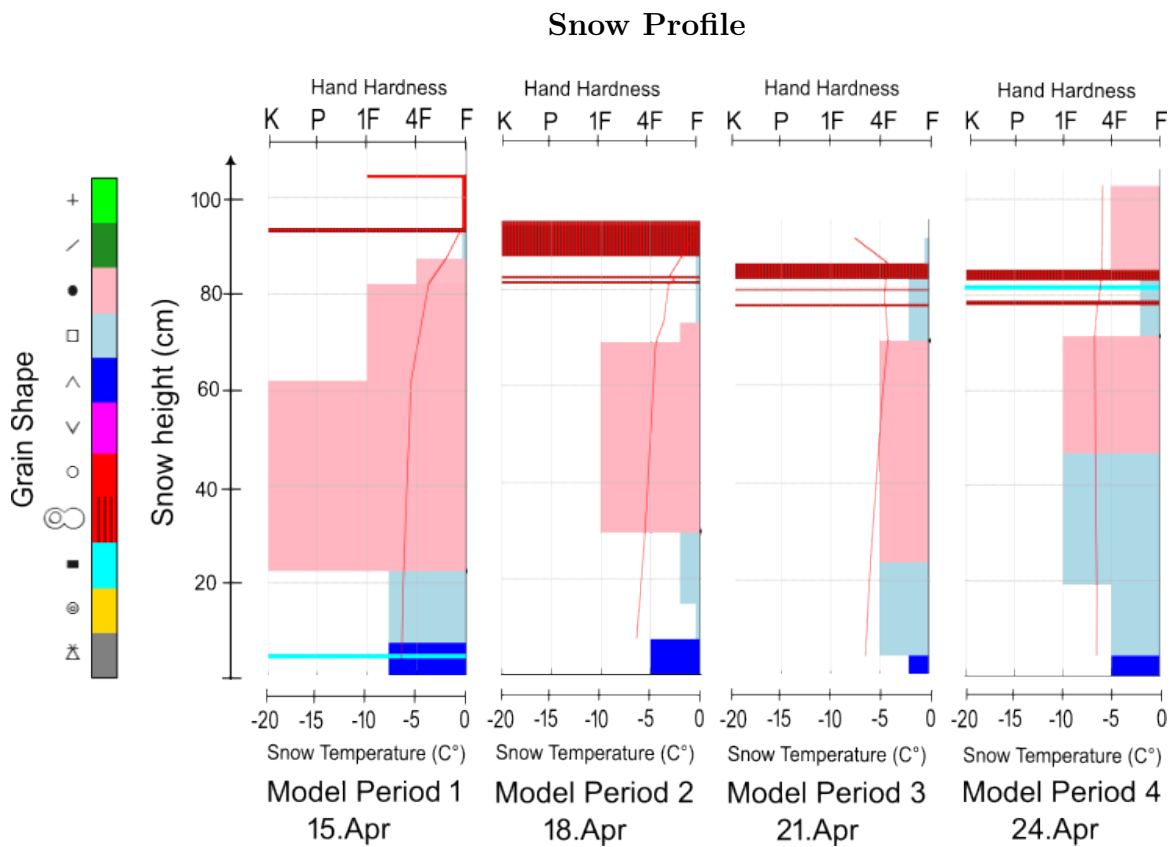


Figure 5.4.5: Simulated snow profile development over four model periods when SNOWPACK was forced by AROME-Arctic output from point A. The Figure should be read the same way as Figure 5.3.4

Chapter 6

Discussion

This Chapter discusses the findings presented in Chapter 5 in the context of the research questions outlined in Section 1.2. It is divided into three main sections, each devoted to discussing the associated research questions in detail.

Section 6.1 discusses AROME-Arctic as a data source for snowpack modeling. The performance of the weather forecast is commented on, followed by an evaluation of how the transformation process from gridded data to point simulation influences the quality of performance. A discussion of the inconsistent data output between grid points is included.

Section 6.2 evaluates the performance of the SNOWPACK and AROME-Arctic model chain based on the four model periods detailed in Section 5.3. Initially, the discussion revolves around the performance related to the specific case study. This is then broadened to consider the possible model performance beyond the tested setting. Furthermore, this Section includes an examination of the sensitivity of the model's performance related to the AROME-Arctic grid point.

Section 6.3 serves as a discussion of the model chain's applicability to avalanche forecasting. It synthesizes all results presented in Chapter 5, as well as insights gleaned from the previous sections in this Chapter in order to explore this final research question.

Section 6.4 provides a discussion of the most pronounced limitations connected to the methodology of the study.

Lastly, Section 6.5 provides suggestions on how findings from the conducted study can encourage further investigations to improve the snowpack modeling forced by numerical weather predictions and manually observed snow profiles for avalanche forecasting.

6.1 AROME-Arctic as data source for SNOWPACK

The similarity between the forecasted and observed weather in Figure 5.1.3, and the high agreement score in Table 5.4.1, indicates that AROME-Arctic has the capability to yield robust results for SNOWPACK modeling.

Further, AROME-Arctic has the advantage that it delivers consistent data sets every third hour, with all parameters needed in order to run snow cover simulations. Additionally, by connecting a snowpack model to the AROME-Arctic NWP, the model chain could, in theory, be set up anywhere within the AROME-Arctic model domain. This methodology introduces flexibility not present when depending on data from a traditional and advanced weather station. These realizations all support AROME-Arctic as a suitable data provider for SNOWPACK.

The AROME-Arctic model predicted snow surface temperatures above 0°C , which is nonphysical. However, this is handled by SNOWPACK when shifting boundary conditions are utilized, as the Neumann boundary conditions are used as the surface temperatures exceed -1°C . Nevertheless, this is a weakness to be noted as it increases uncertainty regarding the quality of the simulated surface temperature.

However, AROME-Arctic as a high-quality data provider aligns with the findings of Myhre (2018) and Zweigel et al. (2021). As AROME-Arctic produces gridded data (Section 2.7), there must be a transformation between grid and point value when AROME-Arctic and SNOWPACK are linked. Even though AROME-Arctic is a high-resolution model in NWP context, a grid resolution of 2.5 km is coarse in the site-specific avalanche forecasting setting. The mesh size of AROME-Arctic makes the model highly sensitive to small-scale local phenomena, indicating that the incorporation of AROME-Arctic into the model chain needs careful consideration.

In this study, a single AROME-Arctic grid point was selected as a data source, similarly as conducted by Bellaire et al. (2011). However, unlike the mentioned authors, the selected point for this study was not one of the closest to the field site. The point was selected based on a consideration of RMSE compartment between possible grid points and the weather data set from the Svalbard Airport weather station and the Adventdalen weather station. It should be highlighted that the observed weather data that were used as a basis for comparison were a combination of data sets, where non of the data sources were located at the research site. Therefore, the data set may not represent the conditions at the research site. In this way, uncertainty regarding the accuracy of the point selection is introduced.

When comparing the four grid points in Figure 5.1.2, it is clear that some parameters are quite consistent over the four model periods while others are highly variable (Section 5.1). Whereas the variance in wind speed can be explained by different topographic channeling effects from the valley systems around Longyearbyen (Section 3.4), the strong variability in bias for the net shortwave parameter is unexpected. There are local features, such as cloud coverage, that would highly influence this parameter and further result in differences between the four simulations. However, the consistent biases over the model period for all four grid points contradict the theory of differences in simulated local cloud coverage, as this phenomenon occurs over a shorter temporal scale. Additionally, the consistency between the four simulated longwave radiation supports the statement that cloud coverage might not explain the variability

in shortwave radiation. Another plausible explanation could be the simulated surface albedo.

As the model is predicting the net shortwave radiation, a parameterization of the snow's albedo is estimated and utilized in AROME- Arctic. Differences in the model's interception of the surface characteristics might introduce different biases in the net shortwave radiation parameter. Again, due to the consistency in outgoing longwave radiation, drastic differences in surface properties are not likely. In this way, explaining the shortwave radiation dynamics proves to be nontrivial. Furthermore, short wave radiation is known to be a challenging parameter for NWP (Gregow et al., 2020), and a model error can not be ruled out.

6.1.1 From grid to point value

These findings exemplify that for the maritime arctic climate, where the topography is dominated by highly local and complex terrain features like valleys, glaciers, and mountains, the selection of grid point for snowpack modeling should involve a thorough investigation. In Horton and Haegeli (2022), the authors gathered all model points in a selected region and utilized the point providing the median value of the most sensitive parameter for their research. However, this method was selected for an inland climate and is not guaranteed to yield the desired output in the Arctic setting. For their Crocus modeling in Svalbard, Zweigel et al. (2021) utilized the closest grid point at a similar elevation, with good results. This study contradicts this finding, as the closest point at a similar elevation where out-performed. Therefore, further exploration of different approaches would be highly interesting and necessary in future setups. The findings of this case study indicate that a validation of the AROME-Arctic model output before setting up the AROME-Arctic and SNOWPACK model chain would increase the credibility of the snowpack predictions, as well as increase the probability of high performance.

6.2 Predicting the development of the snowpack

The AROME-Arctic and SNOWPACK model chain forced by manual snow observations demonstrated considerable success in predicting the snowpack's development throughout all four modeling periods. The average agreement score of 0.88 suggests a near-perfect correspondence between modeled and observed results (Table 5.4.1), signaling a high level of accuracy in all four conducted simulations. The agreement score of 0.97 for grain shape strengthens this claim, as grain type, according to Herla et al. (2021a), constitutes one of the most crucial parameters in such simulations.

It's noteworthy that the stratigraphic parameter indicated the lowest performance, with especially weak performance for the first modeling period. However, the interpretation of these findings must take into account the conditions and context of the observed snow profiles that served as the basis for the initiation and validation of model parameters.

The consistency of the simulated stratigraphy should be assessed in relation to the concordance of the observed snow profiles. The snow profiles in Figure 5.2.1 and Figure 5.2.2 reveal inconsistencies in snow depth, as well as differences in grain shape.

For instance, the changing presence of an ice layer near the ground over the five different profiles cannot be explained by snow metamorphism, as snow melt and refreezing cannot occur due to stable lower half temperatures. Thick ice layers are generally easily detectable in the snowpack, making observational errors less likely. Despite the profiles being conducted with narrow spacing and limited extent, these findings suggest spatial variability influencing the consistency between observations. Figure 5.2.3 supports the statement of variable snow height at the field location. Further, the immediate physical characteristics of the ground might have caused small-scale variations in the presence of the ice layer. The presence of rocks or small water channels could both impact how ice forms early in the development of the seasonal snowpack.

Further, the manually observed snow profiles involved subjective estimation of parameters such as grain shape, size, and hardness (Section 4.3), introducing potential observational errors that might account for the observed variations. These inconsistencies may arguably influence the objective performance of model simulations, potentially underestimating the actual model chain’s performance as recorded in Table 5.4.1.

In light of these considerations, the overall high-performance score is an encouraging testament to the robustness of the model chain. Even with the inherent uncertainties associated with manual observations, the model chain demonstrated resilience to small-scale spatial variability and observational errors. These findings are indeed beneficial, reinforcing the model’s performance and enhancing confidence in its ability to handle naturally occurring inconsistencies.

6.2.1 Performance beyond the case study

There is evidence to suggest that the model chain will maintain its high performance outside the limits of the conducted case study. Firstly, the state of the snowpack (Figure 5.2.1) closely aligns with the typical snow cover of the high-Arctic maritime snowpack (Section 3.3). Thus, if run at different time periods, as well as in other locations in Svalbard, the initial conditions of the snowpack are likely to consist of similar features. The model chain has provided confirmation that it handles this type of snowpack structure well. This finding is in line with Praz (2018) and is encouraging when considering the potential spatial independence of the model chain’s performance. However, the snow cover exhibits a high degree of spatial variability (Section 2.1). Whether the model chain would perform as effectively in areas dominated by other topographic effects, such as deposition or intense erosion, is unlikely due to the one-dimensional character of SNOWPACK (Section 2.5).

Secondly, the four modeling periods all underwent different dominant weather features (Figure 5.1.1), leading to varying processes within the snowpack observed through the manually conducted snow profiles (Figure 5.2.2). The dominant weather during the model period, the processes observed in the snowpack, and the final model performance expressed through the agreement score are summarized in Figure 6.2.1.

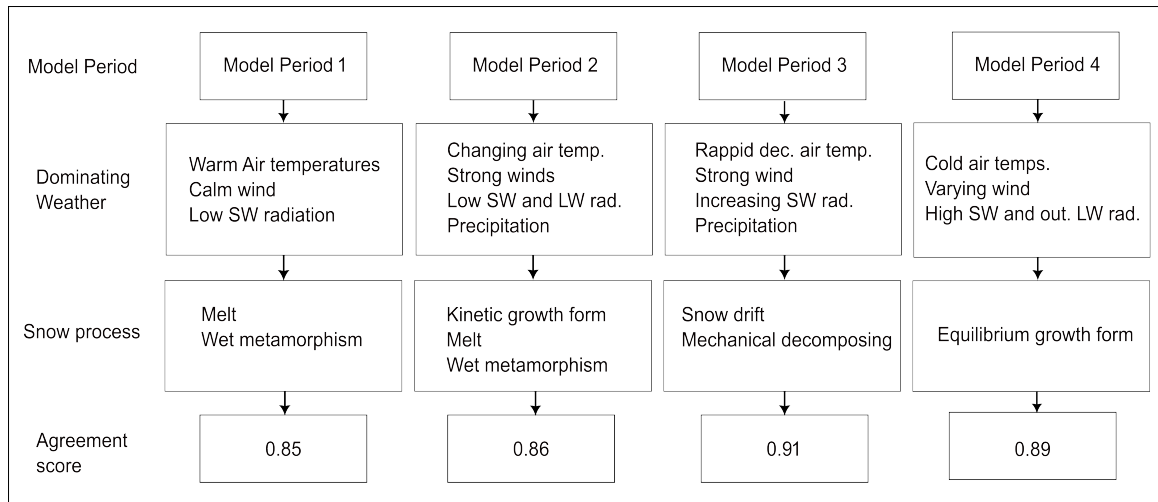


Figure 6.2.1: The Figure describes each of the most dominant weather features occurring in each model period, with the resulting observed snow process. The observed processes within the snowpack are based on five manually conducted snow profiles. Between the first and second profiles (model period 1), both melt and wet metamorphism were detected. The melt-refreeze cycles persisted between the second to the third profile (model period 2), accompanied by a metamorphosis of decomposing and fragmented precipitation particles to faceted crystals near the snowpack’s surface. Between profiles three and four (model period 3), snow drift and mechanical decomposition of the top layer were noted. Minimal changes were observed between the fourth and fifth snow profiles (model period 4), during which the snowpack underwent a slow equilibrium growth. The agreement score of each model period is included.

In this way, despite the model chain’s relatively short testing period, it was subjected to several different snow processes. The two different boundary conditions (Section 2.5.2) were both utilized, mirroring the variability in surface temperatures during the testing period. However, even though a range of processes has been evaluated, there remains a large assortment of untested scenarios. For instance, intense precipitation and warm, wet low-pressure systems causing precipitation (Section 3.2) were not included in the study. These examples highlight that the model chain was only tested with a limited data set and that this should be highlighted when discussing the credibility of the model chain’s capability.

6.2.2 Sensitivity

Upon visual inspection of the conducted sensitivity analysis, it is apparent that the model chain’s output varies based on the grid point utilized. The differences are most notable for model grid point A. This observation corresponds with the results in Figure 5.1.2. The Figure indicates that model point A yields the highest RMSE value, signifying the most substantial differences when compared to the reference weather data set and grid point D.

An examination of the model outputs from point A and point D reveals that the model chain forecasts a warmer snowpack when Point A (Figure B.1.2) is used as a data source compared to point D (Figure B.2.2). Points A and D predict consistent air temperature (Figure 5.1.1). However, notable deviations are seen in the simulated

net shortwave radiation values. As shortwave radiation is treated as a heat source within the SNOWPACK model (Section 2.5), this parameter is expected to influence the simulated snow temperature. Moreover, SNOWPACK simulates the most pronounced absorption of short wave radiation at the surface, decreasing exponentially with snow depth (Section 2.5). This aligns with the described differences apparent in the sensitivity analysis. This deviation in simulated snow temperatures, combined with variations in net shortwave radiation predictions across different grid points, underscores SNOWPACK's sensitivity to the treatment of shortwave radiation. In particular, it reveals that the shortwave radiation parameter considerably impacts the snow temperatures simulated by the SNOWPACK model.

However, it's not only the snow temperature that is influenced by the variations in net shortwave radiation between the grid points. Given that snow temperature governs essential processes within the snowpack, several differences between the simulations for point A and point D are detected. The most notable difference lies in the snowpack's melt predictions and resulting liquid content. Since the snow temperatures were generally near the melting point for model periods 1 and 2, the additional heat derived from grid point A led to increased melt. This manifested as an elevated liquid water content for the first two model periods. Figure 5.4.4 further demonstrates that this is most pronounced in the top 10 cm of the snowpack. This aligns with the expectation that 90% of the energy from shortwave radiation is absorbed within the top 10 cm of a dry snowpack (McClung & Schaerer, 2006).

As the most significant temperature increase occurs at the top of the snow cover when subjected to shortwave radiation, it could potentially lead to a temperature gradient. Given that the temperature gradient is a crucial factor influencing dry metamorphism, it could possibly induce kinetic growth. This effect became noticeable in model period 1 when using point A data, as the formation of kinetic growth and metamorphism to faceted crystals were detected early in the model period.

However, the simulated grain shape development is quite similar for model periods 3 and 4, although the weather output from the two different AROME-Arctic grid points maintains approximately the same biases. Differences were observed in the projected heating of the snowpack, yet these temperature disparities did not result in various metamorphoses in these scenarios. From these findings, it is clear that SNOWPACK's sensitivity towards shortwave radiation impacts a range of processes and results when snow temperature is altered.

Further, the sensitivity analysis confirmed that the model chain, forced by the point with the closest alignment with the reference weather data set, performed best. This finding supports the conducted methodology of grid point selection, even though non of the reference weather data were collected at the study site. However, it is not certain that this would hold true in all situations and for all weather events. Local variation in cloud coverage, wind speed, and precipitation could be influenced by the distances between the research site and the weather stations used to obtain data for the comparison. This could affect the choice of AROME-Arctic grid point in an unfortunate way. However, as shortwave radiation is generally considered a regional parameter, the biases detected by comparing different AROME-Arctic grid points to the reference weather data set appear to be valid.

6.3 Implications for avalanche forecasting

For site-specific avalanche forecasting in Longyearbyen, the model chain has provided an accurate forecast of the snow cover development over four different model periods and different snow development scenarios. The model output is both a visualization of the expected development as well as an independent opinion on the snow cover evolution. This can be compared with the forecasters' evaluations, and therefore strengthen the performance of avalanche forecasting.

This statement is strengthened as the model chain reproduced the observed weak layers during the field period in an accurate way. The observed snow profile all included ECT stability tests. As described in Section 5.2.1, all tests indicated instability in faceted crystals at the upper part of the snowpack (Figure 5.2.2). These layers were all captured by the model chain output, indicating that the avalanche forecaster would be provided with precise information on the most potent layering for these model periods. This is arguably very favorable for the model chain's usefulness in a forecasting scenario.

However, as described in Section 2.5, SNOWPACK is a one-dimensional model. Due to the limitations of this type of modeling (Section 2.4), topographic effects are not captured. Even though both model period 2 and model period 3 yielded a high agreement score, a visual inspection of Figure 5.4.1, shows that these simulations might be problematic regarding avalanche forecasting. Both periods ended with an observed wind slab, which is not captured in the simulations. This finding is in line with the challenges regarding modeling wind-affected snow encountered by Myhre (2018) and Praz (2018) (Section 2.8). Wind slabs are a common part of the avalanche-prone stratigraphy (Section 2.2), and even though the conducted stability tests show that this was not the avalanche problem or concern for these periods, the lack of capturing this process is a drawback.

Further, for model period 3, the model chain simulated a layer of surface faceted crystals instead of the wind slab (Figure 5.4.1). If surface faceted crystals are buried by wind-deposited snow or new precipitation, it might quickly become a potent avalanche problem. This mistake could, therefore, potentially mislead the avalanche forecasters in the wrong direction. On the other side, the relatively frequent updating using observed profiles limits the extent of these misinterpretations and also the consequences of these mistakes. In this way, it can be argued that the frequent model updating utilizing manual snow profiles increases the robustness of the system. Even though the forecasting period then is shorter, it might increase trust in the model chain.

In light of these findings, the method and framework of the model should be revisited. Currently, the model chain is run for one full model run of AROME-Arctic, implying a 66-hour lead time. By shifting the criteria to update the model state with an observed snow profile to be linked to certain weather events, the model chain could both increase capacity and accuracy. Based both on the documentation of SNOWPACK (Section 2.5), as well as observed weaknesses over the four model periods, high wind speeds, as well as precipitation might be utilized as triggering mechanisms. For the four conducted model periods would lead to manual observations performed after both the 2 and 3 model periods (Figure 5.1.3). Model period 2 could be initiated on model period 1 last time step and would probably still yield high performance. If

the field period would have been extended, model period 5 could have been driven by the output of model period 4. It is hard to foresee if the overall observations would increase or decrease. However, it would potentially ensure that fewer resources are used on field observations during stable periods where changes in the snowpack are expected to be limited. Simultaneously, it would increase validation information regarding the state of the snowpack in demanding and challenging conditions, which in turn could be used as model validation and, over time might be used to improve the model performance. However, it is important to highlight that the critical formation of surface hoar could develop during otherwise stable conditions. As this has the potential to become a potent avalanche problem, it should be considered if a new framework is established.

6.3.1 Implications beyond the case study

The successful establishment and validation of the model chain within this specific location highlight a significant potential for its extension. The high performance encourages exploring the possibility of forecasting across varied geographical scales and avalanche forecasting applications.

In the context of Longyearbyen, which encompasses several avalanche paths, the model chain's adaptability could be further investigated. It would be an intriguing exploration to evaluate the performance of the model chain across a spectrum of these avalanche-prone areas.

Furthermore, considering that both MEPS and AROME-Arctic operate within a shared framework (Section 2.7), transitioning the model chain for application in mainland Norway requires minimal adaptations. Encouragingly, the SNOWPACK model has demonstrated favorable results in regions similar to mainland Norway (Section 2.8.1), and MEPS consistently surpasses AROME-Arctic in performance (Section 2.7.1). It would be beneficial to conduct more detailed studies concerning the adaptation and efficiency of the model chain within mainland Norway's conditions, with highly encouraging findings from the Arctic case study. Moreover, the implementation of ensemble simulations in MEPS (Section 2.6) allows for the visualization of uncertainty in snowpack predictions. This can be achieved by running SNOWPACK with the diverse ensemble outputs from the MEPS model run. Such a modification would be of significant interest if AROME-Arctic were to be launched operationally with ensemble simulations (Section 2.7)

At a more expansive level, the model chain's possible incorporation into regional forecasting is another area of interest. Reflecting on the findings from Canadian studies (Section 2.8), the integration of this model chain could be highly interesting for regional avalanche forecasting for Nordenskiöld Land (Section 3.5). The model chain would need extensive updating, as snow profiles would be a limited resource in such a setup. However, considering the findings of Praz (2018), where the snow cover was modeled over a seasonal scale without updating, and the discoveries in this study as well as those of Myhre (2018), it is worth exploring how SNOWPACK coupled with AROME-Arctic could be integrated into the developed framework of Horton and Haegeli (2022) to set up a regional forecast in the Arctic region. If successful, it could revolutionize avalanche forecasting in Svalbard, especially considering the relatively sparse or spatially concentrated manual observations.

6.4 Limitations

The conducted research and chosen methodology have limitations. The three most important limitations, which were considered when the study was planned and set up, are provided in the following summary.

Selection of AROME-Arctic grid point. The observed weather data used as a reference value to compare AROME-Arctic grid points was a synthetic data set constructed based on observations from two weather stations. Neither of these stations was located at the research site. This is important to highlight, as this data set was considered the optimal performance benchmark when choosing an AROME-Arctic grid cell. Even though this was evaluated to be the best approach within the existing framework of weather stations, it might not accurately represent the true events at the research site.

The model chain was tested on a limited data set. The AROME-Arctic and SNOWPACK model chain was tested over fourteen days and at only one location. Further studies, considering a longer temporal scale and multiple research sites, could strengthen the conducted research. Due to the timeframe of this master's thesis, the research was limited to one research site and a field period of two weeks. However, the representativeness of the findings beyond the conducted study period was discussed.

Stability tests are not included. Even though the model chain provides an overview of the stratigraphy of the snowpack, the model chain used in this research does not provide stability indications. To limit the scope of the conducted work, the existing function in the SNOWPACK model was not utilized, and new research on the topic, conducted by Mayer et al. (2023), was not included. Therefore, the output of the model chain provides an overview of the stratigraphy without information on the strength of the layers.

6.5 Future research

Based on the limitations and findings of the conducted study, future studies are encouraged to incorporate the following aspects.

Numerical weather prediction grid point selection. The conducted research found that choosing the optional method to translate the gridded weather data to the point simulation of the snowpack is not straightforward. It is encouraged to research further how this data extraction should be done optimally, considering other methods than utilized in this research. Perhaps an average or even median value over several grid points could be a better approach than using only one grid point as a data provider. Further, the selection method should make sure sensitive parameters are accounted for. This research indicated that net shortwave radiation should be given extra consideration when determining which grid point should be utilized. Lastly, the grid selection should be incorporated in an atomized way.

Forecasting periods. It would be interesting to explore the potential and consequences of optimizing the SNOWPACK model with a more dynamic framework for triggering updates based on specific weather events. Research could be conducted to identify and validate which types of weather should be utilized as triggering events for snow profile updates and when the model could continue to run on AROME-Arctic. This approach could potentially increase the model's capacity and accuracy while conserving resources during stable periods.

Wind drift. As wind drift is an important factor for the Longyearbyen community, it should be evaluated if the current model chain should be expanded to a model that can incorporate this. Even though not used operationally, there are several snow drift models, and looking into incorporating a wind drift model into the AROME-Arctic, SNOWPACK model chain is encouraged.

Stability estimation. As described in Section 6.4, the model chain currently does not provide information on the restiveness of the snowpack. However, the promising findings of Mayer et al. (2023) could potentially improve this aspect of the model chain and thereby improve its usefulness in operational avalanche forecasting. Further investigations of the model chain expansion would be highly interesting.

Expanding the model chain. The overall promising results of the case study encourage further investigations into the expansion of the model chain. Both considering the expansion into regional avalanche forecast utilizing the framework developed by the Canadian avalanche research community (e.g., Horton et al., 2020), as well as expanding the use of the model to mainland Norway. The latter would provide the opportunity to investigate how NWP ensembles could be utilized to highlight and visualize the uncertainty regarding the forecasting of the snowpack.

Chapter 7

Conclusion

Chapter 7 closes this thesis with concluding remarks on acquired insights built on the discussion in Chapter 6.

Section 7.1 provides an overview of how this study helped close the knowledge gap stated in Section 2.8 by answering the research questions stated in Section 1.2.

7.1 Concluding remarks

This study advances knowledge on how numerical snowpack modeling forced by NWP and manually observed snow profiles can improve avalanche forecasting. The progress is achieved by enhancing insight into the convergence between snow cover modeling in avalanche forecasting, SNOWPACK forced with NWP data, and snow cover modeling in the Arctic. This is gained by answering the three stated research questions based on conclusions drawn from Chapter 6.

To what degree does weather prediction data from AROME-Arctic provide suitable input for numerical snowpack modeling?

AROME-Arctic demonstrated the capability to provide high-quality data for SNOWPACK modeling. Nonetheless, notable variability was found between the models' grid points, suggesting that AROME-Arctic is sensitive to localized and complex terrain features. Therefore, substantial attention and careful consideration should be given to the transformation from grid- to point data. Furthermore, a validation period is recommended before setting up an operational AROME-Arctic and SNOWPACK model chain.

How accurately does the SNOWPACK model forced by AROME-Arctic and a manually observed snow profile forecast the development of the snowpack?

The AROME-Arctic and SNOWPACK model chain consistently demonstrated high accuracy in predicting snowpack development throughout the tested period when initiated by a manually observed snow profile. The robust performance was consistent across different weather scenarios leading to a range of snow processes being evaluated. Potential error sources associated with manual observations did not notably affect the impression of overall performance, increasing the model chain's reliability. However, the model chain showed sensitivity to AROME-Arctic grid point selection. Further, shortwave radiation was found to significantly influence the snowpack's temperature and, thereby, the metamorphism of the snowpack.

To what extent is the performance of SNOWPACK forced by AROME-Arctic and a manually observed snow profile useful for avalanche forecasting?

The strong performance of the model chain indicates a significant potential to aid avalanche forecasting. The visualized grain shape, temperature, and liquid water development provide valuable information to an avalanche forecaster. The model's capability to accurately replicate weak layers and capture avalanche problems in the Arctic snowpack underscores its utility in site-specific avalanche forecasting in Svalbard. However, the model chain does not capture wind effects, which should be considered if used operationally. This is especially important in a setting like Svalbard, where avalanche hazard is directly related to wind transport. A potential remedy could be to adjust the frequency of manual model updates based on weather conditions. Moreover, the findings from this case study imply that the model chain might benefit site-specific avalanche forecasting in other locations and possibly be incorporated into a broader framework for regional avalanche forecasting.

By answering the posed research questions, this thesis demonstrates that numerical snowpack modeling, when combined with NWP and manually observed snow profiles, has substantial potential to refine future avalanche forecasting.

References

- Aguado, E., & Burt, J. E. (2015). Chapter 13: Weather Forecasting and Analysis. In *Understanding weather and climate* (7th). Pearson.
- Bellaire, S., & Jamieson, B. (2013). Forecasting the formation of critical snow layers using a coupled snow cover and weather model. *Cold Regions Science and Technology*, *94*, 37–44. <https://doi.org/10.1016/j.coldregions.2013.06.007>
- Bellaire, S., Jamieson, J., & Fierz, C. (2011). Forcing the snow-cover model SNOWPACK with forecasted weather data. *Cryosphere*, *5*(4), 1115–1125. <https://doi.org/10.5194/tc-5-1115-2011>
- Bellaire, S., van Herwijnen, A., Mitterer, C., & Schweizer, J. (2017). On forecasting wet-snow avalanche activity using simulated snow cover data. *Cold Regions Science and Technology*, *144*, 28–38. <https://doi.org/10.1016/j.coldregions.2017.09.013>
- Bennett, N. D., Croke, B. F. W., Guariso, G., Guillaume, J. H. A., Hamilton, S. H., Jakeman, A. J., Marsili-Libelli, S., Newham, L. T. H., Norton, J. P., Perrin, C., Pierce, S. A., Robson, B., Seppelt, R., Voinov, A. A., Fath, B. D., & Andreassian, V. (2013). Characterising performance of environmental models. *Environmental Modelling & Software*, *40*, 1–20. <https://doi.org/10.1016/j.envsoft.2012.09.011>
- Brun, E., David, P., Sudul, M., & Brunot, G. (1992). A numerical model to simulate snow-cover stratigraphy for operational avalanche forecasting. *Journal of Glaciology*, *38*(128), 13–22. <https://doi.org/10.3189/S0022143000009552>
- Brun, E., Martin, Simon, V., Gendre, C., & Coleou, C. (1989). An Energy and Mass Model of Snow Cover Suitable for Operational Avalanche Forecasting. *Journal of Glaciology*, *35*(121), 333–342. <https://doi.org/10.3189/S0022143000009254>
- Brun, E., Yang, Z.-L., Essery, R., & Cohen, J. (2008). Snow-cover parameterization and modeling. In *Snow and climate: Physical processes, surface energy exchange and modeling*. Cambridge University Press.
- Building Acts and Regulations. (2017). *Byggteknisk forskrift (TEK17) med veiledning*. Kommunal- og distriktsdepartementet.
- Casas-Mulet, R., Alfredsen, K., Boissy, T., Sundt, H., & R  ther, N. (2015). Performance of a One-Dimensional Hydraulic Model for the Calculation of Stranding Areas in Hydropeaking Rivers. *River Research and Applications*, *31*(2), 143–155. <https://doi.org/10.1002/rra.2734>
- Christiansen, H. H., Humlum, O., & Eckerstorfer, M. (2013). Central Svalbard 2000–2011 Meteorological Dynamics and Periglacial Landscape Response. *Arctic, Antarctic*

- tic, and Alpine Research*, 45(1), 6–18. <https://doi.org/10.1657/1938-4246-45.16>
- Colbeck, S. C. (1980). Thermodynamics of snow metamorphism due to variations in curvature. *Journal of Glaciology*, 26(94), 291–301. <https://doi.org/10.3189/S0022143000010832>
- Dingman, S. L. (2015). *Physical Hydrology: Third Edition*. Waveland Press.
- Durand, Y., Guyomarc'h, G., Mérindol, L., & Corripio, J. G. (2005). Improvement of a numerical snow drift model and field validation. *Cold Regions Science and Technology*, 43(1), 93–103. <https://doi.org/10.1016/j.coldregions.2005.05.008>
- Dyrørdal, A. V., Isaksen, K., Jacobsen, J. K. S., & Nilsen, I. B. (2020). Present and future changes in winter climate indices relevant for access disruptions in Troms, northern Norway. *Natural Hazards and Earth System Sciences*, 20(6), 1847–1865. <https://doi.org/10.5194/nhess-20-1847-2020>
- Eckerstorfer, M., & Christiansen, H. H. (2011a). The High Arctic Maritime Snow Climate in Central Svalbard. *Arctic, Antarctic, and Alpine Research*, 43(1), 11–21. <https://doi.org/10.1657/1938-4246-43.1.11>
- Eckerstorfer, M., & Christiansen, H. H. (2011b). Topographical and meteorological control on snow avalanching in the Longyearbyen area, central Svalbard 2006–2009. *Geomorphology*, 134(3), 186–196. <https://doi.org/10.1016/j.geomorph.2011.07.001>
- Eckert, N., & Giacona, F. (2023). Towards a holistic paradigm for long-term snow avalanche risk assessment and mitigation. *Ambio*, 52(4), 711–732. <https://doi.org/10.1007/s13280-022-01804-1>
- Endrizzi, S., & Skaugen, T. (2009). Snow simulation and forecasting through all Norway: the SeNorge model. *International Snow Science Workshop Proceedings 2009*.
- Engeset, R. V., Landrø, M., Indreiten, M., Müller, K., Mikkelsen, O. A., & Hoseth, K. I. A. (2020). *Avalanche warning in Svalbard* (Nr. 35/2020). Norwegian Water Resources and Energy Directorate.
- European Avalanche Warning Service. (n.d.). *Avalanche* [Glossary – EAWS]. Retrieved June 11, 2023, from <https://www.avalanches.org/glossary/#avalanche>
- European Avalanche Warning Services. (2022). Site-specific avalanche warning, Definitions and Recommendations. https://www.avalanches.org/wp-content/uploads/2023/04/EN_Site-specific-final-document_final.pdf
- Faber, M. (2007). Risk and safety in civil engineering. lecture notes. *Eidgenössische Technische Hochschule Zürich, ZwiZZ Federal Institute of Technology Zurich*.
- Fierz, C., Armstrong, R. L., Durand, Y., Etchevers, P., Greene, E., McClung, D. M., Nishimura, K., Satyawali, P. K., & Sokratov, S. A. (2009). The international classification for seasonal snow on the ground. *Technical documents in hydrology*, 83.
- Frank, L. (2023). *MET-model_download*. The University Centre in Svalbard. Retrieved May 25, 2023, from <https://github.com/UNISvalbard/unisacsi>
- Fuchs, S., & McAlpin, M. C. (2005). The net benefit of public expenditures on avalanche defence structures in the municipality of Davos, Switzerland [Publisher: Copernicus GmbH]. *Natural Hazards and Earth System Sciences*, 5(3), 319–330. <https://doi.org/10.5194/nhess-5-319-2005>
- Gaume, J., van Herwijnen, A., Gast, T., Teran, J., & Jiang, C. (2019). Investigating the release and flow of snow avalanches at the slope-scale using a unified model

- based on the material point method. *Cold Regions Science and Technology*, 168, 102847. <https://doi.org/10.1016/j.coldregions.2019.102847>
- Gerber, M., Fierz, C., & Haegeli, P. (2013). Visualizing snow profiles. *International Snow Science Workshop Proceedings 2013*.
- Gilrein, E. J., Carvalhaes, T. M., Markolf, S. A., Chester, M. V., Allenby, B. R., & Garcia, M. (2019). Concepts and practices for transforming infrastructure from rigid to adaptable. *Sustainable and Resilient Infrastructure*, 6(3), 213–234. <https://doi.org/10.1080/23789689.2019.1599608>
- Granger, R. (2019). *Crystal growth physics in dry snow metamorphism: characterisation and modeling of kinetic effects* (Doctoral dissertation). Universite Grenoble Alpes.
- Greene, E., Atkins, D., Birkeland, K., Elder, K., Landry, C., Lazar, B., McCammon, I., Moore, M., Sharaf, D., Sternbenz, C., Tremper, B., & Williams, K. (2010). *Snow, Weather, and Avalanches: Observational Guidelines for Avalanche Programs in the United States*. American Avalanche Association.
- Gregow, E., Lindfors, A. V., van der Veen, S. H., Schoenach, D., de Haan, S., & Lindskog, M. (2020). The use of satellite and surface observations for initializing clouds in the HARMONIE NWP model. *Meteorological Applications*, 27(6), e1965. <https://doi.org/10.1002/met.1965>
- Grote, R., Støylen, E., & Ødegaard Køltzow, M. (2022). Arome-arctic - recent developments of a regional high-resolution arctic forecasting system. *EMS Annual Meeting 2022*, (EMS2022-249). <https://doi.org/10.5194/ems2022-249>
- Hagenmuller, P., Viallon, L., Bouchayer, C., Teich, M., Lafaysse, M., & Vionnet, V. (2018). Quantitative Comparison of Snow Profiles. *International Snow Science Workshop Proceedings 2018*.
- Hancock, H. (2021). *Snow avalanche controls, monitoring strategies, and hazard management in Svalbard* (Doctoral dissertation). University of Oslo.
- Hanssen-Bauer, I., Førland, E. J., Hisdal, H., Mayer, S., Sandø, A., & Sorteberg, A. (2019). *Climate in Svalbard 2100 - a knowledge base for climate adaptation* (No. 1/2019). The Norwegian CCS Research Centre.
- Hanssen-Bauer, I., Frøland, E., Haddeland, I., Hisdal, H., Lawrence, D., Mayer, S., Nesje, A., Nilsen, F., Sandven, S., Sandø, A., Sorteberg, A., & Ådlandsvik, B. (2017). *Climate in Norway 2100* (No. 1/2017). Norwegian Environment Agency (Miljødirektoratet).
- Hao, J., Zhang, X., Cui, P., Li, L., Wang, Y., Zhang, G., & Li, C. (2023). Impacts of Climate Change on Snow Avalanche Activity Along a Transportation Corridor in the Tianshan Mountains. *International Journal of Disaster Risk Science*. <https://doi.org/10.1007/s13753-023-00475-0>
- Haslestad, A., & Larsen, H. T. (2022). *Snøprofil* (Fakta No. 01/2022). Norwegian Water Resources and Energy Directorate.
- Herla, F., Horton, S., Mair, P., & Haegeli, P. (2021a). Snow profile alignment and similarity assessment for aggregating, clustering, and evaluating snowpack model output for avalanche forecasting. *Geoscientific Model Development*, 14(1), 239–258. <https://doi.org/10.5194/gmd-14-239-2021>
- Herla, F., Haegeli, P., Horton, S., & Mair, P. (2023, April 13). *A Large-scale Validation of Snowpack Simulations in Support of Avalanche Forecasting Focusing on Critical Layers*. EGUsphere. <https://doi.org/10.5194/egusphere-2023-420>

- Herla, F., Haegeli, P., & Mair, P. (2022). A data exploration tool for averaging and accessing large data sets of snow stratigraphy profiles useful for avalanche forecasting. *The Cryosphere*, *16*(8), 3149–3162. <https://doi.org/10.5194/tc-16-3149-2022>
- Herla, F., Horton, S., Mair, P., & Haegeli, P. (2021b). Supplement of Snow profile alignment and similarity assessment for aggregating, clustering, and evaluating snowpack model output for avalanche forecasting. *Geoscientific Model Development*, *14*, 239–258. <https://doi.org/https://doi.org/10.5194/gmd-14-239-2021-supplement>
- Horton, S., & Haegeli, P. (2022). Using snow depth observations to provide insight into the quality of snowpack simulations for regional-scale avalanche forecasting. *The Cryosphere*, *16*(8), 3393–3411. <https://doi.org/10.5194/tc-16-3393-2022>
- Horton, S., Nowak, S., & Haegeli, P. (2020). Enhancing the operational value of snowpack models with visualization design principles. *Natural Hazards and Earth System Sciences*, *20*(6), 1557–1572. <https://doi.org/10.5194/nhess-20-1557-2020>
- Humlum, O., Instanes, A., & Sollid, J. L. (2003). Permafrost in Svalbard: a review of research history, climatic background and engineering challenges. *Polar Research*, *22*(2), 191–215. <https://doi.org/10.3402/polar.v22i2.6455>
- Isaksen, K., Nordli, Ø., Førland, E. J., Łupikasza, E., Eastwood, S., & Niedźwiedź, T. (2016). Recent warming on Spitsbergen—Influence of atmospheric circulation and sea ice cover. *Journal of Geophysical Research: Atmospheres*, *121*(20), 11, 913–11, 931. <https://doi.org/10.1002/2016JD025606>
- Isaksen, K., Nordli, Ø., Ivanov, B., Køltzow, M. A. Ø., Aaboe, S., Gjelten, H. M., Mezghani, A., Eastwood, S., Førland, E., Benestad, R. E., Hanssen-Bauer, I., Brækkan, R., Sviashchennikov, P., Demin, V., Revina, A., & Karandasheva, T. (2022). Exceptional warming over the Barents area. *Scientific Reports*, *12*(1), 9371. <https://doi.org/10.1038/s41598-022-13568-5>
- Jaedicke, C., & Sandvik, A. D. (2002). High resolution snow distribution data from complex Arctic terrain: a tool for model validation. *Natural Hazards and Earth System Sciences*, *2*(3), 147–155. <https://doi.org/10.5194/nhess-2-147-2002>
- Jaedicke, C., Studerregger, A., Monti, F., Dellavedova, P., Stoffel, L., Azzarello, S., Garcia, C., Molné, T., & Bellido, G. M. (2018). Local avalanche warning in Europe. *International Snow Science Workshop Proceedings 2018*.
- Jóhannesson, T., Gauer, P., Hákonardóttir, K. M., Margreth, S., Pálsson, H., & Sigtryggsdóttir, F. G. (2019). International Symposium on Mitigation Measures against Snow Avalanches and other Rapid Gravity Mass Flows. *Science steering and Editorial committee*, 242.
- Jordan, R., Albert, M. R., & Brun, E. (2008). Physical processes within the snow cover and their parameterization. In *Snow and climate: Physical processes, surface energy exchange and modeling* (pp. 12–69). Cambridge University Press.
- Køltzow, M., Casati, B., Bazile, E., Haiden, T., & Valkonen, T. (2019). An NWP Model Intercomparison of Surface Weather Parameters in the European Arctic during the Year of Polar Prediction Special Observing Period Northern Hemisphere 1. *Weather and Forecasting*, *34*(4), 959–983. <https://doi.org/10.1175/WAF-D-19-0003.1>
- Krinner, G., Derksen, C., Essery, R., Flanner, M., Hagemann, S., Clark, M., Hall, A., Rott, H., Brutel-Vuilmet, C., Kim, H., Ménard, C. B., Mudryk, L., Thack-

- eray, C., Wang, L., Arduini, G., Balsamo, G., Bartlett, P., Boike, J., Boone, A., . . . Zhu, D. (2018). ESM-SnowMIP: Assessing snow models and quantifying snow-related climate feedbacks. *Geoscientific Model Development*, *11*(12), 5027–5049. <https://doi.org/10.5194/gmd-11-5027-2018>
- LaChapelle, E. R. (1980). The Fundamental Processes in Conventional Avalanche Forecasting. *Journal of Glaciology*, *26*(94), 75–84. <https://doi.org/10.3189/S0022143000010601>
- Landrø, M., Hetland, A., Engeset, R. V., & Pfuhl, G. (2020). Avalanche decision-making frameworks: Factors and methods used by experts. *Cold Regions Science and Technology*, *170*, 102897. <https://doi.org/10.1016/j.coldregions.2019.102897>
- Le Roux, E., Evin, G., Eckert, N., Blanchet, J., & Morin, S. (2021). Elevation-dependent trends in extreme snowfall in the French Alps from 1959 to 2019. *The Cryosphere*, *15*(9), 4335–4356. <https://doi.org/10.5194/tc-15-4335-2021>
- Lehning, M., Bartelt, P., Brown, B., Russi, T., Stöckli, U., & Zimmerli, M. (1999). SNOWPACK model calculations for avalanche warning based upon a new network of weather and snow stations. *Cold Regions Science and Technology*, *30*(1), 145–157. [https://doi.org/10.1016/S0165-232X\(99\)00022-1](https://doi.org/10.1016/S0165-232X(99)00022-1)
- Lehning, M., Löwe, H., Ryser, M., & Raderschall, N. (2008). Inhomogeneous precipitation distribution and snow transport in steep terrain. *Water Resources Research*, *44*(7). <https://doi.org/10.1029/2007WR006545>
- Lehning, M., & Bartelt, P. (2002). A physical SNOWPACK model for the Swiss avalanche warning Part I: Numerical model. *Cold Regions Science and Technology*, *35*. [https://doi.org/10.1016/S0165-232X\(02\)00074-5](https://doi.org/10.1016/S0165-232X(02)00074-5)
- Lehning, M., Bartelt, P., Brown, B., & Fierz, C. (2002a). A physical SNOWPACK model for the Swiss avalanche warning Part III: Meteorological forcing, Thin layer formation and evaluation. *Cold Regions Science and Technology*, *35*. [https://doi.org/10.1016/S0165-232X\(02\)00072-1](https://doi.org/10.1016/S0165-232X(02)00072-1)
- Lehning, M., Bartelt, P., Brown, B., Fierz, C., & Satyawali, P. (2002b). A physical SNOWPACK model for the Swiss avalanche warning Part II: Snow microstructure. *Cold Regions Science and Technology*, *35*. [https://doi.org/10.1016/S0165-232X\(02\)00073-3](https://doi.org/10.1016/S0165-232X(02)00073-3)
- Lehning, M., Fierz, C., & Lundy, C. (2001). An objective snow profile comparison method and its application to SNOWPACK. *Cold Regions Science and Technology*, *33*(2), 253–261. [https://doi.org/10.1016/S0165-232X\(01\)00044-1](https://doi.org/10.1016/S0165-232X(01)00044-1)
- Lied, K., & Kristensen, K. (2003). *Snøskred. Håndbok om snøskred*. Vett & Viten as i samarbeid med NGI.
- Lindin, I. (2023). *Over 49 000 bygninger trenger bedre sikring mot skred* [Faktisk]. Retrieved June 1, 2023, from <https://www.faktisk.no/artikler/jn293/over-49-000-bygninger-trenger-bedre-sikring-mot-skred>
- Liston, G. E., Haehnel, R. B., Sturm, M., Hiemstra, C. A., Berezovskaya, S., & Tabler, R. D. (2007). Simulating complex snow distributions in windy environments using SnowTran-3d. *Journal of Glaciology*, *53*(181), 241–256. <https://doi.org/10.3189/172756507782202865>
- Mayer, S. I., Techel, F., Schweizer, J., & van Herwijnen, A. (2023). Prediction of natural dry-snow avalanche activity using physics-based snowpack simulations. *EGUsphere*, 1–33. <https://doi.org/10.5194/egusphere-2023-646>

- McClung, D. M. (2000). Predictions in avalanche forecasting. *Annals of Glaciology*, 31, 377–381. <https://doi.org/10.3189/172756400781820507>
- McClung, D. M. (2002). The Elements of Applied Avalanche Forecasting, Part I: The Human Issues. *Natural Hazards*, 26(2), 111–129. <https://doi.org/10.1023/A:1015665432221>
- McClung, D., & Schaerer, P. A. (2006). *The Avalanche Handbook*. The Mountaineers Books.
- Morin, S., Horton, S., Techel, F., Bavay, M., Coléou, C., Fierz, C., Gobiet, A., Hagenmuller, P., Lafaysse, M., Ližar, M., Mitterer, C., Monti, F., Müller, K., Olefs, M., Snook, J. S., van Herwijnen, A., & Vionnet, V. (2020). Application of physical snowpack models in support of operational avalanche hazard forecasting: A status report on current implementations and prospects for the future. *Cold Regions Science and Technology*, 170, 102910. <https://doi.org/10.1016/j.coldregions.2019.102910>
- Müller, K., Landrø, M., Haslestad, A., Dahlstrup, J., & Engset, R. (2015). *Systematisk snødekkeundersøkelse* (No. 1/2015). Norwegian Water Resources and Energy Directorate.
- Müller, M., Batrak, Y., Kristiansen, J., Køltzow, M. A. Ø., Noer, G., & Korosov, A. (2017a). Characteristics of a Convective-Scale Weather Forecasting System for the European Arctic. *Monthly Weather Review*, 145(12), 4771–4787. <https://doi.org/10.1175/MWR-D-17-0194.1>
- Müller, M., Homleid, M., Køltzow, M. A. Ø., Lindskog, M., Midtbø, K., Andrae, U., Aspelien, T., Berggren, L., Bjørge, D., Dahlgren, P., Kristiansen, J., Randriamampianina, R., Ridal, M., Vignes, O., & Ivarsson, K. (2017b). AROME-MetCoOp: A Nordic Convective-Scale Operational Weather Prediction Model. *Weather and Forecasting*, 32(2), 609–627. <https://doi.org/10.1175/WAF-D-16-0099.1>
- Myhre, M. (2018). *Model Based Snow Cover Analysis Regarding the Avalanches in Longyearbyen 2015 and 2017* (Master's Thesis). University of Oslo.
- Norwegian Meteorological Institute. (2019). *About AROME-Arctic* [Norwegian Meteorological Institute]. Retrieved May 24, 2023, from <https://www.met.no/en/projects/The-weather-model-AROME-Arctic/about>
- Norwegian Water Resources and Energy Directorate. (2022). *Felthåndbok for snø- og skredobservasjoner*.
- Nuth, C., Kohler, J., König, M., von Deschwanden, A., Hagen, J. O., Käab, A., Moholdt, G., & Pettersson, R. (2013). Decadal changes from a multi-temporal glacier inventory of Svalbard. *The Cryosphere*, 7(5), 1603–1621. <https://doi.org/10.5194/tc-7-1603-2013>
- Olefs, M., Schöner, W., Suklitsch, M., Wittmann, C., Niedermoser, B., Neururer, A., & Wurzer, A. (2013). SNOWGRID - A new operational snow cover model in Austria. *International Snow Science Workshop Proceedings 2013*.
- Onarheim, I. H., Smedsrud, L. H., Ingvaldsen, R. B., & Nilsen, F. (2014). Loss of sea ice during winter north of Svalbard. *Tellus A: Dynamic Meteorology and Oceanography*, 66(1). <https://doi.org/10.3402/tellusa.v66.23933>
- Peeters, B., Pedersen, Å. Ø., Loe, L. E., Isaksen, K., Veiberg, V., Stien, A., Kohler, J., Gallet, J.-C., Aanes, R., & Hansen, B. B. (2019). Spatiotemporal patterns of rain-on-snow and basal ice in high Arctic Svalbard: detection of a climate-

- cryosphere regime shift. *Environmental Research Letters*, 14(1), 015002. <https://doi.org/10.1088/1748-9326/aaefb3>
- Pomeroy, J. W., Gray, D. M., & Landine, P. G. (1993). The Prairie Blowing Snow Model: characteristics, validation, operation. *Journal of Hydrology*, 144(1), 165–192. [https://doi.org/10.1016/0022-1694\(93\)90171-5](https://doi.org/10.1016/0022-1694(93)90171-5)
- Praz, M. (2018). *Modelling the Arctic snowpack properties in Svalbard using SNOWPACK* (Master's Thesis). École polytechnique fédérale de Lausanne & The University Centre in Svalbard.
- Randriamampianina, R., Bormann, N., Køltzow, M. A. Ø., Lawrence, H., Sandu, I., & Wang, Z. Q. (2021). Relative impact of observations on a regional Arctic numerical weather prediction system. *Quarterly Journal of the Royal Meteorological Society*, 147(737), 2212–2232. <https://doi.org/10.1002/qj.4018>
- Randriamampianina, R., Schyberg, H., & Mile, M. (2019). Observing System Experiments with an Arctic Mesoscale Numerical Weather Prediction Model. *Remote Sensing*, 11(8), 981. <https://doi.org/10.3390/rs11080981>
- Rantanen, M., Karpechko, A. Y., Lipponen, A., Nordling, K., Hyvärinen, O., Ruosteenoja, K., Vihma, T., & Laaksonen, A. (2022). The Arctic has warmed nearly four times faster than the globe since 1979. *Communications Earth & Environment*, 3(1), 1–10. <https://doi.org/10.1038/s43247-022-00498-3>
- Rudolf-Miklau, F., Sauermoser, S., & Mears, A. I. (2015). *The Technical Avalanche Protection Handbook*. <https://doi.org/10.1002/9783433603840>
- Saloranta, T. M. (2012). Simulating snow maps for Norway: description and statistical evaluation of the seNorge snow model. *The Cryosphere*, 6(6), 1323–1337. <https://doi.org/10.5194/tc-6-1323-2012>
- Schweizer, J., Bartelt, P., & van Herwijnen, A. (2015). Snow avalanches. In *Snow and ice-related hazards, risks, and disasters* (pp. 395–436). <https://doi.org/10.1016/B978-0-12-394849-6.00012-3>
- Schweizer, J., Kronholm, K., Jamieson, J. B., & Birkeland, K. W. (2008). Review of spatial variability of snowpack properties and its importance for avalanche formation. *Cold Regions Science and Technology*, 51(2), 253–272. <https://doi.org/10.1016/j.coldregions.2007.04.009>
- Schweizer, J., & Wiesinger, T. (2001). Snow profile interpretation for stability evaluation. *Cold Regions Science and Technology*, 33(2), 179–188. [https://doi.org/10.1016/S0165-232X\(01\)00036-2](https://doi.org/10.1016/S0165-232X(01)00036-2)
- Simenhois, R., & Birkeland, K. (2006). The extended column test: a field test for fracture initiation and propagation. *Proceedings of the International Snow Science Workshop 2006*.
- Singleton, A. (2022). *Addressing predictability in the AROME-Arctic ensemble using Stochastically Perturbed Parameters (SPP) and Ensemble Data Assimilation (EDA)* (METreport No. 13/2022). Norwegian Meteorological Institute.
- Statham, G., Haegeli, P., Greene, E., Birkeland, K., Israelson, C., Tremper, B., Stethem, C., McMahan, B., White, B., & Kelly, J. (2018). A conceptual model of avalanche hazard. *Natural Hazards*, 90(2), 663–691. <https://doi.org/10.1007/s11069-017-3070-5>
- Stoll, P. J., Valkonen, T. M., Graverson, R. G., & Noer, G. (2020). A well-observed polar low analysed with a regional and a global weather-prediction model. *Quarterly Journal of the Royal Meteorological Society*, 146(729), 1740–1767. <https://doi.org/10.1002/qj.3764>

- Strapazzon, G., Schweizer, J., Chiambretti, I., Brodmann Maeder, M., Brugger, H., & Zafren, K. (2021). Effects of Climate Change on Avalanche Accidents and Survival. *Frontiers in Physiology*, 12. Retrieved February 17, 2023, from <https://www.frontiersin.org/articles/10.3389/fphys.2021.639433>
- Sysselmesteren på Svalbard. (2023). *Lokal snøskredvarsling for bebyggelse i Longyearbyen* [Sysselmesteren på Svalbard]. Retrieved May 29, 2023, from <https://www.sysselmesteren.no/nb/om-sysselmesteren/samfunnssikkerhet-og-beredskap/lokal-snoskredvarsling-for-bebyggelse-i-longyearbyen/>
- Techel, F., Jarry, F., Kronthaler, G., Mitterer, S., Nairz, P., Pavšek, M., Valt, M., & Darms, G. (2016). Avalanche fatalities in the European Alps: long-term trends and statistics. *Geographica Helvetica*, 71(2), 147–159. <https://doi.org/10.5194/gh-71-147-2016>
- The Norwegian Directorate for Civil Protection. (2016). *Skredulykken i Longyearbyen 19. desember 2015*. The Norwegian Directorate for Civil Protection.
- Tremper, B. (2018). *Staying Alive in Avalanche Terrain* (3rd Edition). Mountaineers Books.
- Varsom. (2023). *Om snøskredvarslingen*. Retrieved May 30, 2023, from <https://www.varsom.no/snoskred/snoskredvarsling/om-snoskredvarslingen/>
- Vikhamar-Schuler, D., Müller, K., & Engen-Skaugen, T. (2011). *Snow modeling using SURFEX with the CROCUS snow scheme* (No. 7/2011). Norwegian Water Resources and Energy Directorate.
- Vikhamar-Schuler, D., Førland, E., Lutz, J., & Gjelten, H. (2019, February 1). *Evaluation of downscaled reanalysis and observations for Svalbard - Background report for Climate in Svalbard 2100*.
- Vionnet, V., Martin, E., Masson, V., Guyomarc'h, G., Naaim-Bouvet, F., Prokop, A., Durand, Y., & Lac, C. (2014). Simulation of wind-induced snow transport and sublimation in alpine terrain using a fully coupled snowpack/atmosphere model. *The Cryosphere*, 8(2), 395–415. <https://doi.org/10.5194/tc-8-395-2014>
- Wickström, S., Jonassen, M. O., Cassano, J. J., & Vihma, T. (2020). Present Temperature, Precipitation, and Rain-on-Snow Climate in Svalbard. *Journal of Geophysical Research: Atmospheres*, 125(14). <https://doi.org/10.1029/2019JD032155>
- Wilhelm, C., Wiesinger, T., Brundl, M., & Ammann, W. (2000). The avalanche winter 1999 in Switzerland - an overview. *International Snow Science Workshop Proceedings 2000*.
- Zweigel, R. B., Westermann, S., Nitzbon, J., Langer, M., Boike, J., Eitzelmüller, B., & Vikhamar Schuler, T. (2021). Simulating Snow Redistribution and its Effect on Ground Surface Temperature at a High-Arctic Site on Svalbard. *Journal of Geophysical Research: Earth Surface*, 126(3), e2020JF005673. <https://doi.org/10.1029/2020JF005673>

Appendices

The appendices that follow offer additional information, context, and detail to support and expand upon the research presented in this thesis. These resources provide comprehensive insight for readers interested in further exploring relevant terms from snow science, detailed model output, and results from the conducted sensitivity analysis.

Appendix A provides a more detailed explanation of the key concepts in snow science that are utilized throughout this research.

Appendix B offers more in-depth model output from the model chain simulations, supplementing the overview presented within the main report.

Appendix C presents the model chain output for AROME-Arctic grid points B and Point D. These investigations were part of the sensitivity analysis performed according to Section 4.5.7.

Appendix A

Snow Science

Appendix A provides more detailed descriptions of the concepts introduced in Section 2.1 and used throughout this thesis.

Section A.1 provides an overview of snow stratigraphy, including the typical processes resulting in a layered snow cover.

Further, Section A.2 describes snow metamorphism, including a description of wet and dry metamorphism, as well as the two different forms of dry metamorphism: equilibrium- and kinetic growth forms. The section is summarized with a figure visualizing the different processes, the related temperature gradients driving the transformations, and the resulting grain shape.

Section A.3 concludes Appendix A with a brief overview of the spatial variability, including a depiction of spatial variability at different scales.

A.1 Stratigraphy

A seasonal snowpack is formed when average atmospheric temperatures predominantly fall below the freezing point. Then the snowpack grows progressively as the cumulative output of precipitation events throughout the winter. Each event contributes a novel layer of precipitation particles to the terrain or existing snow cover (Dingman, 2015; Lied & Kristensen, 2003). Factors such as the meteorological conditions within the precipitation cloud, the velocity and direction of the wind, and the ground-level air temperature at deposition collectively influence the structure of the precipitation particles. Given the inherent variation in these events, different crystal types are deposited, forming stratification within the snowpack (Dingman, 2015; Fierz et al., 2009). Each stratigraphic layer differs in at least one respect from the layer above or below (Fierz et al., 2009). The snowpack’s stability is primarily connected to the stratigraphic arrangement of the snowpack and the properties of each layer (McClung & Schaerer, 2006). Figure A.1.1 shows an example of a stratified snowpack, with especially two ice layers detectable.



Figure A.1.1: An example of snow stratigraphy, showing two distinct ice layers close to the snowpack’s surface. The picture is taken during this study.

A.2 Metamorphism

The initial state of a stratigraphic layer depends on the configuration of the original precipitation particles. However, the vast variability in snow microstructure results from the multitude of transformations the crystals undergo due to the thermodynamic relationships among the water phases (Jordan et al., 2008). This process, known as metamorphism, begins as soon as snow accumulates on the surface and continues until melting is completed (Dingman, 2015). Given that the temperature of snow is usually close to the melting point, the mass interchange between ice, water vapor, and possibly liquid water is highly dynamic. The main factor resulting in variations in metamorphism is whether liquid water is present. This leads to the classification of metamorphism into dry and wet types (Jordan et al., 2008). An overview of the different types of snow metamorphism, the related temperature gradient, and snow crystals are given in Figure A.2.1.

A.2.1 Dry metamorphism

Dry metamorphism occurs in dry snow where the pore spaces are solely occupied by air, typically saturated with water vapor. The differences in saturated vapor pressure due to variations in temperature and curvature facilitate the onset of two distinct processes, equilibrium- and kinetic growth form (Jordan et al., 2008).

A.2.1.1 Equilibrium growth form

The geometry of a snowflake causes local curvature variations that give rise to differences in saturation vapor pressure. The highest surface tension occurs at the convex ends of the ice branches, instigating sublimation. This vapor is subsequently deposited in concave depressions, with lower saturation vapor pressure. This phenomenon is articulated by Kelvin's expression for the equilibrium vapor pressure over a curved surface and is detailed further in Colbeck (1980). The outcome of this process is a rounding of the snow crystal. However, this effect is slow and only transpires without imposed temperature gradients. Given that temperature within the snow cover typically varies on daily and hourly timescales, metamorphosis is driven solely by curvature differences. It cannot dominate in long-term changes to the snowpack (Colbeck, 1980).

A.2.1.2 Kinetic growth form

Temperature variations induce alterations in saturated vapor pressure. Consequently, vapor diffusion from the warmer crystal surface to the colder one where condensation occurs is stimulated. Given a sufficiently high-temperature gradient, the accelerated growth on the colder surfaces prompts the formation of facets and striations, representing the faceted crystals and depth hoar (Jordan et al., 2008).

A distinct instance of the kinetic growth form, or constructive metamorphosis, is surface hoar development. Surface hoar formation arises during clear, calm, and cold conditions when moist air is instantly sublimated. This process is facilitated by a substantial temperature gradient between the snow surface and the overlaying air, stimulating the transition of water vapor into solid ice, which culminates in the formation of large, feather-like ice crystals (McClung & Schaerer, 2006).

A.2.2 Wet metamorphism

When the snow begins to retain a substantial amount of liquid water, the subsequent metamorphosis significantly alters. At this stage, the snow operates as a tri-phase system composed of ice, air, and liquid water. Nevertheless, as with dry equilibrium metamorphism, the differences in curvature serve as a driving force. The melting temperature over curved ice surfaces is in inverse proportion to the radius of curvature, indicating that the melting temperature reduces as the crystal surface becomes more convex (McClung & Schaerer, 2006). In this way, the smallest crystals melt before the liquid water refreezes onto the bigger crystals. When wet snow refreezes, liquid menisci are encapsulated within the neighboring ice grains, accounting for the accelerated expansion of grains during melting and freezing (Jordan et al., 2008).

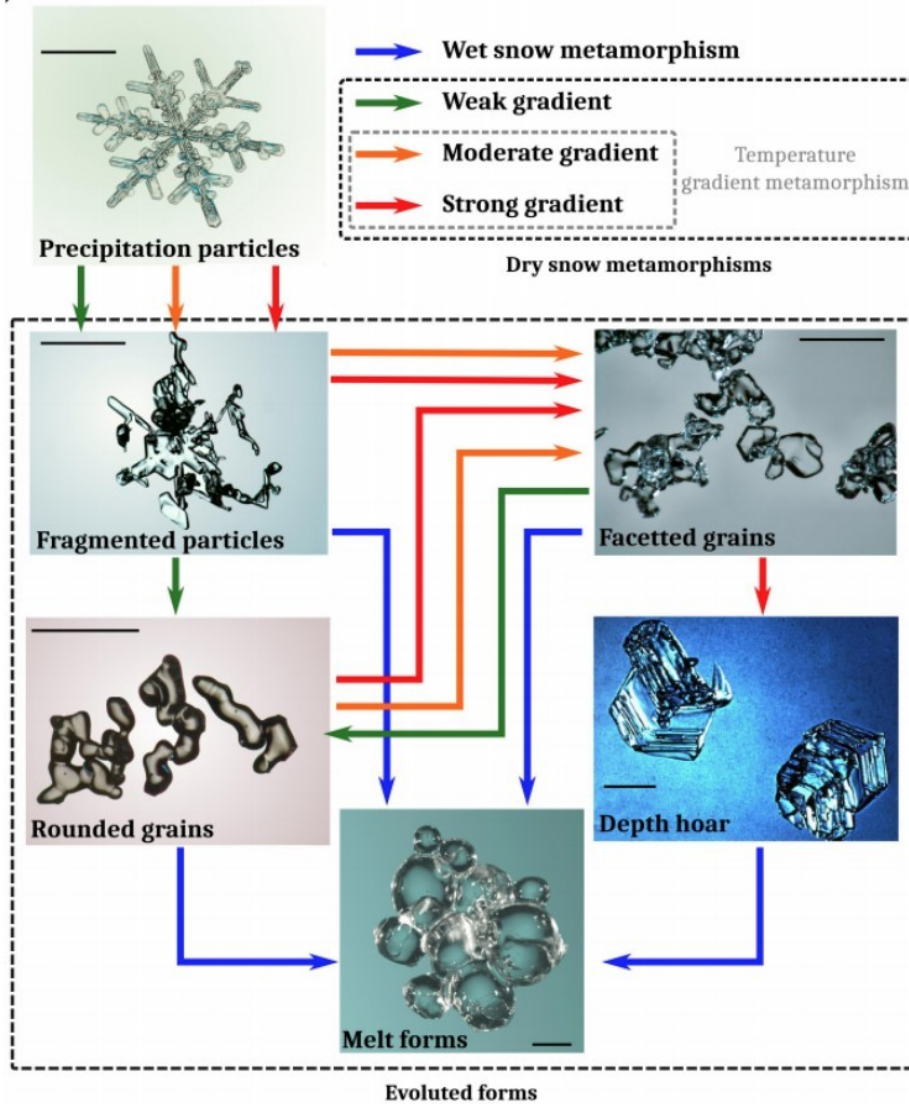


Figure A.2.1: Summary of the relationship between the different metamorphism processes and microscope pictures of grain shape. The horizontal black line in all pictures represents a scale equivalent to 1 mm. The figure is taken from Granger (2019).

A.3 Spatial variability

The seasonal snow cover exhibits substantial spatial variability, a phenomenon most manifested in the heterogeneity of snow depth. Nonetheless, from the standpoint of snow stability assessments, the properties of individual layers are of greater interest due to their critical implications for stability (Schweizer et al., 2008). Spatial variability is caused by external and internal processes, which interact with topography during and post-deposition. Key drivers of this variability are precipitation, sublimation, wind, radiation, and temperature. However, the most pronounced source of spatial variability is the conditions during deposition, with wind-induced dynamics serving as the most influential (Schweizer et al., 2008). Figure A.3.1 provides an example of spatial variability across multiple scales. At the base of the image, there are several abrupt changes in snow height and differences in snow surface characteristics. The mountain in the background shows significant spatial variability at a

larger scale, oscillating between snow-covered areas and those without. It is plausible that wind erosion and deposition have contributed to both the small- and big-scale features.



Figure A.3.1: The picture shows the spatial variable snow cover at the Hiorthfjellet, Longyearbyen. Further, the picture shows spatial differences in snow height over small distances in the picture’s foreground. The picture is taken on 21. April, from this study’s field site.

Numerous studies have additionally shown that layers, especially weak layers, frequently exhibit spatial continuity on a slope scale. It is found that layer properties and structural instability indicators are expected to be less subject to spatial variability than stability scores. Further, it is found that the impact of spatial variability is highly contingent on the methodological approach, specifically the chosen scale triplet (Schweizer et al., 2008).

The scale triplet is defined by support, spacing, and extent. Support refers to the area or volume of each measurement, spacing to the distance between samples, and extent to the maximum distance between two measurement locations, as visualized in Figure A.3.2. The interplay of these three factors significantly influences the interpretation of spatial variability in snowpack studies (Schweizer et al., 2008).

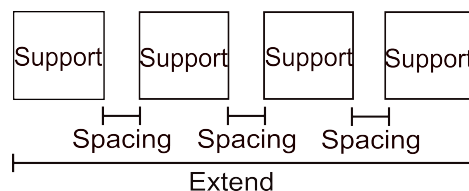


Figure A.3.2: The scale triplet in spatial variability research.

Appendix B

SNOWPACK simulations

The following Appendix gives a detailed presentation of the AROME-Arctic and SNOWPACK model chain predictions and manually observed snow profiles. An overview and the most important features are pointed out in Chapter 5. However, insight gained from considering the detailed output of the model chain where utilized in the discussion in Chapter 6.

For each of the four model periods, the temporal tracking of grain shape, temperature, and liquid water is presented. Where no liquid water is simulated, the Figure is not included.

B.1 Model period 1

Figure B.1.1 shows the SNOWPACK model's temporal tracking of grain shape development during Model Period 1. The model predicts a transition to melt forms for the top 2 cm between 16:00 and 21:00 on 14. April, before a transition back to a melt refreeze crust phase. Another melt metamorphosis is modeled for the same layer, beginning at the last time step of the model output, 08:00 on 15. April. Outside these key transformations, the grain shapes remain consistent across the 66-hour model period.

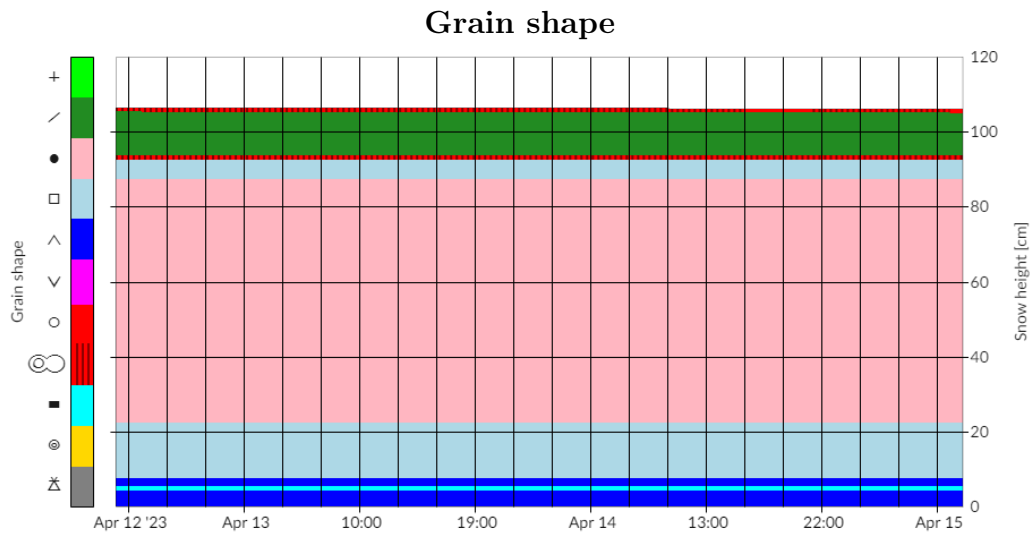


Figure B.1.1: Detailed grain shape development for model period 1.

The modeled thermal development of the snowpack suggests an increase in temperature during the model run, with a convergence towards the melting point at the end of the model period (Figure B.1.2). The temperature decreased during the initial two nights, which was not significantly observed on the night before the closing phase of the model period.

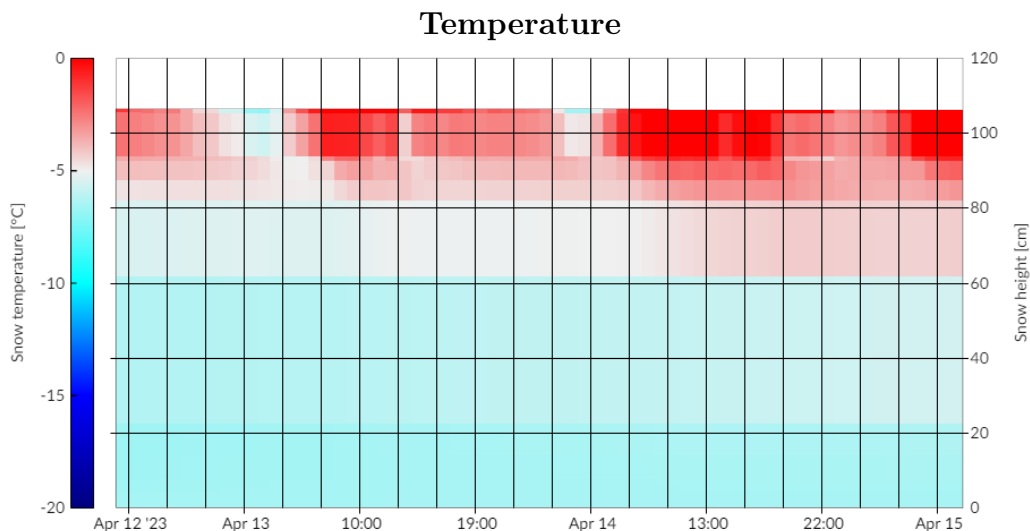


Figure B.1.2: Detailed thermal development model period 1.

The appearance of meltwater is simulated between 16:00 and 21:00 on 14. April, and commencing at 08:00 on 15. April (Figure B.1.3). This temporal distribution coincides with the temperature escalation (Figure B.1.2) and the metamorphic changes (Figures B.1.1).

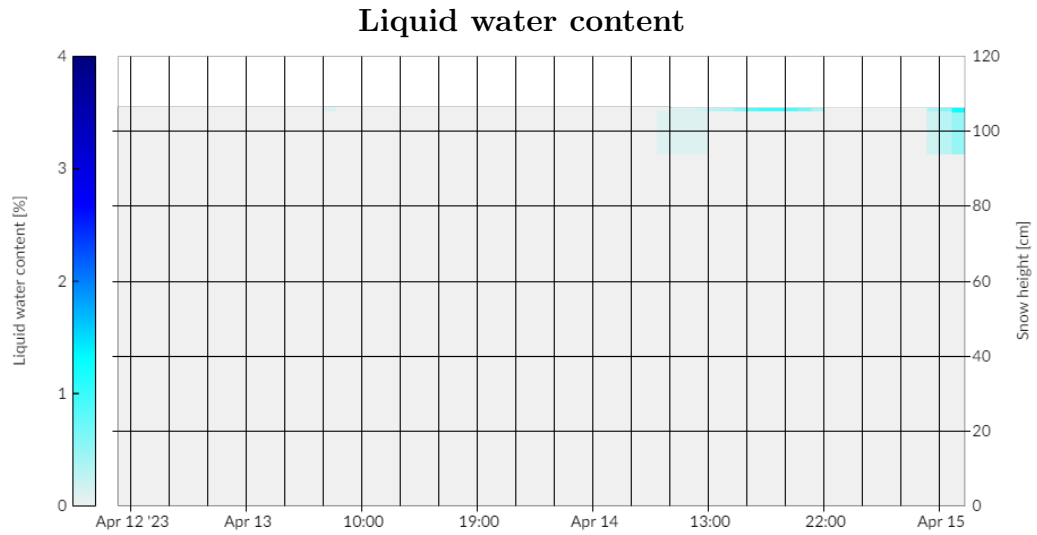


Figure B.1.3: Detailed simulated liquid water content for model period 1.

B.2 Model period 2

In Model Period 2, the model chain forecasts four grain shape transformations (Figure B.2.1). The uppermost 2 cm of the snowpack undergoes a melt/refreeze cycle, predicted to be in a frozen state from 14:00 on 15. April to 08:00 on 16. April, subsequently transitioning to melt forms until 14:00 on 17. April. Following this, a freezing phase is anticipated until the simulation's termination. The second stratigraphic layer is projected to transition from decomposing and fragmented precipitation particles to faceted crystals at midday on 16. April.

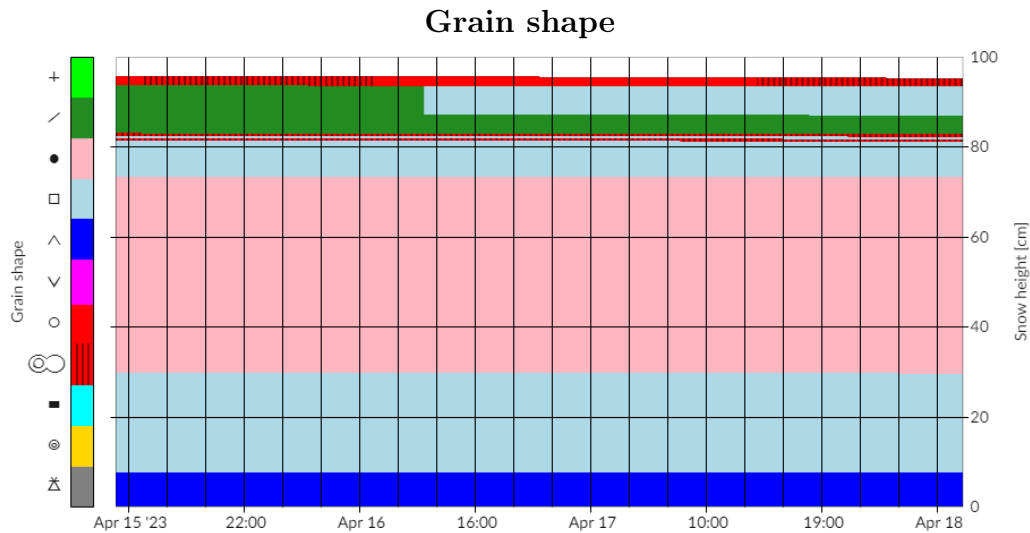


Figure B.2.1: Detailed grain shape development for model period 2.

The modeled thermal development illustrates a relatively warm snowpack for the initial half of model period 2, with a subsequent cooling phase (Figure B.2.2). A notable temperature gradient is evident within the snowpack on 16. April. The interval from the start of 16. April to 17. April manifests particularly elevated temperatures, with correspondingly high liquid water content (Figure B.2.3).

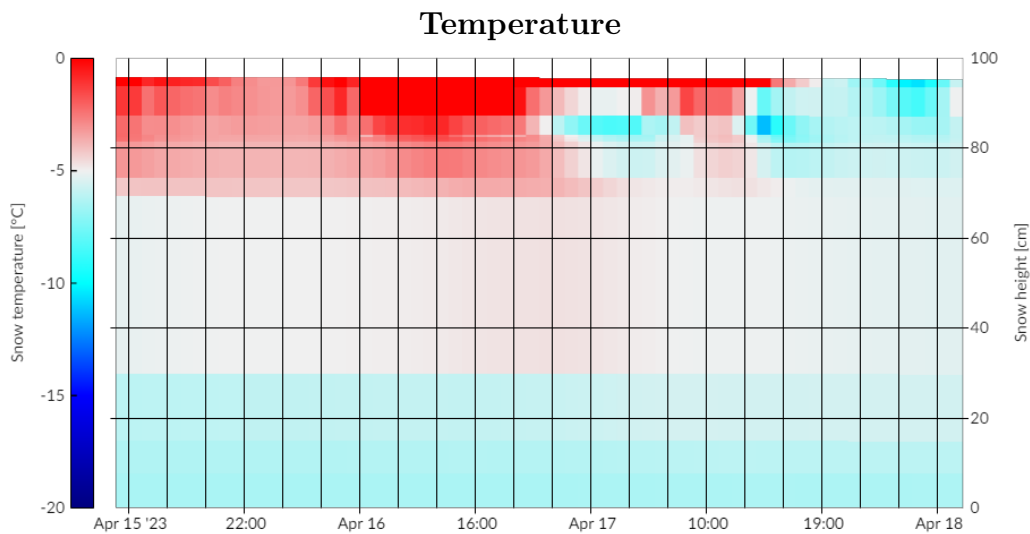


Figure B.2.2: Detailed thermal development model period 3.

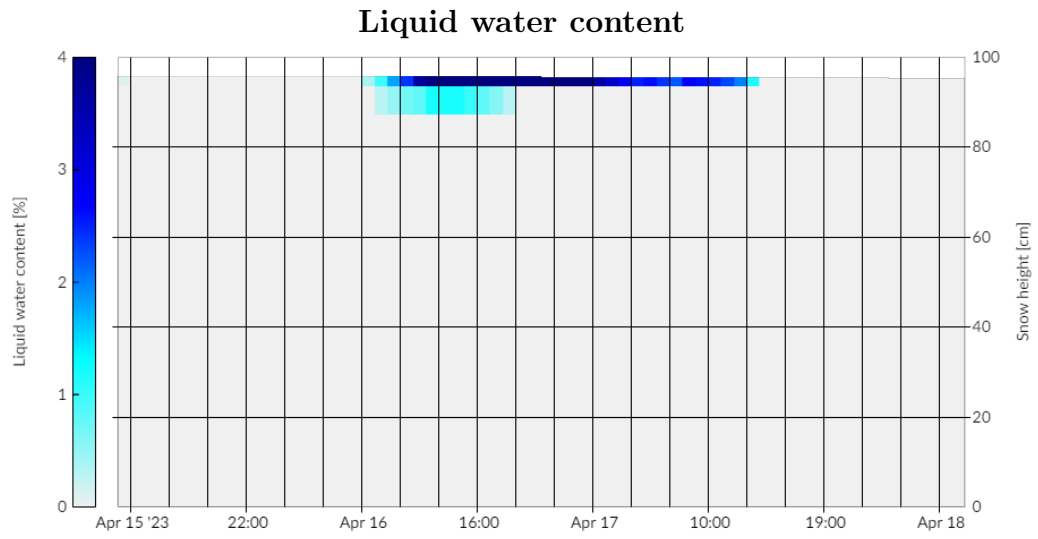


Figure B.2.3: Detailed simulated liquid water content for model period 4.

B.3 Model period 3

Model period 3 anticipates a modest increase in snow depth due to precipitation on the evening of 18. April. Then a swift metamorphism to rounded grains is foreseen prior to the occurrence of surface faceting (Figure B.3.1) By 20. April, the model chain predicts a complete metamorphosis of all snow layers above the melt refreeze layer into faceted crystals. The model output of liquid water is not included, as no liquid water was modeled during the time series.

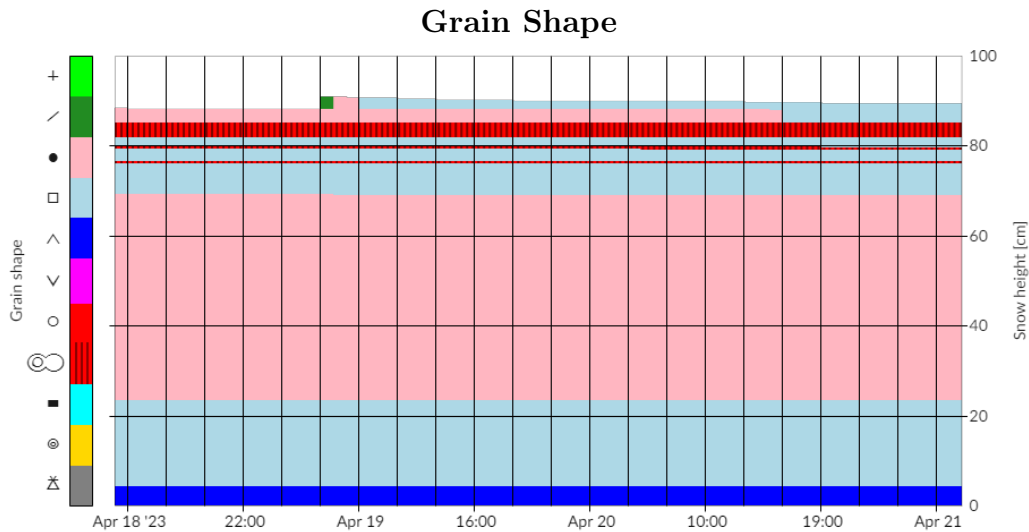


Figure B.3.1: Detailed grain shape development for model period 3.

The simulation predicts a swift cooling of the snowpack. The surface temperature is projected to cool from 0°C to approximately -15°C. This pronounced cooling process began on 20. April, and induced a significant temperature gradient (Figure B.3.2).

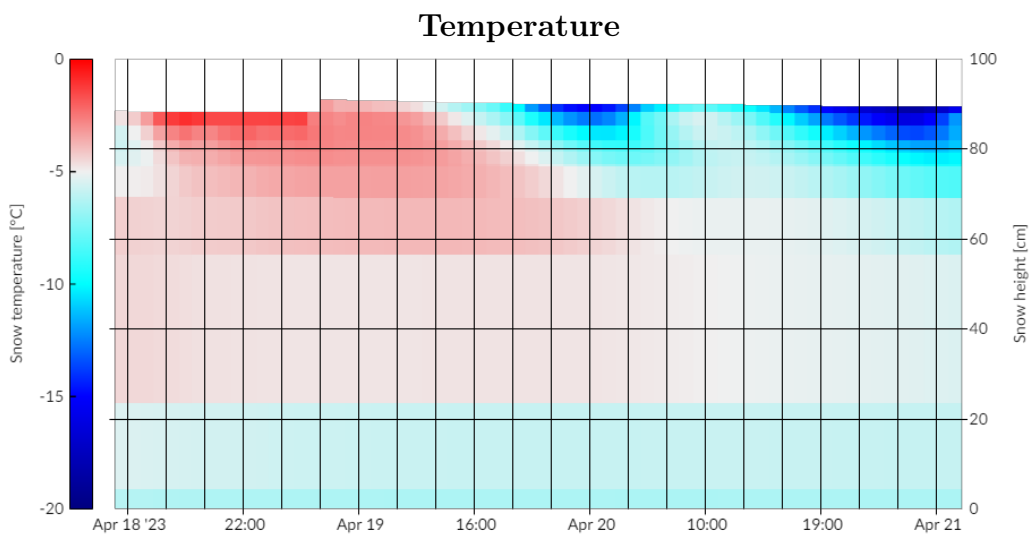


Figure B.3.2: Detailed thermal development model period 3.

B.4 Model period 4

The simulation predicts unchanged grain shapes within the snowpack throughout Model Period 4 (Figure B.4.1). The model output of liquid water is not included, as no liquid water was modeled during the time series.

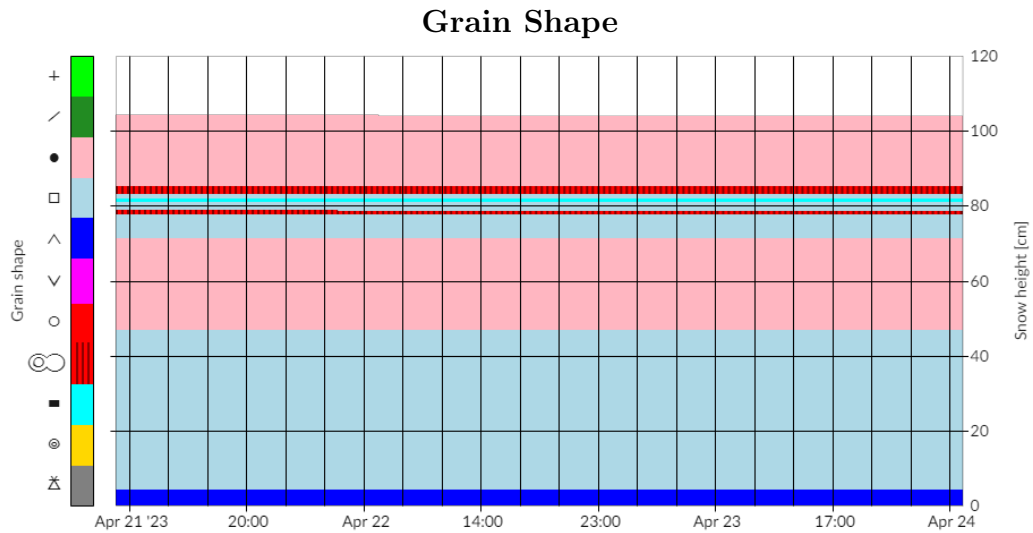


Figure B.4.1: Detailed grain shape development for model period 4.

However, the simulation projects an increase in temperature over Model Period 4, culminating in a near-isothermal state at the last time step of the simulation (Figure B.4.2).

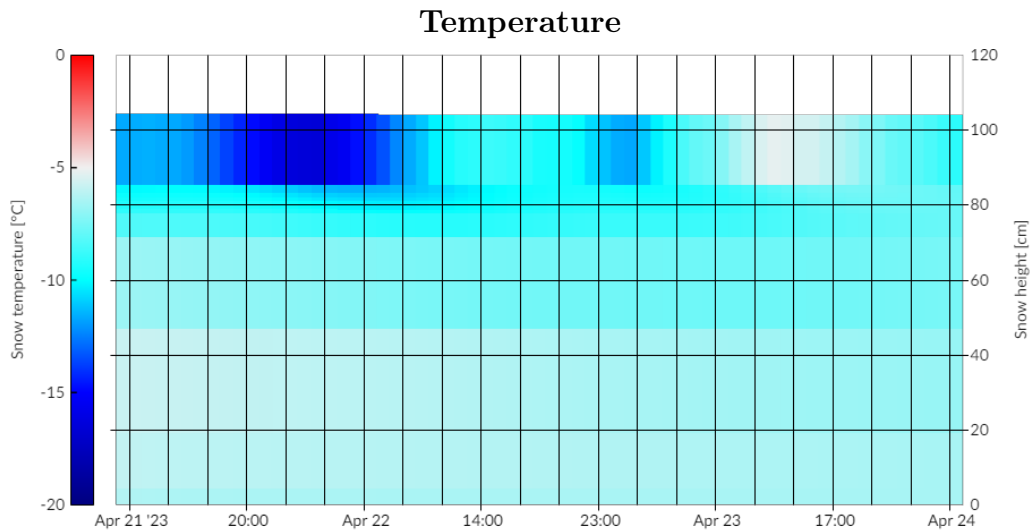


Figure B.4.2: Detailed thermal development model period 4.

Appendix C

Sensitivity analysis

The following Appendix includes the results from the AROME-Arctic, SNOWPACK model chain when running on AROME-Arctic grid point B and point C. The experiences were carried out as part of the sensitivity analysis described in Section 4.5.7 and discussed in Section 6.2.2. Even though these results are not explicitly mentioned in the report, insight from these results was utilized for the discussion and the drawn conclusions.

C.1 Point B

The model chain output when ran on data from AROME-Arctic, grid point C.

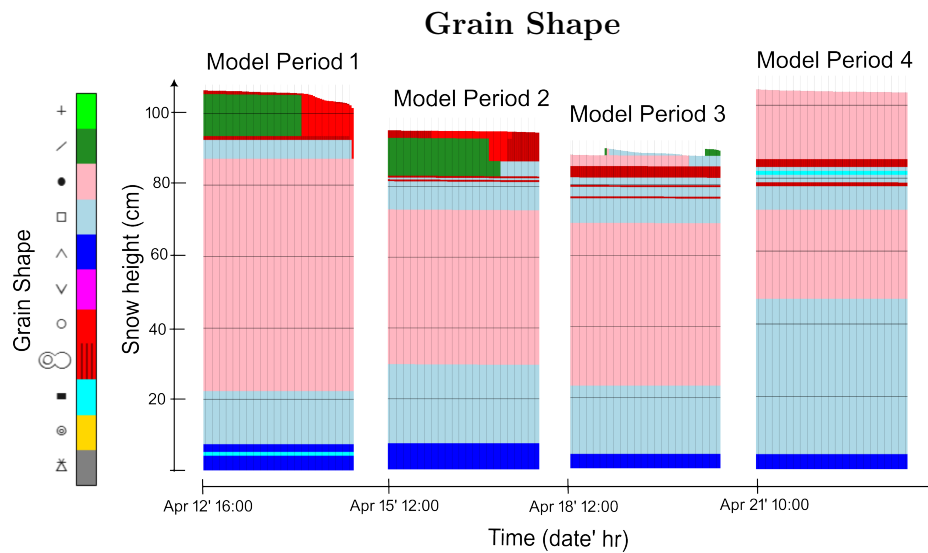


Figure C.1.1: The simulated grain shape evolution over four model periods as generated by the model chain point B.

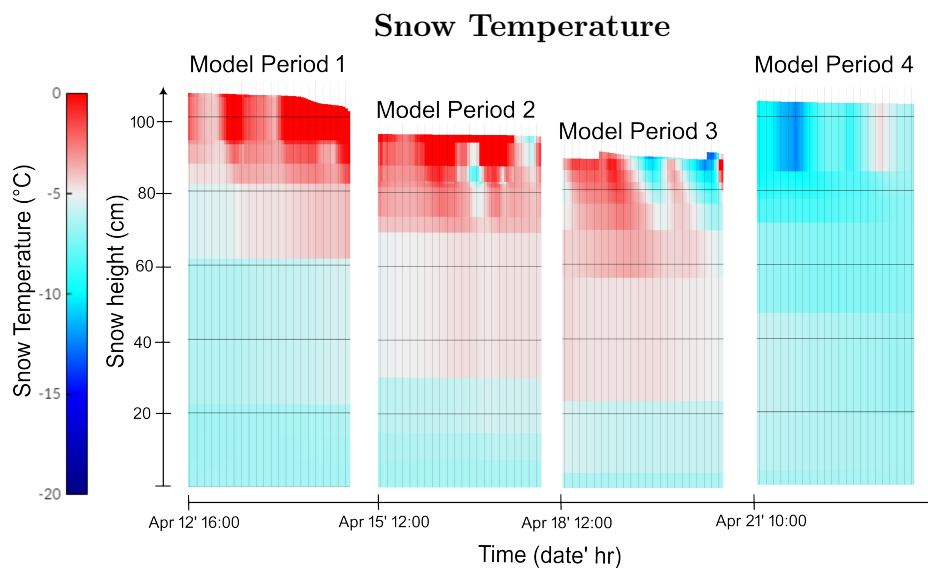


Figure C.1.2: The simulated temperature evolution over four model periods as generated by the model chain point B.

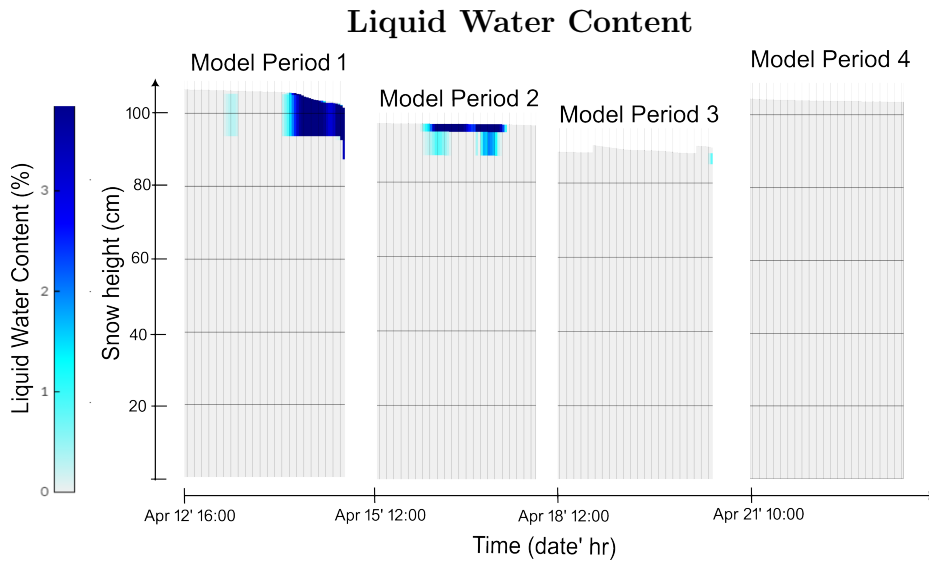


Figure C.1.3: The simulated liquid water content evolution over four model periods as generated by the model chain point B.

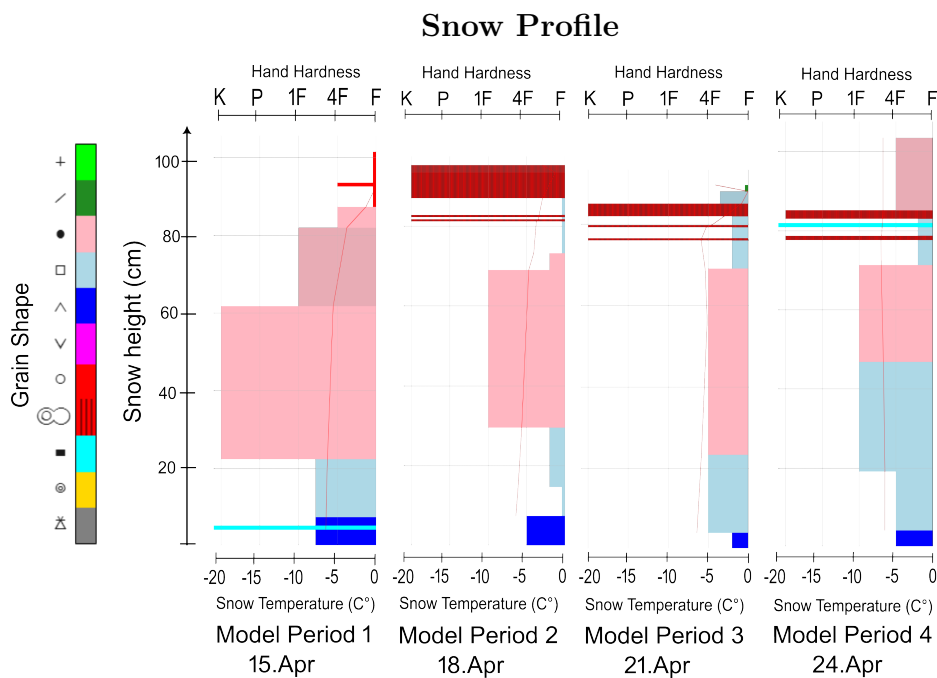


Figure C.1.4: The simulated snow profiles for the last time step of the over four model periods, as generated by the model chain point B.

C.2 Point C

The model chain output when ran on data from AROME-Arctic, grid point C.

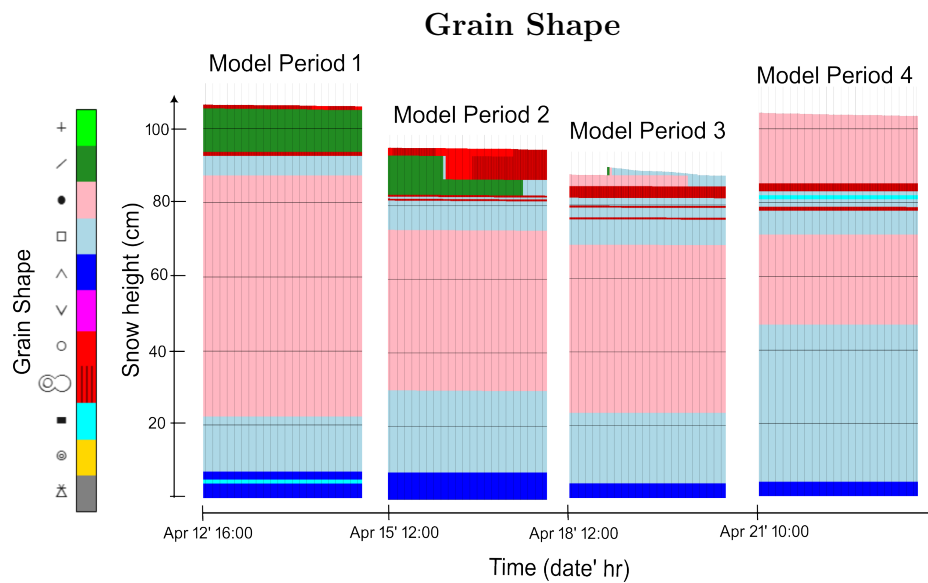


Figure C.2.1: The simulated grain shape evolution over four model periods as generated by the model chain point C.

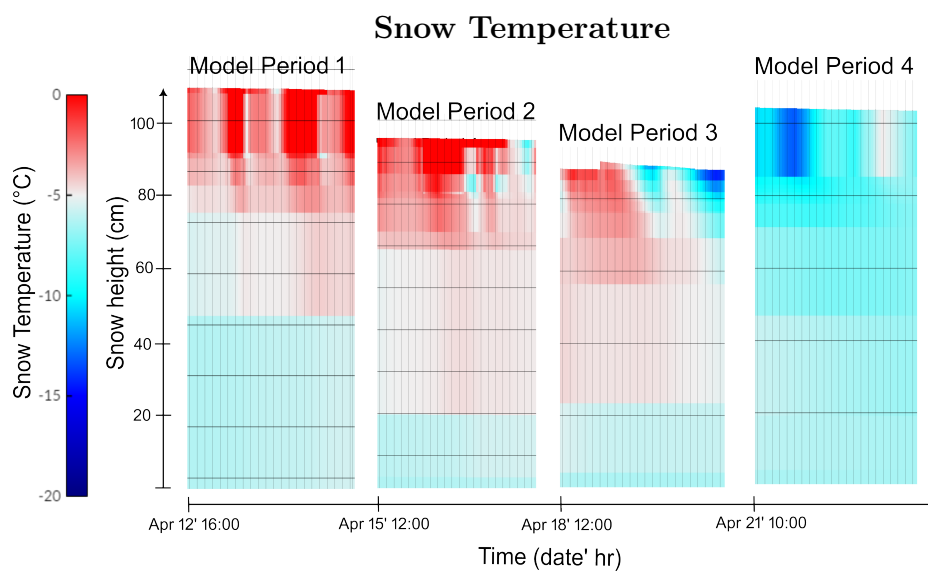


Figure C.2.2: The simulated temperature evolution over four model periods as generated by the model chain point C.

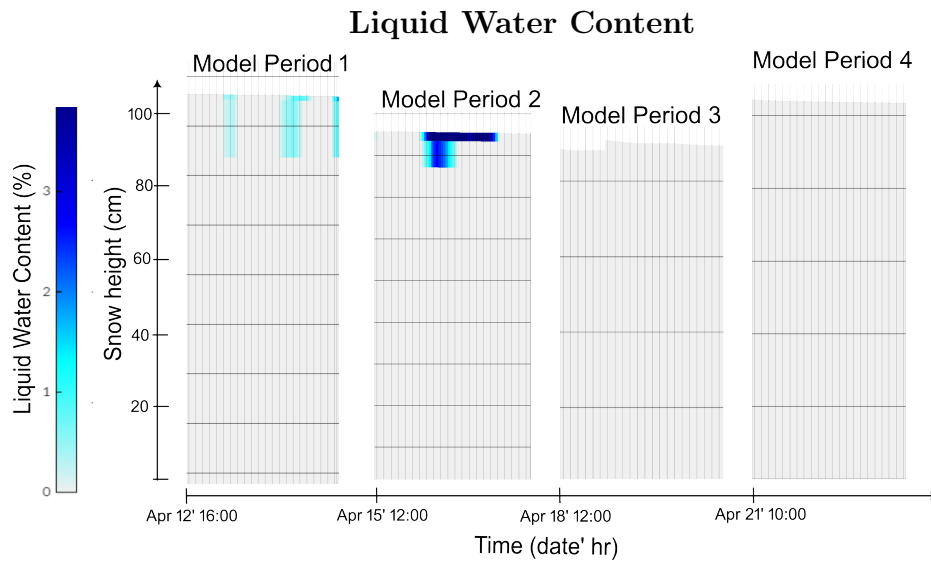


Figure C.2.3: The simulated liquid water content evolution over four model periods as generated by the model chain point C.

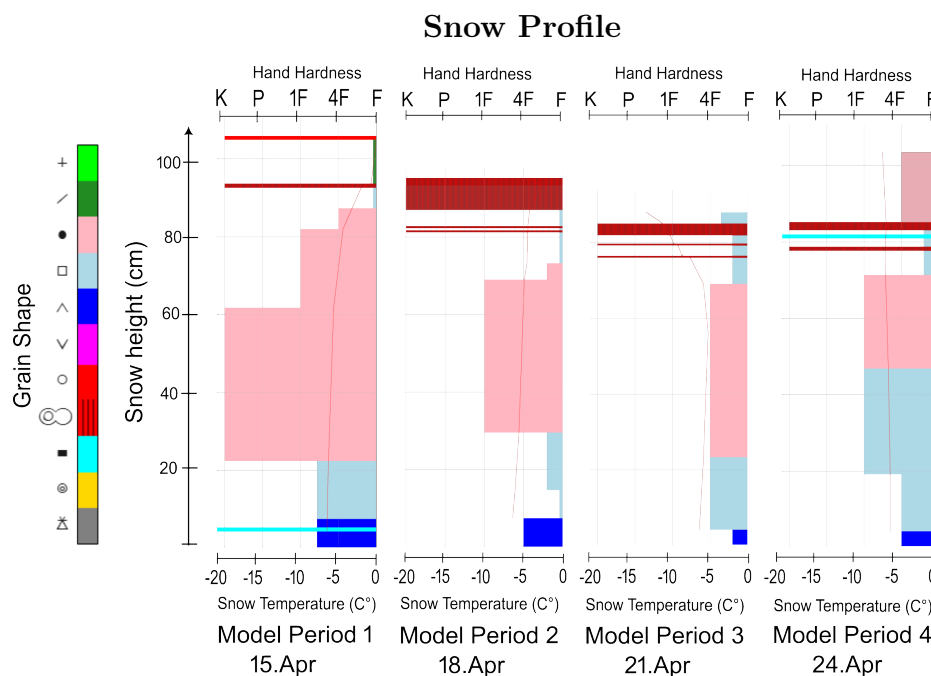


Figure C.2.4: The simulated snow profiles for the last time step of the over four model periods, as generated by the model chain point C.



 **NTNU**

Norwegian University of
Science and Technology